

分類:	
編號:	
總號:	

Chapter 8

Barriers and Wells

General Discussions.

Conservation of probability

Probability flux (current)

Existence of probability density, probability flux

Requirement for acceptable solution.



Special treatment of δ -functions.
boundary conditions.

Simple examples



one dimensional problem.

no need of differential equation.

emphasize on matching the boundary conditions

Potential Step

$$E > V_0 > 0$$

Reflection coefficient, Transmission coefficient

$$0 < E < V_0$$

Penetrating depth.

Potential Barrier.

Tunneling

Resonance

Tunneling of Particles

分類:	
編號:	
總號:	

General Discussion of Tunneling Problem.

Overview

General shape.

Approximation.

Triangular and Trapezoidal Barrier

α -Decay.

Scanning Tunnelling Microscopy.

Field Emission

Other Application on Electronic Devices will be discussed
in Solid State Section

分類:
編號:
總號:

Wells.

Potential Well

Parity operator

$$P\psi(x) = p\psi(-x)$$

$$P^2\psi(x) = \psi(x)$$

$$P^2 = 1$$

$$P\psi(x) = p\psi(x) \quad \text{eigenvalue equation}$$

$$P^2\psi(x) = p^2\psi(x) = \psi(x)$$

$$p = \pm 1$$

$$\psi(x) = \psi(-x) \quad \text{even}$$

$$P\psi(x) = \psi(-x) = \psi(x)$$

\Rightarrow it is an eigenfunction of parity P with ^{eigen}value $+1$
with eigenfunction of parity P with eigenvalue -1

$$[H, P] = 0 \quad \text{is valid if } V(x) = V(-x)$$

\downarrow
we can find simultaneous eigenfunctions
of H, P

Compare with infinite potential well and
simple harmonic oscillator potential.

Singe δ -function Potential

Double δ -function Potential.

分類:
編號:
總號:

Barrier and Wells

Schrodinger Equation and Conservation of Probability

↓
probability flux

Requirement of Acceptable Solutions

Potential Step

Reflection Coefficient and Transmission Coefficient

Potential Barrier

↓
Tunneling problem

Potential Well.

分類:
編號:
總號:

Appendix

The Dirac Delta Function

Reference: David J. Griffiths "Introduction to Electrodynamics" Third Edition, P 45 - 51

5 The Dirac Delta Function

1.5.1 The Divergence of \hat{r}/r^2

Consider the vector function

$$\mathbf{v} = \frac{1}{r^2} \hat{r}. \quad (1.83)$$

At every location, \mathbf{v} is directed radially outward (Fig. 1.44); if ever there was a function that ought to have a large positive divergence, this is it. And yet, when you actually *calculate* the divergence (using Eq. 1.71), you get precisely *zero*:

$$\nabla \cdot \mathbf{v} = \frac{1}{r^2} \frac{\partial}{\partial r} \left(r^2 \frac{1}{r^2} \right) = \frac{1}{r^2} \frac{\partial}{\partial r} (1) = 0. \quad (1.84)$$

(You will have encountered this paradox already, if you worked Prob. 1.16.) The plot thickens if you apply the divergence theorem to this function. Suppose we integrate over a sphere of radius R , centered at the origin (Prob. 1.38b); the surface integral is

$$\begin{aligned} \oint \mathbf{v} \cdot d\mathbf{a} &= \int \left(\frac{1}{R^2} \hat{r} \right) \cdot (R^2 \sin \theta \, d\theta \, d\phi \, \hat{r}) \\ &= \left(\int_0^\pi \sin \theta \, d\theta \right) \left(\int_0^{2\pi} d\phi \right) = 4\pi. \end{aligned} \quad (1.85)$$

But the *volume* integral, $\int \nabla \cdot \mathbf{v} \, d\tau$, is *zero*, if we are really to believe Eq. 1.84. Does this mean that the divergence theorem is false? What's going on here?

The source of the problem is the point $r = 0$, where \mathbf{v} blows up (and where, in Eq. 1.84, we have unwittingly divided by zero). It is quite true that $\nabla \cdot \mathbf{v} = 0$ everywhere *except* the origin, but right *at* the origin the situation is more complicated. Notice that the surface integral (1.85) is *independent of R* ; if the divergence theorem is right (and it *is*), we should get $\int (\nabla \cdot \mathbf{v}) \, d\tau = 4\pi$ for *any* sphere centered at the origin, no matter how small. Evidently the entire contribution must be coming from the point $r = 0$! Thus, $\nabla \cdot \mathbf{v}$ has the bizarre property that it vanishes everywhere except at one point, and yet its *integral* (over any volume containing that point) is 4π . No ordinary function behaves like that. (On the other hand, a *physical* example *does* come to mind: the density (mass per unit volume) of a point particle. It's zero except at the exact location of the particle, and yet its *integral* is finite—namely, the mass of the particle.) What we have stumbled on is a mathematical object known to physicists as the **Dirac delta function**. It arises in many branches of theoretical physics. Moreover, the specific problem at hand (the divergence of the function \hat{r}/r^2) is not just some arcane curiosity—it is, in fact, central to the whole theory of electrodynamics. So it is worthwhile to pause here and study the Dirac delta function with some care.

1.5.2 The One-Dimensional Dirac Delta Function

The one dimensional Dirac delta function, $\delta(x)$, can be pictured as an infinitely high, infinitesimally narrow “spike,” with area 1 (Fig. 1.45). That is to say:

$$\delta(x) = \begin{cases} 0, & \text{if } x \neq 0 \\ \infty, & \text{if } x = 0 \end{cases} \quad (1.86)$$

and

$$\int_{-\infty}^{\infty} \delta(x) dx = 1. \quad (1.87)$$

Technically, $\delta(x)$ is not a function at all, since its value is not finite at $x = 0$. In the mathematical literature it is known as a **generalized function**, or **distribution**. It is, if you

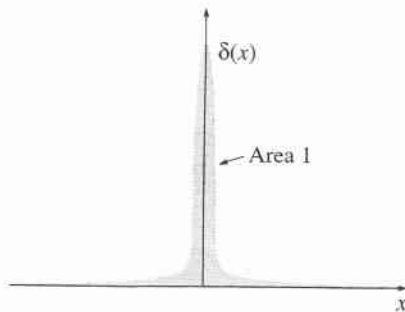


Figure 1.45

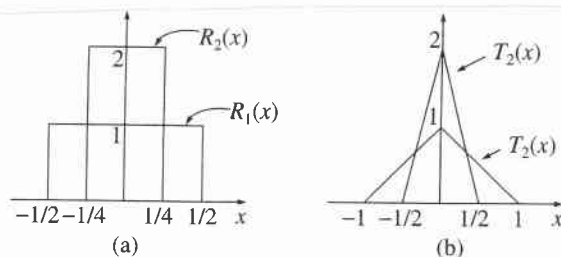


Figure 1.46

like, the *limit* of a *sequence* of functions, such as rectangles $R_n(x)$, of height n and width $1/n$, or isosceles triangles $T_n(x)$, of height n and base $2/n$ (Fig. 1.46).

If $f(x)$ is some “ordinary” function (that is, *not* another delta function—in fact, just to be on the safe side let’s say that $f(x)$ is *continuous*), then the *product* $f(x)\delta(x)$ is zero everywhere except at $x = 0$. It follows that

$$f(x)\delta(x) = f(0)\delta(x). \quad (1.88)$$

(This is the most important fact about the delta function, so make sure you understand why it is true: since the product is zero anyway *except* at $x = 0$, we may as well replace $f(x)$ by the value it assumes at the origin.) In particular

$$\int_{-\infty}^{\infty} f(x)\delta(x) dx = f(0) \int_{-\infty}^{\infty} \delta(x) dx = f(0). \quad (1.89)$$

Under an integral, then, the delta function “picks out” the value of $f(x)$ at $x = 0$. (Here and below, the integral need not run from $-\infty$ to $+\infty$; it is sufficient that the domain extend across the delta function, and $-\epsilon$ to $+\epsilon$ would do as well.)

Of course, we can shift the spike from $x = 0$ to some other point, $x = a$ (Fig. 1.47):

$$\delta(x - a) = \begin{cases} 0, & \text{if } x \neq a \\ \infty, & \text{if } x = a \end{cases} \text{ with } \int_{-\infty}^{\infty} \delta(x - a) dx = 1. \quad (1.90)$$

Equation 1.88 becomes

$$f(x)\delta(x - a) = f(a)\delta(x - a), \quad (1.91)$$

and Eq. 1.89 generalizes to

$$\int_{-\infty}^{\infty} f(x)\delta(x - a) dx = f(a). \quad (1.92)$$

Example 1.14

Evaluate the integral

$$\int_0^3 x^3 \delta(x-2) dx.$$

類:
號:
號:

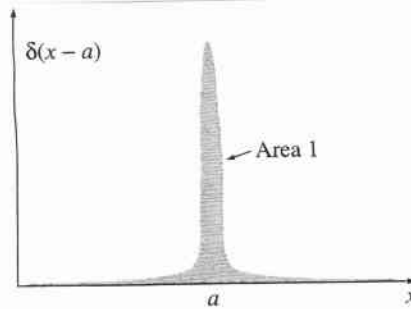


Figure 1.47

Solution: The delta function picks out the value of x^3 at the point $x = 2$, so the integral is $2^3 = 8$. Notice, however, that if the upper limit had been 1 (instead of 3) the answer would be 0, because the spike would then be outside the domain of integration.

Although δ itself is not a legitimate function, *integrals* over δ are perfectly acceptable. In fact, it's best to think of the delta function as something that is *always intended for use under an integral sign*. In particular, two expressions involving delta functions (say, $D_1(x)$ and $D_2(x)$) are considered equal if⁶

$$\int_{-\infty}^{\infty} f(x) D_1(x) dx = \int_{-\infty}^{\infty} f(x) D_2(x) dx, \quad (1.93)$$

for all ("ordinary") functions $f(x)$.

Example 1.15

Show that

$$\delta(kx) = \frac{1}{|k|} \delta(x), \quad (1.94)$$

where k is any (nonzero) constant. (In particular, $\delta(-x) = \delta(x)$.)

Solution: For an arbitrary test function $f(x)$, consider the integral

$$\int_{-\infty}^{\infty} f(x) \delta(kx) dx.$$

Changing variables, we let $y \equiv kx$, so that $x = y/k$, and $dx = 1/k dy$. If k is positive, the integration still runs from $-\infty$ to $+\infty$, but if k is *negative*, then $x = \infty$ implies $y = -\infty$, and

⁶This is not as arbitrary as it may sound. The crucial point is that the integrals must be equal for *any* $f(x)$. Suppose $D_1(x)$ and $D_2(x)$ actually *differed*, say, in the neighborhood of the point $x = 17$. Then we could pick a function $f(x)$ that was sharply peaked about $x = 17$, and the integrals would not be equal.

分類:
編號:
總號:

vice versa, so the order of the limits is reversed. Restoring the "proper" order costs a minus sign. Thus

$$\int_{-\infty}^{\infty} f(x)\delta(kx) dx = \pm \int_{-\infty}^{\infty} f(y/k)\delta(y) \frac{dy}{k} = \pm \frac{1}{k} f(0) = \frac{1}{|k|} f(0).$$

(The lower signs apply when k is negative, and we account for this neatly by putting absolute value bars around the final k , as indicated.) Under the integral sign, then, $\delta(kx)$ serves the same purpose as $(1/|k|)\delta(x)$:

$$\int_{-\infty}^{\infty} f(x)\delta(kx) dx = \int_{-\infty}^{\infty} f(x) \left[\frac{1}{|k|} \delta(x) \right] dx.$$

According to criterion 1.93, therefore, $\delta(kx)$ and $(1/|k|)\delta(x)$ are equal.

Problem 1.43 Evaluate the following integrals:

(a) $\int_2^6 (3x^2 - 2x - 1) \delta(x - 3) dx.$

(b) $\int_0^5 \cos x \delta(x - \pi) dx.$

(c) $\int_0^3 x^3 \delta(x + 1) dx.$

(d) $\int_{-\infty}^{\infty} \ln(x + 3) \delta(x + 2) dx.$

Problem 1.44 Evaluate the following integrals:

(a) $\int_{-2}^2 (2x + 3) \delta(3x) dx.$

(b) $\int_0^2 (x^3 + 3x + 2) \delta(1 - x) dx.$

(c) $\int_{-1}^1 9x^2 \delta(3x + 1) dx.$

(d) $\int_{-\infty}^a \delta(x - b) dx.$

Problem 1.45

(a) Show that

$$x \frac{d}{dx} (\delta(x)) = -\delta(x).$$

[Hint: Use integration by parts.]

(b) Let $\theta(x)$ be the **step function**:

$$\theta(x) \equiv \left\{ \begin{array}{ll} 1, & \text{if } x > 0 \\ 0, & \text{if } x \leq 0 \end{array} \right\}. \quad (1.95)$$

Show that $d\theta/dx = \delta(x)$.

1.5.3 The Three-Dimensional Delta Function

It is an easy matter to generalize the delta function to three dimensions:

$$\delta^3(\mathbf{r}) = \delta(x) \delta(y) \delta(z). \quad (1.96)$$

(As always, $\mathbf{r} \equiv x \hat{\mathbf{x}} + y \hat{\mathbf{y}} + z \hat{\mathbf{z}}$ is the position vector, extending from the origin to the point (x, y, z)). This three-dimensional delta function is zero everywhere except at $(0, 0, 0)$, where it blows up. Its volume integral is 1:

$$\int_{\text{all space}} \delta^3(\mathbf{r}) d\tau = \int_{-\infty}^{\infty} \int_{-\infty}^{\infty} \int_{-\infty}^{\infty} \delta(x) \delta(y) \delta(z) dx dy dz = 1. \quad (1.97)$$

And, generalizing Eq. 1.92,

$$\int_{\text{all space}} f(\mathbf{r}) \delta^3(\mathbf{r} - \mathbf{a}) d\tau = f(\mathbf{a}). \quad (1.98)$$

As in the one-dimensional case, integration with δ picks out the value of the function f at the location of the spike.

We are now in a position to resolve the paradox introduced in Sect. 1.5.1. As you will recall, we found that the divergence of $\hat{\mathbf{r}}/r^2$ is zero everywhere except at the origin, and yet its *integral* over any volume containing the origin is a constant (to wit: 4π). These are precisely the defining conditions for the Dirac delta function; evidently

$$\nabla \cdot \left(\frac{\hat{\mathbf{r}}}{r^2} \right) = 4\pi \delta^3(\mathbf{r}). \quad (1.99)$$

More generally,

$$\nabla \cdot \left(\frac{\hat{\mathbf{r}}}{r^2} \right) = 4\pi \delta^3(\mathbf{r}), \quad (1.100)$$

where, as always, \mathbf{r} is the separation vector: $\mathbf{r} \equiv \mathbf{r} - \mathbf{r}'$. Note that differentiation here is with respect to \mathbf{r} , while \mathbf{r}' is held constant. Incidentally, since

$$\nabla \left(\frac{1}{r} \right) = -\frac{\hat{\mathbf{r}}}{r^2} \quad (1.101)$$

(Prob. 1.13), it follows that

$$\nabla^2 \frac{1}{r} = -4\pi \delta^3(\mathbf{r}). \quad (1.102)$$

分類:
編號:
總號:

Example 1.16

Evaluate the integral

$$J = \int_{\mathcal{V}} (r^2 + 2) \nabla \cdot \left(\frac{\hat{\mathbf{r}}}{r^2} \right) d\tau,$$

where \mathcal{V} is a sphere of radius R centered at the origin.

Solution 1: Use Eq. 1.99 to rewrite the divergence, and Eq. 1.98 to do the integral:

$$J = \int_{\mathcal{V}} (r^2 + 2) 4\pi \delta^3(\mathbf{r}) d\tau = 4\pi(0 + 2) = 8\pi.$$

This one-line solution demonstrates something of the power and beauty of the delta function, but I would like to show you a second method, which is much more cumbersome but serves to illustrate the method of integration by parts, Sect. 1.3.6.

Solution 2: Using Eq. 1.59, we transfer the derivative from $\hat{\mathbf{r}}/r^2$ to $(r^2 + 2)$:

$$J = - \int \frac{\hat{\mathbf{r}}}{r^2} \cdot [\nabla(r^2 + 2)] d\tau + \oint (r^2 + 2) \frac{\hat{\mathbf{r}}}{r^2} \cdot d\mathbf{a}.$$

The gradient is

$$\nabla(r^2 + 2) = 2r\hat{\mathbf{r}},$$

so the volume integral becomes

$$\int \frac{2}{r} d\tau = \int \frac{2}{r} r^2 \sin\theta dr d\theta d\phi = 8\pi \int_0^R r dr = 4\pi R^2.$$

Meanwhile, on the boundary of the sphere (where $r = R$),

$$d\mathbf{a} = R^2 \sin\theta d\theta d\phi \hat{\mathbf{r}},$$

so the surface integral becomes

$$\int (R^2 + 2) \sin\theta d\theta d\phi = 4\pi(R^2 + 2).$$

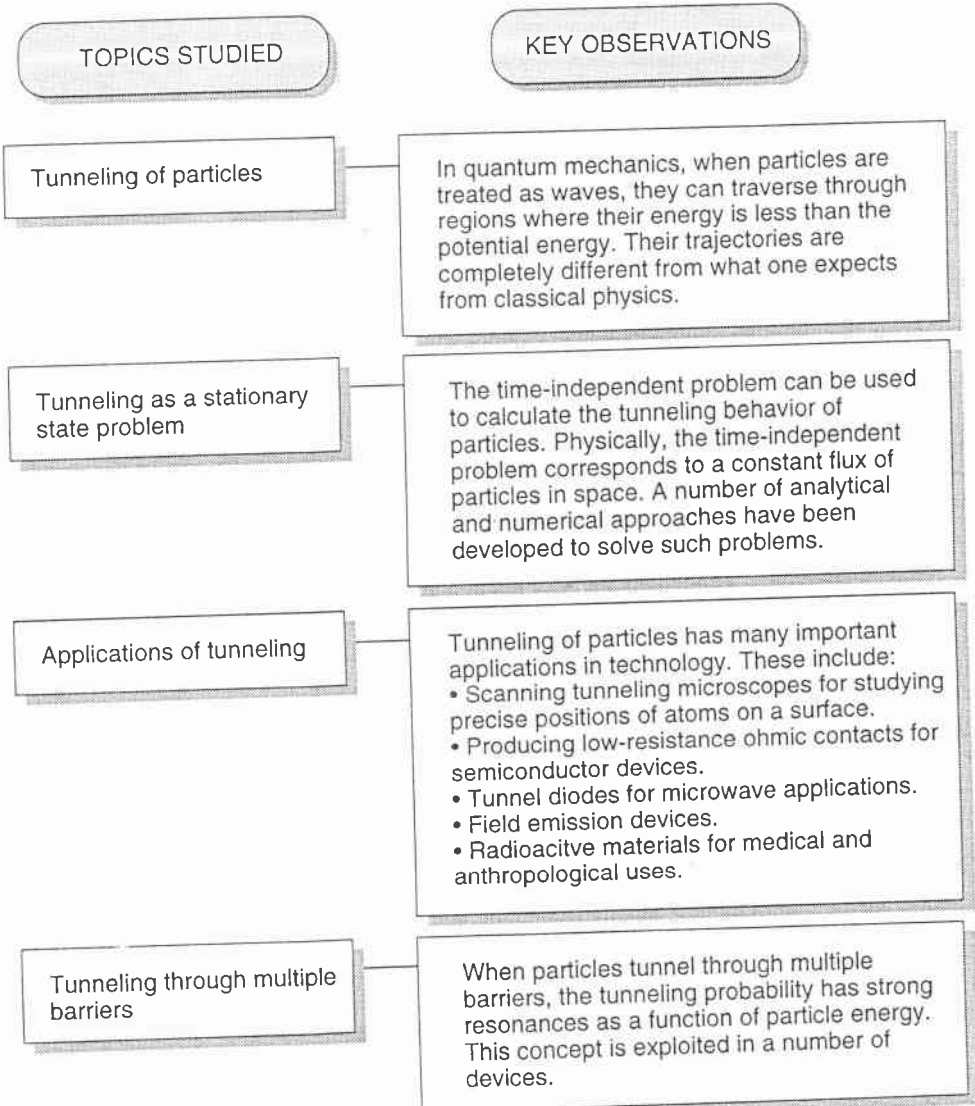
Putting it all together, then,

$$J = -4\pi R^2 + 4\pi(R^2 + 2) = 8\pi,$$

as before.

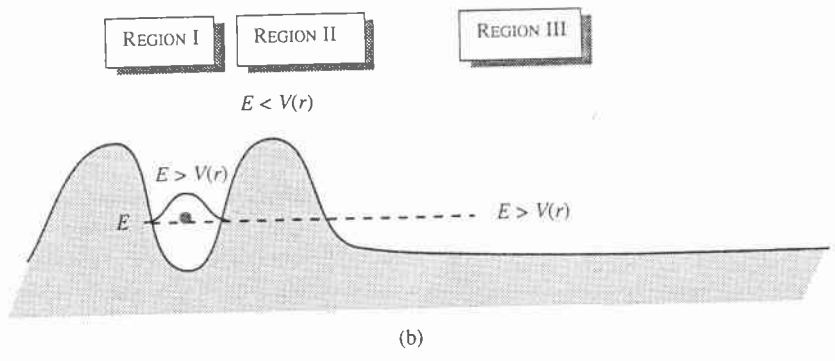
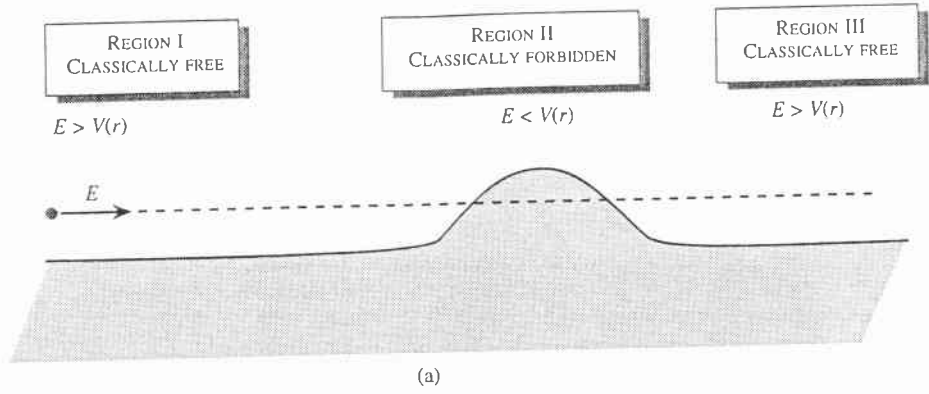
TUNNELING OF PARTICLES

- The general problem of quantum mechanical tunneling
- Tunneling as a stationary state problem:
Tunneling through a barrier
- Important technological applications of tunneling
- Tunneling through multiple barriers: Resonant tunneling

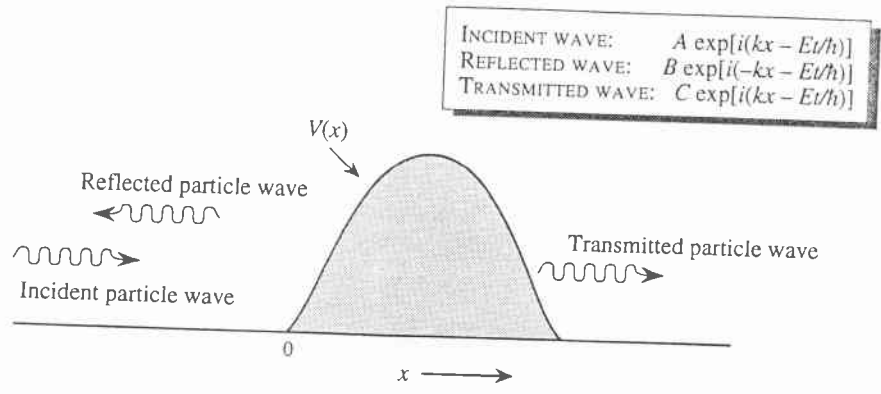


Applications

General Tunneling Problem

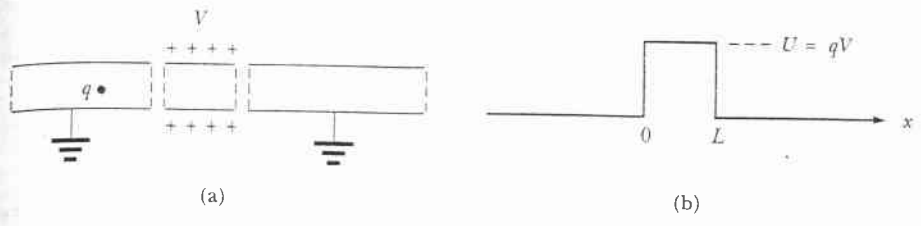


A schematic view of two categories of tunneling problems. (a) A particle starts from the unbound state on the left in region I where it is free to move classically (i.e., $E \geq V(r)$) and tunnels through a classically "forbidden" region (II) into a classically allowed region (III). In (b) the particle is initially in "bound region" and tunnels through a "forbidden" region (II) into a classically allowed region (III).



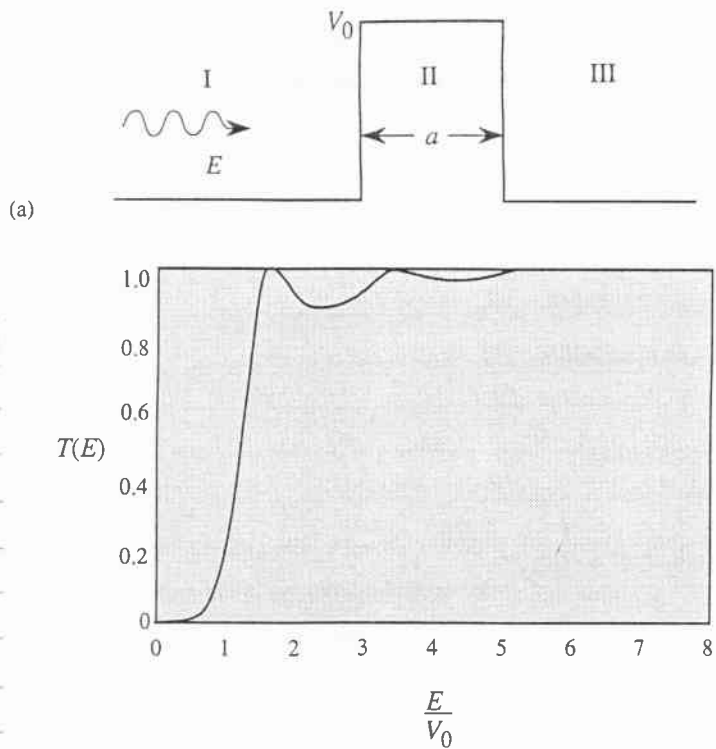
A generic description of the tunneling problem. Particles are incident from the left with an energy E . A certain fraction of the particle current is reflected and the rest is transmitted.

分類:
編號: 8-25a
總號:

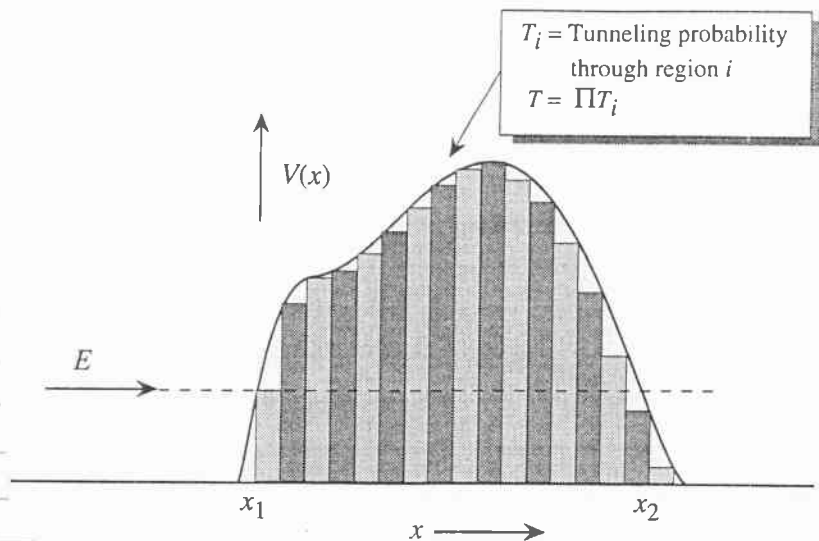


(a) Aligned metallic cylinders serve as a potential barrier to charged particles. The central cylinder is held at some positive electric potential V , and the outer cylinders are grounded. A charge q whose total energy is less than qV is unable to penetrate the central cylinder classically, but can do so quantum mechanically by a process called *tunneling*. (b) The potential energy seen by this charge in the limit where the gaps between the cylinders have shrunk to zero size. The result is the square barrier potential of height U .

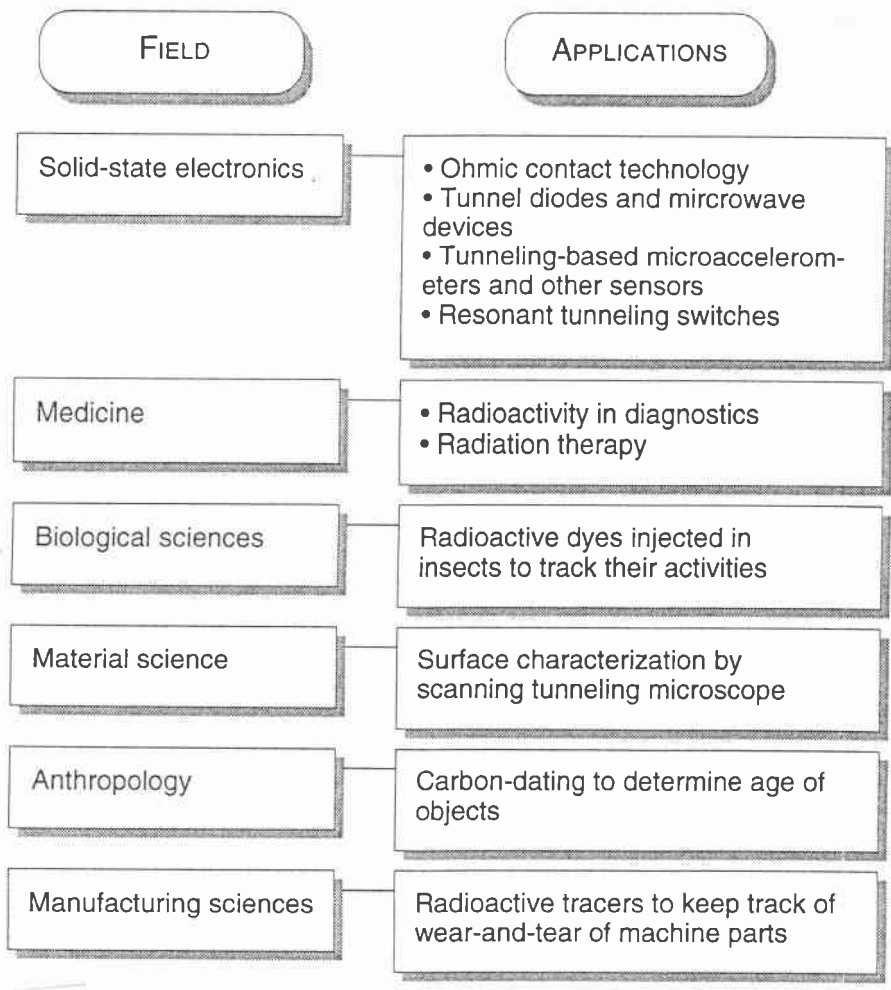
Simplest way to realize a potential barrier



(a) Tunneling of a particle through a potential barrier. (b) The transmission coefficients for an electron as a function of energy for $V_0 = 1.0$ eV, $a = 7.77$ Å. The results are typical of transmittance through a barrier. Notice that even for $E > V_0$, the probability goes through values less than unity; i.e., some reflection occurs.



: An approximation scheme used to calculate particle tunneling with energy E through a smoothly varying potential.



Important applications of particle tunneling in various fields.

Basic Formula

We have developed an analytical expression for the tunneling probability for simple square barriers

In the "wide" barrier approximation ($d \ll a$)

$$T \sim \frac{16 E (V_0 - E)}{V_0^2} e^{-2\gamma a} \quad \gamma = \sqrt{\frac{2m(V_0 - E)}{\hbar^2}} = \frac{1}{2d}$$

[The tunneling expression is dominated by the exponential term]

As a further approximation, we take the prefactor to be unity

$$T \sim e^{-2\gamma a}$$

Now we will develop a simple approximation which is quite accurate and yet can be applied analytically to many problems of interest.

Divide the potential into hatched region

$$T \sim \prod_i T_i = e^{-\frac{1}{\hbar} \sum_i \int_{x_i}^{x_{i+1}} [8mV(x) - E]^{\frac{1}{2}} dx}$$

[This is valid only if the potential is smoothly varying compared to the de Broglie wavelength]

Now increasing the number of subdivisions while ensuring $d_i \ll \lambda$

[Note, when $E > V(x_i)$, $T_i \sim 1$]

$$\Rightarrow T = e^{-\frac{1}{\hbar} \int_{x_1}^{x_2} [8mV(x) - E]^{\frac{1}{2}} dx}$$

where x_1 and x_2 are points where $E = V(x)$

\downarrow \downarrow
 turning points

This is the starting point for the application of tunneling.

Example: Triangular Barrier and Trapezoidal Barrier

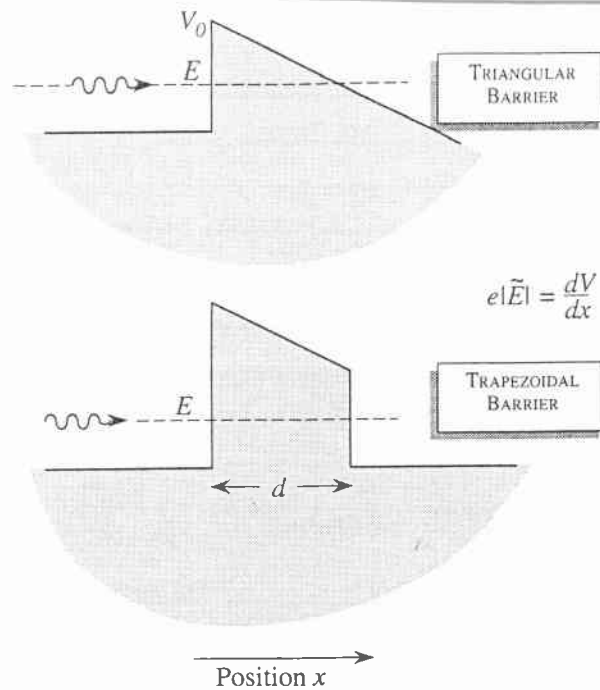


Figure 6.6: (a) Triangular and (b) trapezoidal barriers through which an electron with energy E can tunnel. Such barriers are encountered in many electronic device structures. The potential shape is described by an electric field \tilde{E} .

Triangle $T = e^{-\frac{4(2m)^{\frac{1}{2}}}{3e|\tilde{E}|\hbar} (V_0 - E)^{\frac{3}{2}}}$ Fowler - Nordheim formula

Trapezoidal, $T = e^{-\frac{4(2m)^{\frac{1}{2}}}{3\hbar e|\tilde{E}|} [(V_0 - E)^{\frac{3}{2}} - (V_0 - E - e|\tilde{E}|d)^{\frac{3}{2}}]}$

Task, find the good model for $V(x)$
 ↓
 in application.

6.2 GENERAL TUNNELING PROBLEM

The general problem of particle tunneling can be loosely classified into two categories, both of which involve the propagation of a particle with energy E through a region of potential energy $V(r)$, where in some regions, the particle energy is smaller than the potential energy. This region is classically forbidden to the particle, but, as discussed in the Introduction, when the particle is described through a wave description, tunneling can occur. In the first category of problems we have a situation, as shown in Fig. 6.2a, where there is a region of space where the particle can be represented by a "free" state. The particle can be represented by a momentum in this free space region where the electron energy E is greater than the background potential energy, which may be considered to be uniform. In this example, the tunneling problem involves the particle coming from the left and striking the potential barrier, with the particle having a finite probability of tunneling through and a finite probability of being reflected back.

In the second category of tunneling problems, the particle is initially confined to a "quantum well" region in a "quasi-bound" state, as shown in Fig. 6.2b. In the quasi-bound state, the particle is primarily confined to the quantum well, but has a finite probability of tunneling out of the well and escaping. The key difference between the two cases is that in the first problem the wavefunction corresponding to the initial state is essentially unbound, whereas in the second case it is primarily confined to the quantum well region.

Tunneling Through Wide Barriers

In many applications, the transmission probability for tunneling is very small. Inside a barrier, the wave function is essentially proportional to $e^{-\alpha x}$, or $e^{-x/\delta}$, where $\delta \equiv 1/\alpha$ is the penetration depth.² If $L \gg \delta$, very little of the wave will "survive" to $x = L$. The condition for a "wide" barrier is thus

$$\frac{1}{\delta}L = \alpha L = \frac{\sqrt{2m(U_0 - E)}}{\hbar}L \gg 1 \quad (5-11)$$

It is wide if L is large, or E is much less than U_0 , or both.

It is left as an exercise to show that if (5-11) holds, the transmission probability of (5-10) is given by the approximation

$$T \cong 16 \frac{E}{U_0} \left(1 - \frac{E}{U_0}\right) e^{-2[\sqrt{2m(U_0 - E)}/\hbar]L} \quad (5-12)$$

Example 5.2

An electron encounters a barrier of height 0.100 eV and width 15 nm. What is the transmission probability if its energy is (a) 0.040 eV? (b) 0.060 eV?

²The solution within the barrier is not strictly a decaying exponential, but contains an exponentially increasing part $e^{+\alpha x}$. In most cases, this part is inconsequential small.

Solution

First we see if condition (5-11) holds.

For 0.040 eV:

$$\frac{L}{\delta} = \frac{\sqrt{2(9.11 \times 10^{-31} \text{ kg})(0.100 - 0.040) \times 1.6 \times 10^{-19} \text{ J}}}{1.055 \times 10^{-34} \text{ J}\cdot\text{s}} 15 \times 10^{-9} \text{ m}$$

$$= 18.8$$

For 0.060 eV:

$$\frac{L}{\delta} = \frac{\sqrt{2(9.11 \times 10^{-31} \text{ kg})(0.100 - 0.060) \times 1.6 \times 10^{-19} \text{ J}}}{1.055 \times 10^{-34} \text{ J}\cdot\text{s}} 15 \times 10^{-9} \text{ m}$$

$$= 15.4$$

In both cases, the barrier is wide, many times the penetration depth. Now, noting that we have just calculated the arguments of the exponential in (5-12),

$$T_{0.040 \text{ eV}} = 16 \frac{0.04}{0.1} \left(1 - \frac{0.04}{0.1}\right) e^{-2 \times 18.8} = 1.8 \times 10^{-16}$$

$$T_{0.060 \text{ eV}} = 16 \frac{0.06}{0.1} \left(1 - \frac{0.06}{0.1}\right) e^{-2 \times 15.4} = 1.8 \times 10^{-13}$$

As expected, for both barriers the transmission probability for a single event is very small. But in many real situations, barriers are constantly bombarded by particles. If electrons at either of these energies were to strike the barrier 10^{20} times each second, there would be a significant flux of escaping particles. Such high frequency is not at all unrealistic; alpha-particles almost trapped in an atomic nucleus typically get 10^{20} chances to tunnel out every second. Alpha decay is discussed in the next section.

The example illustrates another important point: When transmission probabilities are very small, they vary sharply with energy. Both probabilities are small, but a modest 50% increase in particle energy results in a transmission probability about a thousand times larger. This sensitivity is due to the exponential dependence in (5-12), and the smaller the probability, the more pronounced is the variation.³

Electrons with energies of 1.0 eV and 2.0 eV are incident on a barrier 10.0 eV high and 0.50 nm wide. (a) Find their respective transmission probabilities. (b) How are these affected if the barrier is doubled in width?

Solution

(a) For the 1.0-eV electrons

$$k_2 = \frac{\sqrt{2m(U - E)}}{\hbar}$$

$$= \frac{\sqrt{(2)(9.1 \times 10^{-31} \text{ kg})(10.0 - 1.0) \text{ eV}(1.6 \times 10^{-19} \text{ J/eV})}}{1.054 \times 10^{-34} \text{ J}\cdot\text{s}}$$

$$= 1.6 \times 10^{10} \text{ m}^{-1}$$

Since $L = 0.50 \text{ nm} = 5.0 \times 10^{-10} \text{ m}$, $2k_2L = (2)(1.6 \times 10^{10} \text{ m}^{-1})(5.0 \times 10^{-10} \text{ m}) = 16$, and the approximate transmission probability is

$$T_1 = e^{-2k_2L} = e^{-16} = 1.1 \times 10^{-7}$$

One 1.0-eV electron out of 8.9 million can tunnel through the 10-eV barrier on the average. For the 2.0-eV electrons a similar calculation gives $T_2 = 2.4 \times 10^{-7}$. These electrons are over twice as likely to tunnel through the barrier.

(b) If the barrier is doubled in width to 1.0 nm, the transmission probabilities become

$$T_1' = 1.3 \times 10^{-14} \quad T_2' = 5.1 \times 10^{-14}$$

Evidently T is more sensitive to the width of the barrier than to the particle energy here.

The Tunnel Diode

A tunnel diode is an electronic element whose response to applied voltages is unusual and very fast

Tunneling in Semiconductor

p-n diode which is made by placing a p-type region next to an n-type region

↓
exploit tunneling across the bandgap

(or Esaki diode)

The tunnel diode, in certain biasing regions, the current decreases with increasing voltage.

↗ band-band tunneling
The Zener diode has the property that its resistance changes from a very large value to a very small value over a narrow biasing region.

To understand these devices

- Need to understand the band structure

↓
solid state physics

↓
will be studied in later chapters

(A brief summary is given in Appendix D)

- The important result is the current-voltage relation:

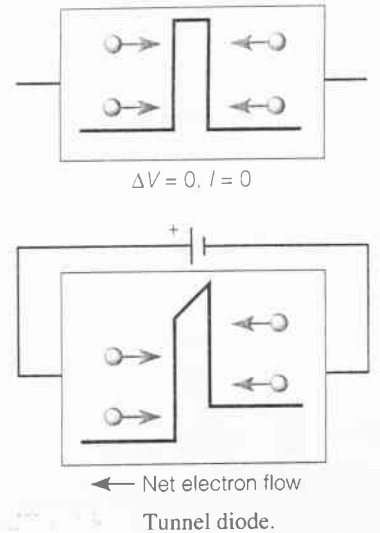
Ohmic contact

Metal semi-conductor junctions which have a linear I-V characteristic with very low resistivity.

The Tunnel Diode

A tunnel diode is an electronic circuit element whose response to applied voltages is unusual and very fast. In a narrow region between the device's two ends (leads), there is a change in the material's physical properties that prevents simple conduction of electrons from one end to the other. In essence, the electrons at the ends are separated by an electrostatic potential barrier they cannot classically surmount, crudely depicted in Figure 5.11. By design, however, the barrier is not wide and significant tunneling occurs. With no applied voltage, tunneling occurs equally in both directions; there is no *net* flow. When a potential difference is applied, the situation becomes asymmetric. Right- and left-tunneling transmission rates differ, and a net current flows.

The tunnel diode may seem to have little utility, as an applied voltage will induce current flow in many materials. But one of its distinctive features is *how* the current varies with voltage. It does not always increase as applied voltage is increased; at some points it decreases (see Exercise 9.32). Moreover, changing the applied voltage changes the transmission rates almost instantly, and quick response is very desirable at high frequencies. The more common devices that control current via voltage changes rely upon relatively slow thermal diffusion of the charge carriers (see Section 9.9). Although its early promise as a high-frequency switch in integrated circuits has dimmed, the tunnel diode has found use in a variety of modern electronic circuits.



Tunneling in Semiconductor Diodes

An important semiconductor device is the *p-n* diode which is made by placing a *p*-type region next to an *n*-type region. In most diode applications, tunneling is not of importance, but there are some special purpose diodes that exploit tunneling across the bandgap. These include the tunnel diode (or Esaki diode) and the Zener diode. The tunnel diode has the unusual characteristic that in certain biasing regions, the current decreases with increasing voltage. This leads to negative differential resistance which can be exploited for generating microwave power. The Zener diode has the property that its resistance changes from a very large value to a very small value over a narrow biasing range.

Let us apply our tunneling theory to understand band-to-band tunneling in semiconductors. In Fig. 6.11a, we show a profile of the conduction and valence

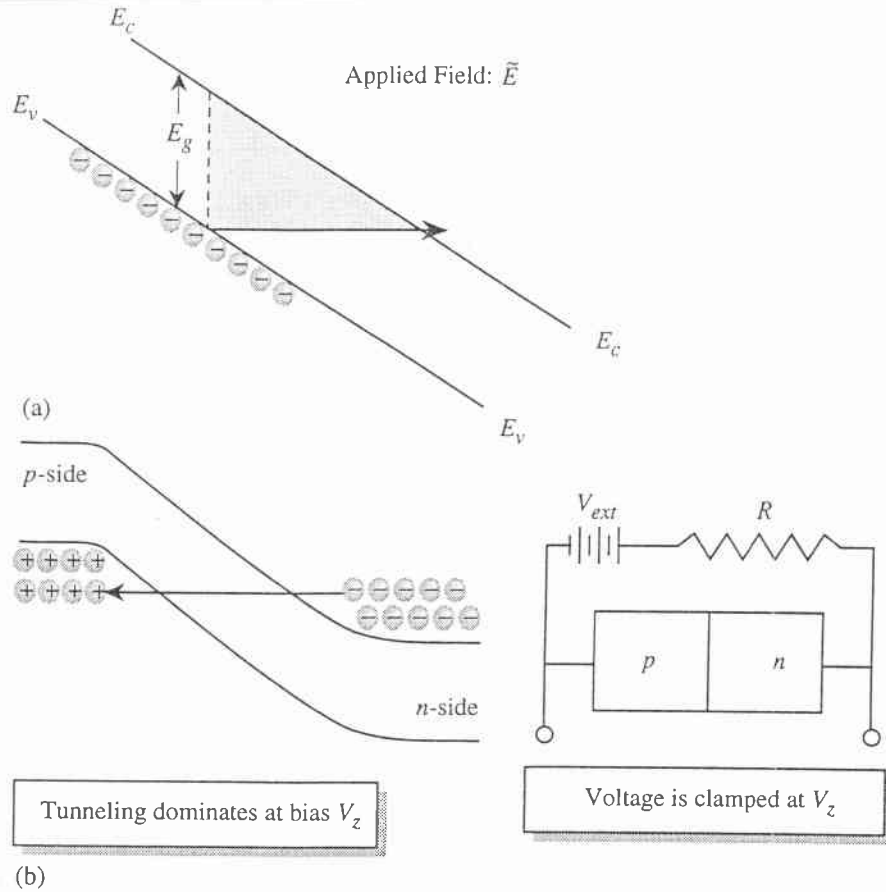


Figure 6.11: (a) Schematic of how band-to-band tunneling takes place. (b) Tunneling in a *p-n* diode across which a bias is applied. Also shown is the use of a reverse-biased *p-n* diode for a voltage-clamping circuit. The current saturates to a value determined by the external circuit resistor, while the output voltage is clamped at the diode breakdown voltage. The circuit is thus very useful as a voltage regulator.

bands in a semiconductor across which some bias is applied. Electrons from the valence band can tunnel across the forbidden bandgap and go into the conduction band. Similarly, electrons in the conduction band can tunnel into the valence band provided there are holes in the valence band. As shown in Fig. 6.11a, the electrons see a triangular barrier and the tunneling probability is

$$T = \exp\left(\frac{-4\sqrt{2m^*}E_g^{3/2}}{3e\hbar\tilde{E}}\right) \quad (6.18)$$

where \tilde{E} is the field across the semiconductor.

The band-to-band tunneling is exploited to make the Zener diode. When a *p-n* junction is reverse biased (i.e., a negative voltage is applied to the *p*-side

and a positive one to the n -side), a strong electric field is produced in the diode junction region, as shown in Fig. 6.11b. Once the reverse bias voltage reaches a certain value, V_z , the tunneling process becomes dominant. At this point, the diode resistance becomes negligible. The voltage across the diode is then clamped at V_z regardless of how high the external bias becomes. This voltage-clamping property of the Zener diode is very useful in many circuit applications.

The tunnel diode also exploits band-to-band tunneling, but couples it with clever energy band alignment to create negative differential resistance. The tunnel diode is designed from very heavily doped n and p sides. The high doping ensures a very large electric field in the junction so that band-to-band tunneling is possible at all biasing conditions.

The operation of the device is shown in Fig. 6.12. At a small forward bias, some of the electrons on the n -side can tunnel into the holes on the p -side. As the bias is increased, the band alignment is such that more and more of the electrons find holes to tunnel into and the current increases as shown. Beyond the point marked B, the empty states on the p -side move higher in energy with respect to the electron energies as the n -side. Eventually, at point C, there are no empty state (holes) available for electrons to tunnel into. This causes the current to decrease to a minimum value. Eventually the current increases because the electrons and holes are able to overcome the reduced barrier due to their thermal distribution.

The negative resistance of the tunnel diode is an important feature that allows one to use it in microwave applications (eg., radar detectors).

EXAMPLE 6.5 Calculate the band-to-band tunneling probability in InAs ($E_g = 0.4$ eV; $m^* = 0.02 m_0$) and GaAs ($E_g = 1.43$ eV; $m^* = 0.07 m_0$) under an applied field of 5×10^5 V/cm.

The exponent in the tunneling probability has the following value for InAs:

$$\frac{-4(2 \times 0.02 \times 9.1 \times 10^{-31} \text{ kg})^{1/2} (0.4 \times 1.6 \times 10^{-19} \text{ J})^{3/2}}{3(1.6 \times 10^{-19} \text{ C})(1.05 \times 10^{-34} \text{ J.s})(5 \times 10^7 \text{ V/m})} = -4.9032$$

This gives

$$T = 7.423 \times 10^{-3}$$

For GaAs we get

$$T = \exp(-62) = 1.18 \times 10^{-27}$$

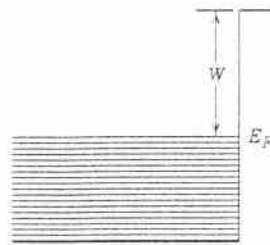
We see that while band tunneling can be responsible for breakdown in InAs, it is not the cause for breakdown in GaAs. For GaAs, the value of T can increase with higher fields, but there are other mechanisms that are responsible for breakdown.

Ohmic Contact

Current flow in semiconductor device, electrons or holes must be able to flow in and out of semiconductor

Cannot happen through a vacuum - semiconductor interface (or air)

↓
there is a large barrier (workfunction)

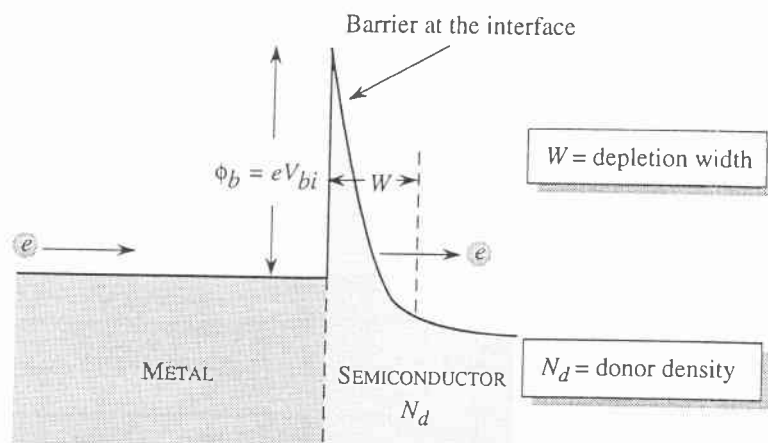


$W = \text{work function.}$

metal - vacuum interface

Metal - semiconductor junctions which have a linear I - V characteristic with very low resistivity

↓
ohmic contacts.



: Potential profile in an ohmic contact. The contact depends upon the tunneling of electrons with very small energies ($E \sim 0$) through the narrow triangular barrier.

Barrier height $\phi_b = e V_{bi}$
↳ Schottky barrier

height is determined by the nature of semiconductor surface and the metal

W = depletion width.

$$W = \left[\frac{2\epsilon V_{bi}}{eN_d} \right]^{1/2}$$

ϵ → relative dielectric constant

N_d → doping density in the semiconductor

The resistance can be reduced by using a low Schottky barrier height doping the semiconductor as heavily as possible.

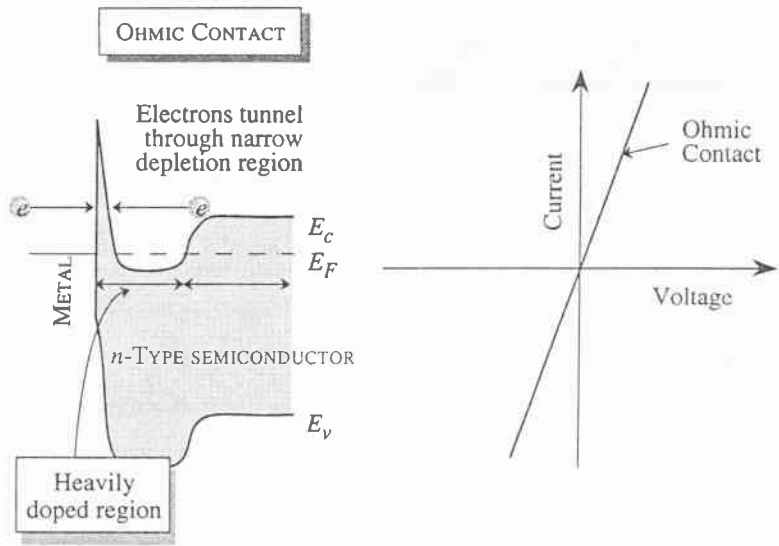


Figure 6.8: Band diagrams of metal - n^+ - n contact. The heavy doping reduces the depletion width to such an extent that the electrons can tunnel through the spiked barrier easily in either direction. This leads to a highly linear current-voltage relation.

Thus

$$\ln(r_c) \propto \frac{1}{\sqrt{N_d}} \quad (6.17)$$

The resistance can be reduced by using a low Schottky barrier height and doping the semiconductor as heavily as possible. The current-voltage relation of a good ohmic contact is highly linear, as shown in Fig. 6.8.

EXAMPLE 6.1 Assume that the potential profile of the barrier in the semiconductor side is described by an electric field \tilde{E} . Calculate the tunneling probability if $\tilde{E} = 10^8$ V/cm; $\phi_b = 0.5$ eV and the electron mass in the semiconductor is $0.1 m_0$. Note that if the tunneling probability approaches unity the electrons can go across the junction without "feeling" the barrier. This is a requirement of good ohmic contact.

The tunneling probability is given by (choosing the electron energy to be ~ 0)

$$T = \exp \left\{ \frac{-4(2m^*)^{1/2} \phi_b^{3/2}}{3e|\tilde{E}|\hbar} \right\}$$

$$(2m^*)^{1/2} = (2 \times 0.1 \times 0.091 \times 10^{-30})^{1/2} = 4.27 \times 10^{-16} (\text{kg})^{1/2}$$

$$\phi_b^{3/2} = (0.5 \times 1.6 \times 10^{-19})^{3/2} = 2.26 \times 10^{-29} (\text{J})^{3/2}$$

$$e = 1.6 \times 10^{-19} \text{ C}$$

$$\tilde{E} = 10^8 \text{ V/m}$$

This gives

$$T = \exp(-8.41) \sim 2.2 \times 10^{-4}$$

EXAMPLE 6.2 Consider a metal-Si interface on silicon doped at 10^{18} and 10^{21} cm^{-3} . The Schottky barrier height is 0.66 V. Calculate the tunneling probability for electrons with energies near the conduction band in the two doping cases. Use an effective mass of $0.34 m_0$ for electrons in the semiconductor. The relative dielectric constant of Si is 11.9.

Let us first calculate the depletion width corresponding to a Schottky barrier height of 0.66 V. The depletion width is

$$W(n = 10^{18} \text{ cm}^{-3}) = \left[\frac{2 \times (11.9 \times 8.84 \times 10^{-14} \text{ F/cm}) \times (0.66 \text{ V})}{(1.6 \times 10^{-19} \text{ C})(10^{18} \text{ cm}^{-3})} \right]^{1/2}$$

$$= 2.9 \times 10^{-6} \text{ cm} = 290 \text{ \AA}$$

$$W(n = 10^{21} \text{ cm}^{-3}) = \frac{W(n = 10^{18} \text{ cm}^{-3})}{\sqrt{1000}} = 9.17 \text{ \AA}$$

The electrons with energy just at the conduction bandedge will have to tunnel through an approximately triangular well. We can use the tunneling probability through a triangular well, using an average electric field in the depletion region

$$\tilde{E}(n = 10^{18} \text{ cm}^{-3}) = \frac{0.66 \text{ V}}{2.9 \times 10^{-6} \text{ cm}} = 2.3 \times 10^5 \text{ V/cm}$$

$$\tilde{E}(n = 10^{21} \text{ cm}^{-3}) = 7.2 \times 10^6 \text{ V/cm}$$

The tunneling probability is now

分類:

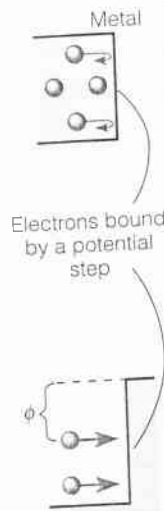
編號: 8-38

總號:

Field Emission.

To remove an electron from a given kind of metal requires a certain minimum amount of energy
 \Rightarrow the work function ϕ

\downarrow
in effect, the metal's electrons reside in a potential well, the result of their attraction to the positive ions



Due to the random thermal distribution of speeds, at a given temperature a small fraction of the electrons have sufficient kinetic energy to escape the metal.

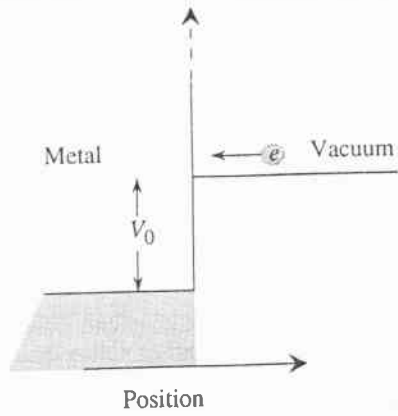
Heating a metal filament to enhance this effect
 \Rightarrow thermionic emission

\downarrow
used a source of electron beams

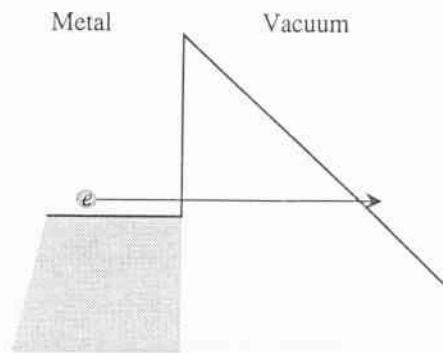
\downarrow
such as those in the conventional (elongated) cathode ray tubes used in TV and computer monitors.

Positive electrode modifies the potential energy function "seen" by the electrons
 \Rightarrow tunneling \Rightarrow field emission (cold)

Field Emission Devices

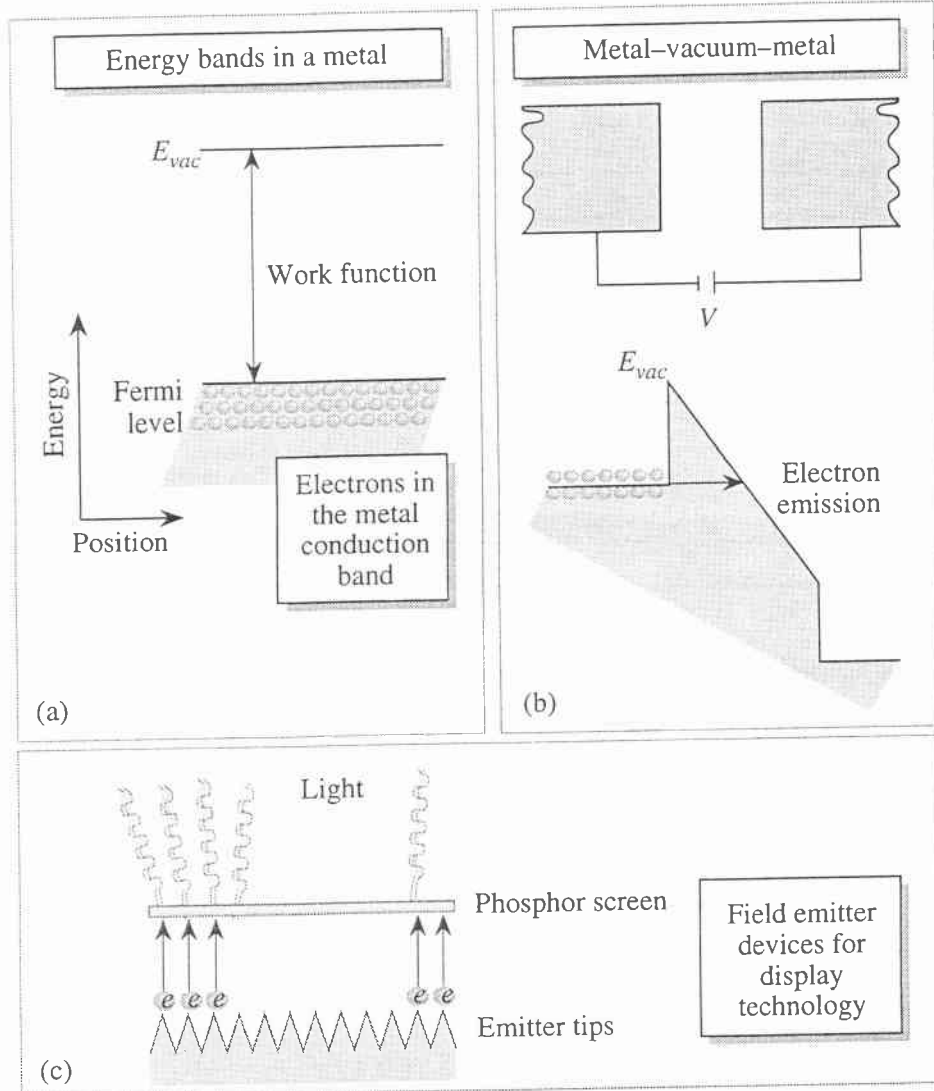
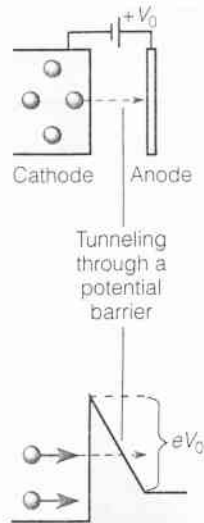


Potential profile of a metal-vacuum interface region.



Potential profile of a metal-vacuum interface with a field across the junction.

✓



(a) Schematic of the electronic energies in a solid-state material. (b) Metal-vacuum-metal junction under applied field. (c) Schematic of a display device based on field emission tips.

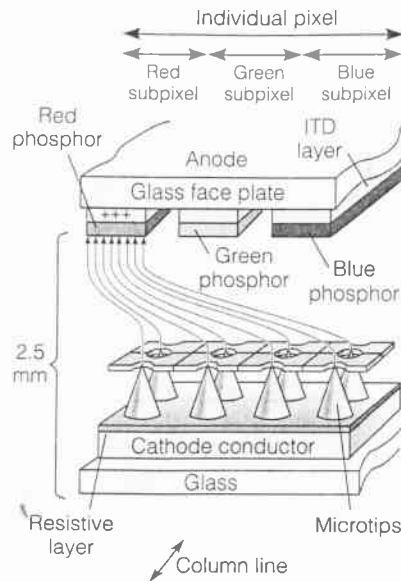
Flat panel display

The metal (or semiconductor) emitters are formed into sharp tips to enhance the field produced by the applied potential

The voltage across tips is controlled by a driver circuitry.

The phosphor screen is separated from the tips by a very small gap (submicron) \Rightarrow entire system is "paper-thin."

Each pixel (picture element) is "illuminated" by its own set of tips \Rightarrow thin, low-power-consuming display system.

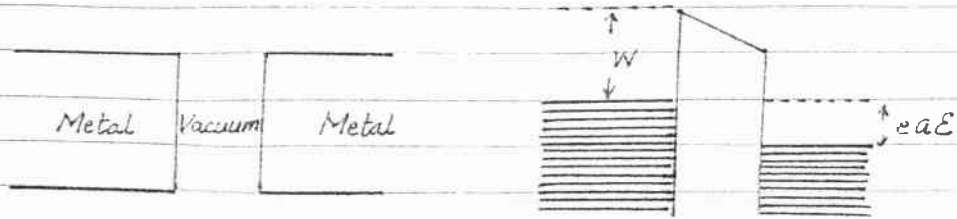


(a) (b)
Figure 5.12 Electrons in a metal (a) behave as though in a finite well. An electric field (b) alters the "wall," so that tunneling may occur.

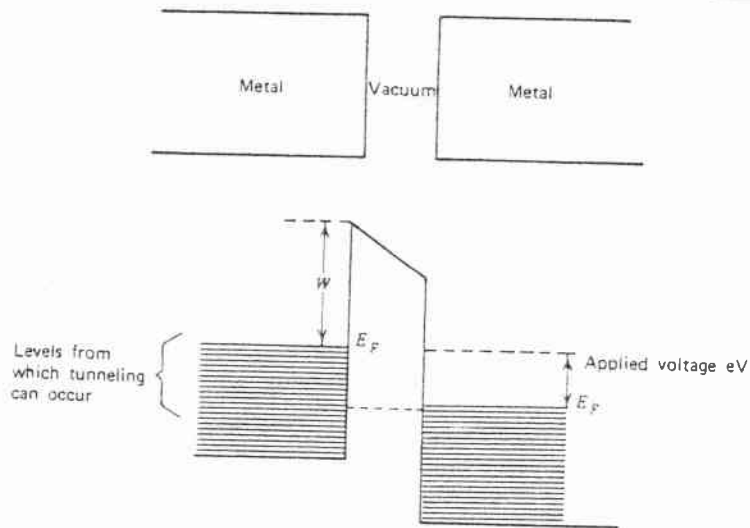
Figure 5.13 One pixel of a field emission display. Applying a positive bias turns on any of the three different colors of subpixel.

Field emission is now being tried as the source of illumination in a new kind of flat-screen display, the aptly named Field Emission Display (FED) shown in Figure 5.13. Its potential advantages over the liquid crystal displays commonly used in laptop computers include wider viewing angle and quicker response.

Tunneling between two metals seperated by vacuum



Ni - NiO - Pb with gap of 50 \AA



Energy diagram for tunneling between two metals separated by vacuum. Tunneling between metals is possible only when there are empty states on the right. Such empty states are created when eV is applied to lower the Fermi level on the right.

$$|T|^2 \sim e^{-2\sqrt{\frac{2mW}{\hbar^2}} a}$$

Metal - superconductor tunneling

Gap in energy level

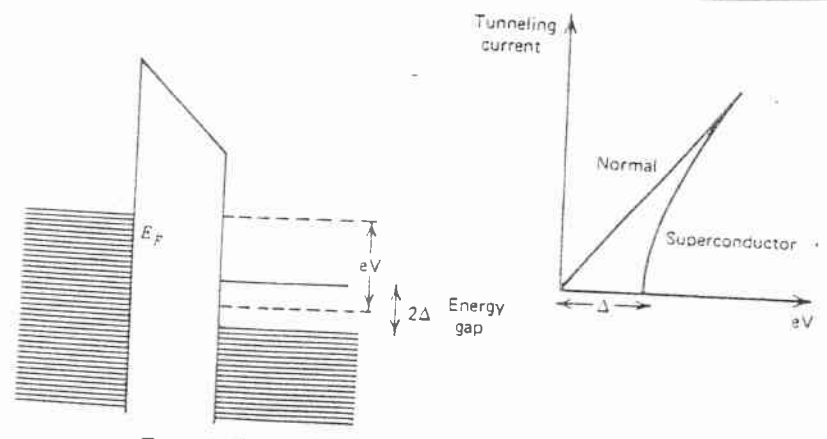
$$E_F - \Delta \quad \text{and} \quad E_F + \Delta$$

$$\Delta \sim 10^{-3} \text{ eV} \quad E_F \sim 10 \text{ eV}$$

Level density just below and just above the gap is very large
 $eV \leq \Delta$ there will be no tunneling

Superconductor - oxide - superconductor

"Photon-assisted" tunneling \rightarrow photon energy cause breakup of the electron pairs



Energy diagram for tunneling from metal to superconductor. In contrast to the metal-metal tunneling shown in Figure 5-6, no tunneling is allowed into the energy gap. This affects the current-voltage characteristic as shown.

分類:

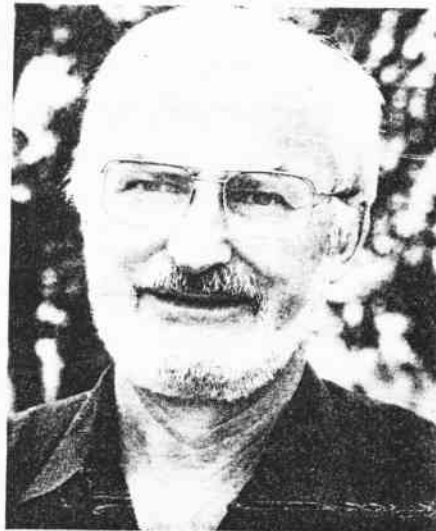
編號: 8-42

總號:

Scanning Tunneling Microscope (STM)



BINNIG



ROHRER

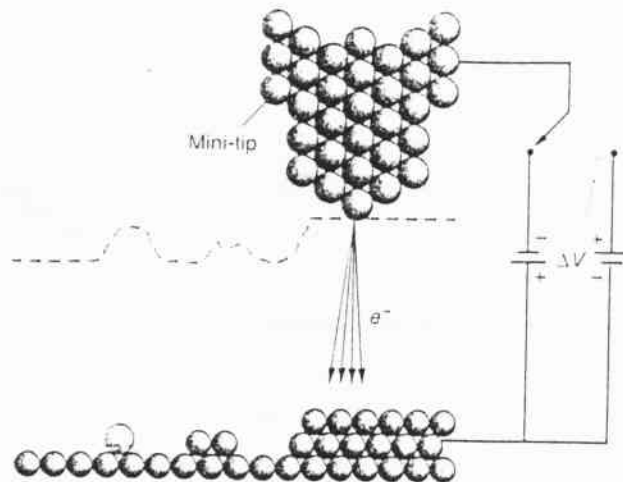
Study surfaces on an atomic scale of size.

STM was invented in 1981 by Gert Binnig and Heinrich Rohrer, who shared the 1986 Nobel Prize in physics with Ernst Ruska, the inventor of the electron microscopy.

The extreme sensitivity of tunneling probability to width in a wide barrier is the root of the utility of the STM

A narrow gap between a conducting specimen and the tip of a tin probe acts a potential barrier to electrons bound in the specimen.

A small bias voltage applied between the probe and the specimen causes the electrons to tunnel through the barrier sepering the two surfaces if the s are close enough together.

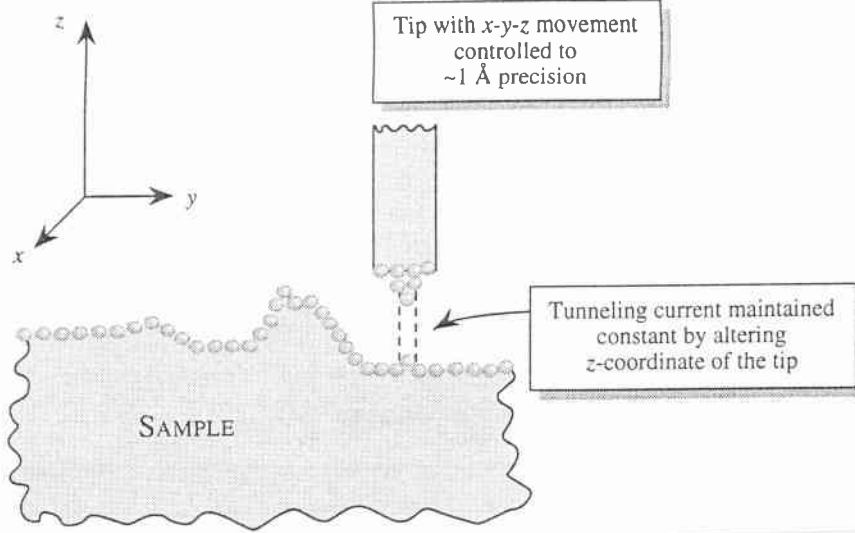


The tunneling current is extremely sensitive to the size of the gap.. i.e., the width of the barrier, between the probe and specimen

A change of only 0.5 nm (about the diameter of one atom) in the width of the barrier can cause the tunneling current change by as much as a factor of 10^4 .

As the probe scans the specimen, a constant tunneling current is maintained by a piezoelectric feedback system that keeps the gap constant.

⇒ the surface of the specimen can be mapped out by the vertical motion of the probe.



✓

Key:

Tip with $x-y-z$ movement controlled to $\sim 1 \text{ \AA}$ precision.

Early work of Binnig and Rohrer.

- a vacuum environment
- a very elaborate system for the suppression of vibration.

relative position of
probe and specimen
remain fixed.

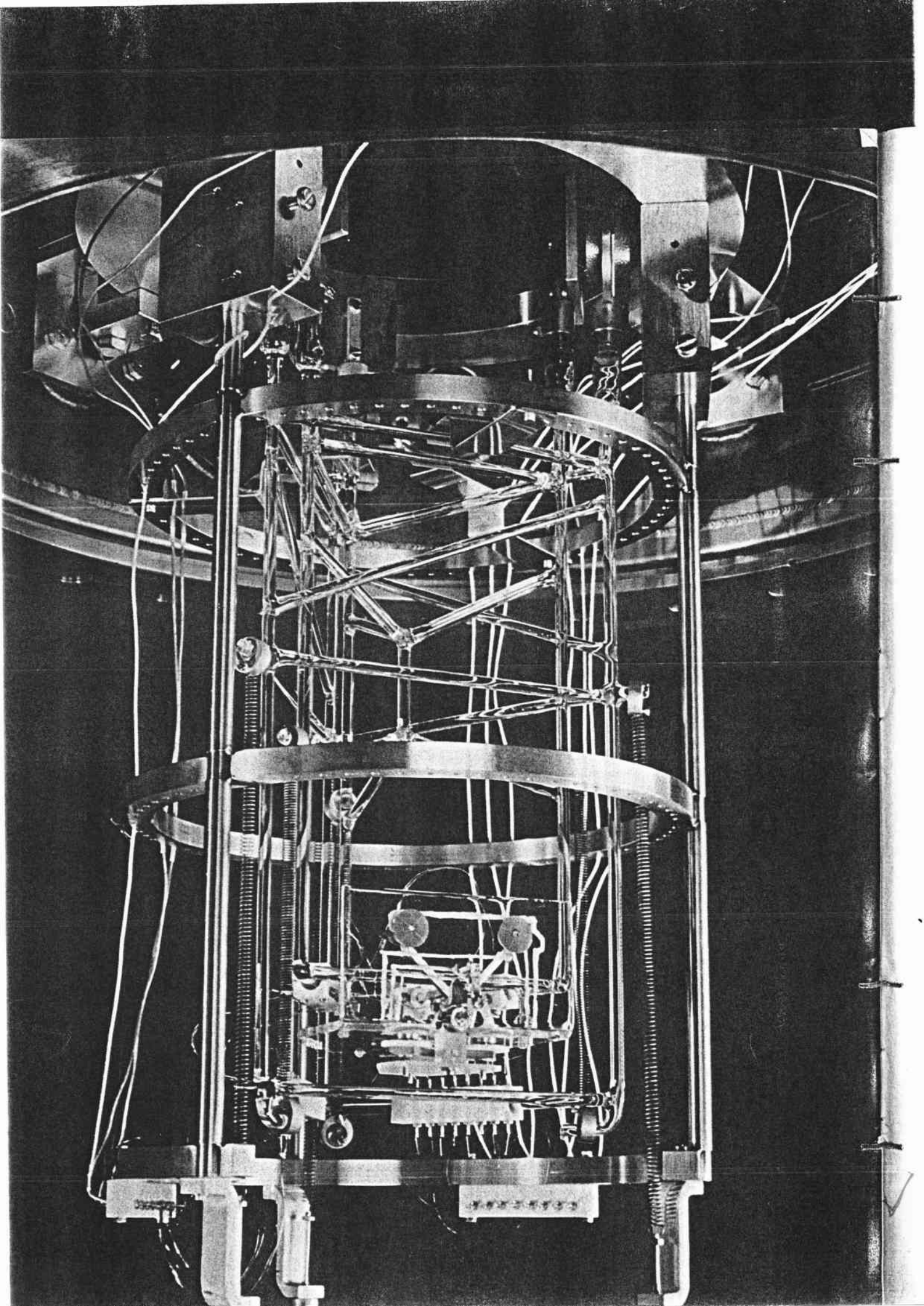
SCANNING TUNNELING MICROSCOPE has two stages, suspended from springs, that nestle within a cylindrical stainless-steel frame. The innermost stage contains the microscope mechanism. To achieve high-resolution images of surface structures the microscope must be shielded from even such small vibrations as those caused by footsteps and sound. The copper plates (attached to the bottom of the stainless-steel frame) and the magnets (attached to the bottom of the inner and outer stages) damp vibrations. Any disturbance causes the copper plates to move up and down in the field generated by the magnets. The movement induces eddy currents in the plates. The interaction of the eddy currents with the magnetic field retards the motion of the plates and hence the motion of the stages. For work required in a vacuum a steel cover is placed over the outer frame of the microscope.

The original apparatus was magnetically levitated on a superconducting lead bowl resting on a heavy stone slab atop a bed of inflated rubber tires

Two stages, or sections, suspended from springs, nestle within the stainless-steel cylindrical frame of the microscope and protect the tunneling gap from vibration. Both stages, triangular in cross section, are made of glass rods. The second stage slips into the first stage, from which it is suspended by three springs. The first stage in turn is suspended from the outer frame, also by three springs. The second stage carries the heart of the microscope: it contains both the sample and the scanning needle.

When the entire microscope sits in a vacuum, air resistance is minimal and the first and second stages could, if they were disturbed, bounce up and down almost indefinitely. To stop this motion we rely on the phenomenon of eddy-current damping. We let copper plates attached to the bottom of the first and second stages slide between magnets attached to the outer frame. As each plate slides up and down, the magnetic field causes the conducting electrons of the copper to move around, inducing a so-called eddy current. The reaction between the eddy current and the magnetic field retards

the motion of the plate and thereby protects the microscope from even the smallest vibrations.



• Piezoelectric drive

The thickness of certain ceramics changes when a voltage is applied across them

↓
piezoelectricity

Once the gross vibrations have been stopped the sample can be positioned. This is done with a specially developed drive that carries the sample across a horizontal metal plate on the second stage. The body of the drive consists of a slab of piezoelectric material that expands or contracts when voltage is applied. The drive has three metallic feet, arranged in triangular fashion, that are coated with a thin layer of insulating material. They can be clamped to the metal plate by establishing a voltage between them and the metal plate.

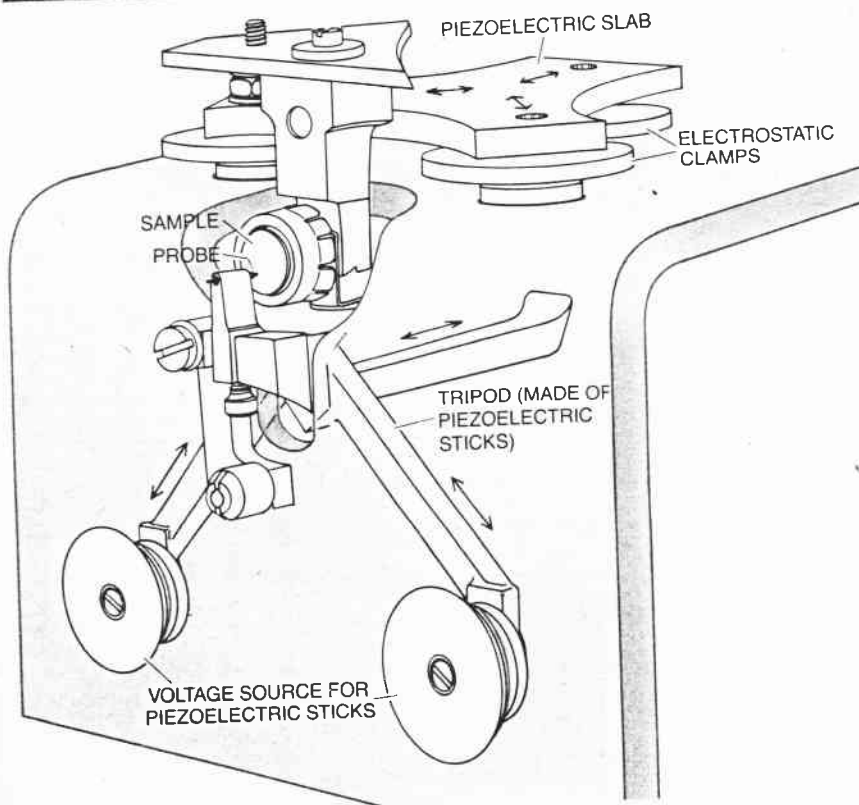
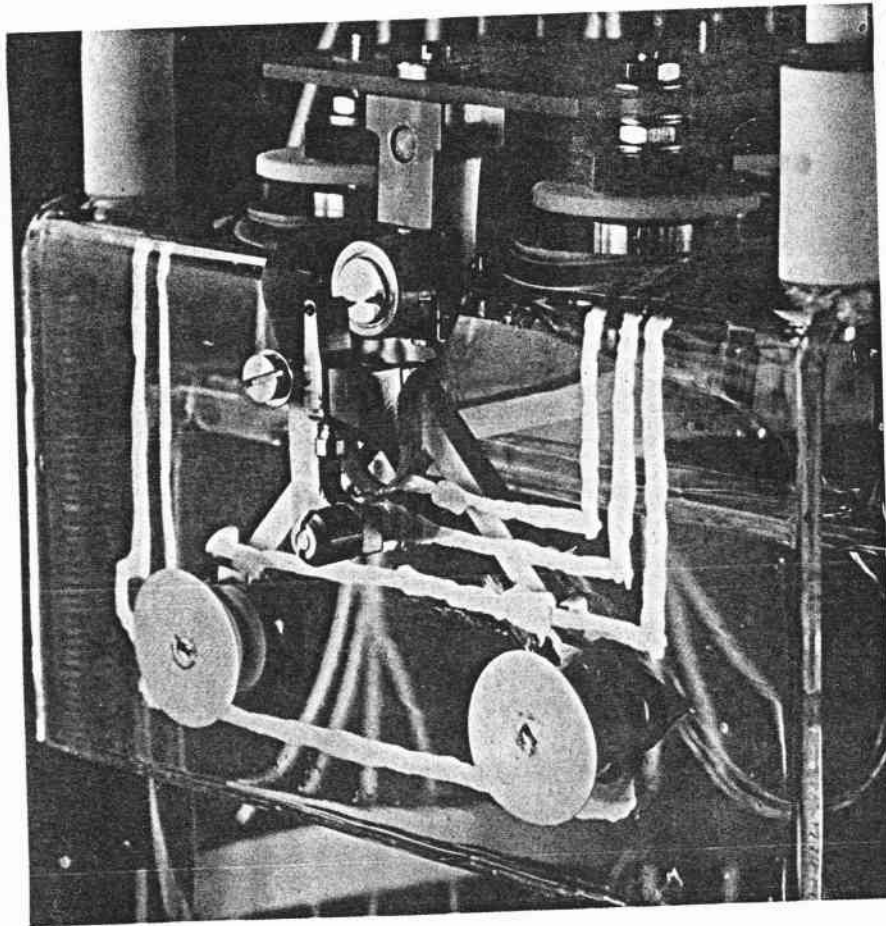
We move the drive in the following manner. Suppose, for instance, we clamp only one foot and apply a voltage to the piezoelectric body so that it contracts. The other two feet will move slightly. We then clamp those two feet, release the third foot and remove the applied voltage so that the

body expands back to its original size. The drive has just moved one step. The step width can be varied between 100 and 1,000 angstroms. Since the drive can rotate about each of its feet, it can walk along the plate in any desired direction.

When the drive has carried the sample to the wanted tunneling position, we begin scanning the surface of the sample. We use a rigid tripod made of three piezoelectric sticks to move the tip of the scanning needle. When we apply a voltage to expand or contract one of the sticks, the other two bend slightly. Consequently the tip moves in a straight line over distances as great as 10,000 angstroms. Furthermore, this motion is quite sensitive to the magnitude of the applied voltage: a voltage on the order of .1 volt results in a motion of 1.0 angstrom. The precision of the tripod's drive is so good that at present only vibration limits the vertical resolution of the sample's surface. This resolution at present is in the

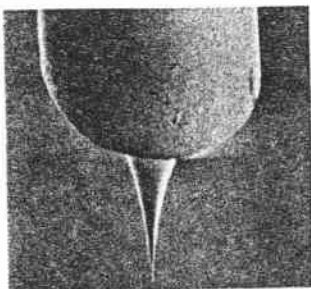
range of approximately a few hundredths of an angstrom.

分類:	
編號:	8-48
總號:	



MICROSCOPE DEVICE contains a sample and a scanning needle. Piezoelectric materials, which expand or contract when voltage is applied to them, enable the device to resolve features that are only about a hundredth the size of an atom. A piezoelectric drive positions the sample on a horizontal metal plate. A piezoelectric tripod then sweeps the scanning needle over the surface of the sample, simultaneously achieving high stability and precision.

Sharpness of the tip of the probe.



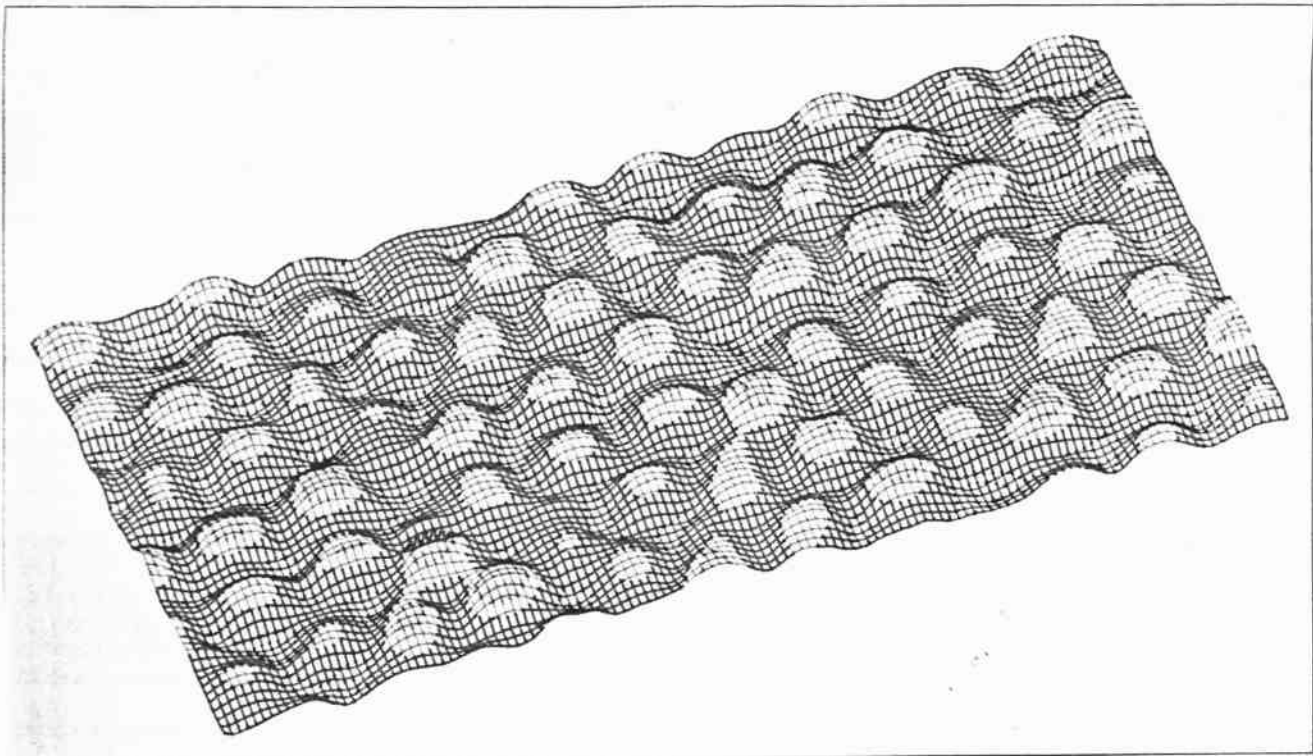
The tungsten probe of a scanning tunneling microscope.

The lateral resolution of the surface is limited by the sharpness of the tip. In this instance nature has been kind to the vacuum tunneler. It is relatively easy to make a sharp tip that yields a lateral resolution of about six to 12 angstroms: one simply grinds the end of a needle, which is usually made of tungsten.

To achieve a lateral resolution of two angstroms, however, the needle must have a single atom sitting securely on top of its tip. Such an atom usually comes from the sample itself. It is dislodged by high electric fields that are caused by applying a voltage difference of from two to 10 volts between the sample and the tip. Since luck plays a large role in the final stage, we are trying to sharpen the tip by bombarding it with a high-energy beam of ions. This causes the atoms on the surface to sputter away in a highly controlled manner.

The probe turned out to be even more local than their fondest hopes. Employing stylus tips with curvature radii on the order of a thousand angstroms, Binnig and Rohrer had expected a horizontal resolution of about 50 Å—not nearly good enough to resolve individual atoms. But when they started scanning, they certainly did see atoms. “We had thought this kind of resolution would require a big effort,” Binnig told us. “But we got atomic scale resolution more or less as a gift.”

The gift comes from the fact that these 1000-Å tips are inevitably rough on a smaller scale, with accidental protuberances serving as tips only a few atoms wide. With these protuberances doing the probing, the scanning instruments achieved a horizontal resolution of about 4 Å very early on. Now it's down to 1 Å. In recent months the IBM Zurich group has been replacing these fortuitous probing tips with monatomic tips carefully created by field-ion microscopy techniques devised by Hans-Werner Fink. The end of the tip is the world's smallest manmade pyramid: three layers consisting respectively of seven, three and finally one single atom. Putting the last single atom in place is “a miracle,” says Rohrer.



SURFACE OF SILICON as disclosed by the scanning tunneling microscope consists of a pattern of diamond-shaped unit cells. Each cell measures 27 angstrom units (one angstrom unit is one ten-billionth of a meter) on a side. The cell is called the 7-by-7 because each side measures seven atomic units. Each 7-by-7 contains 12

bumps that are arranged in two groups of six. The bumps, which have never before been resolved, apparently correspond to the surfaces of individual atoms. They stand as much as 1.3 angstroms above the rest of the surface. The image was formed by applying a voltage so that electrons flowed from the needle tip to the surface.

The STM must be ranked as one of the most indispensable tools in modern technology. Its uses are already legion—studying geometry and composition of a seeming endless list of surfaces; locating important biological molecular groups, such as the fundamental building blocks of DNA; mapping microscopic “vortices” in certain kinds of superconductors; nudging atoms from one point on a surface to another—and they continue to expand.

Actually, the result of an STM scan is not a true topographical map of surface height but a contour map of constant electron density on the surface. This means that atoms of different elements appear differently, which greatly increases the value of the STM as a research tool.

Although many biological materials conduct electricity, they do so by the flow of ions rather than of electrons and so cannot be studied with STMs. A more recent development, the atomic force microscope (AFM) can be used on any surface, although with somewhat less resolution than an STM. In an AFM, the sharp tip of a fractured diamond presses gently against the atoms on a surface. A spring keeps the pressure of the tip constant, and a record is made of the deflections of the tip as it moves across the surface. The result is a map showing contours of constant repulsive force between the electrons of the probe and the electrons of the surface atoms. Even relatively soft biological materials can be examined with an AFM and changes in them monitored. For example, the linking together of molecules of the blood protein fibrin, which occurs when blood clots, has been watched with an AFM.

Articles by Roger A. Freedman and Paul K. Hansma
Binnig and Rohrer are given in Appendix E ✓

α Decay (Alpha)

Certain heavy nuclei are observed to decay by emission of an α particle (made of two protons and two neutrons) with a kinetic energy of a few MeV

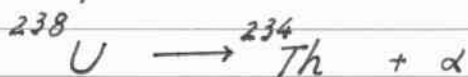
In an α decay, the daughter nucleus has two fewer protons and two fewer neutrons than the parent nucleus

The kinetic energy of the α -particles are measured to be in a relatively small range from 4 to 9 MeV

The lifetime of the α -decay process vary dramatically from 10^{-7} sec to 10^{10} years.

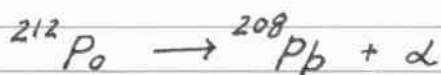
(The half-life is defined as the time required for one half the nuclei in a sample to decay)

For example



$$E_k \text{ of } \alpha \text{ particle} = 4.18 \text{ MeV}$$

$$t_{1/2} = 4.5 \times 10^9 \text{ years}$$



$$E_k = 8.78 \text{ MeV}$$

$$t_{1/2} = 0.3 \mu\text{sec.}$$

"Why do similar decays yield α -particle energies of the same order of magnitude while the lifetimes differ by more than 23 order of magnitude?"

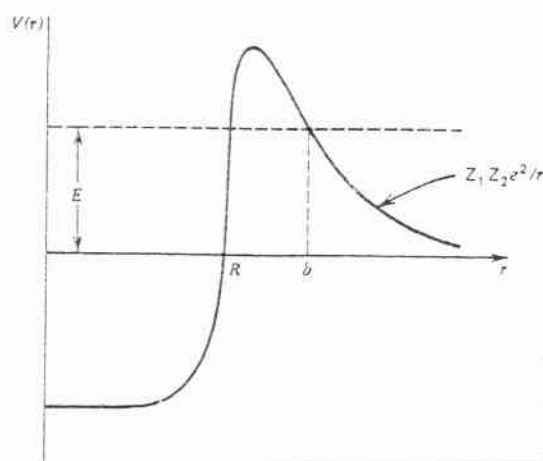
The answer is to be found in quantum tunneling.

↓
first proposed by
Gamow
in 1928



George Gamow, 1904–1968, whose work in 1928 showed that alpha particles can behave as waves. In so doing, he solved the long-standing puzzle about the half-life of alpha decay. This demonstrated for the first time that quantum mechanics applies to nuclei. (AIP Emilio Segrè Visual Archives.)

$V(r)$ between the daughter nucleus and the α particle.



We approximate $V(r)$ as an attractive "square well" (short-range) due to the strong interaction plus a repulsive Coulomb component outside the nucleus.

$$|T|^2 \sim e^{-G}$$

with

$$G \cong 2 \int_R^b \left(\frac{2m}{\hbar^2} \right)^{\frac{1}{2}} \left(\frac{Z_1 Z_2 e^2}{r} - E \right)^{\frac{1}{2}} dr$$

($m = \text{mass of the } \alpha \text{ particle}$)

b is determined by $E = \frac{Z_1 Z_2 e^2}{b} \sim \frac{1}{2} m v^2$

$$G \sim 2 \int_R^b \left(\frac{2m}{\hbar^2} \right)^{\frac{1}{2}} Z_1 Z_2 e^2 \left(\frac{1}{r} - \frac{1}{b} \right) dr$$

$Z_1 = \text{charge of the daughter nucleus}$

$$\int_R^b dr \left(\frac{1}{r} - \frac{1}{b} \right)^{\frac{1}{2}} = \sqrt{b} \left[\cos^{-1} \left(\frac{R}{b} \right)^{\frac{1}{2}} - \left(\frac{R}{b} - \frac{R^2}{b^2} \right)^{\frac{1}{2}} \right]$$

For $b \gg R$ (valid for low energy α)

$$\Rightarrow G \sim \frac{2\pi Z_1 Z_2 e^2}{\hbar v} \sim \frac{Z_1}{\sqrt{E}}$$

$$t_{1/2} \sim \frac{2R}{v} e^G *$$

$$\ln t_{1/2} \sim C_2 + C_1 \frac{Z_1}{\sqrt{E}}$$

↓
very rough result

Comparison with experimental result are shown in the next graph.

分類:

編號: 8-53a

總號:

$$\text{number of decays / time} = \frac{\text{number of times \& strikes}}{\text{time}}$$

\times transmission probability

$$= \frac{\text{one strike}}{\text{time to cross diameter}} \times \text{transmission probability}$$

$$= \frac{1}{\text{diameter of nucleus / speed}} \times \text{transmission probability}$$

$$= \frac{v}{2R_{\text{nucl.}}} \times \text{transmission} = \lambda$$

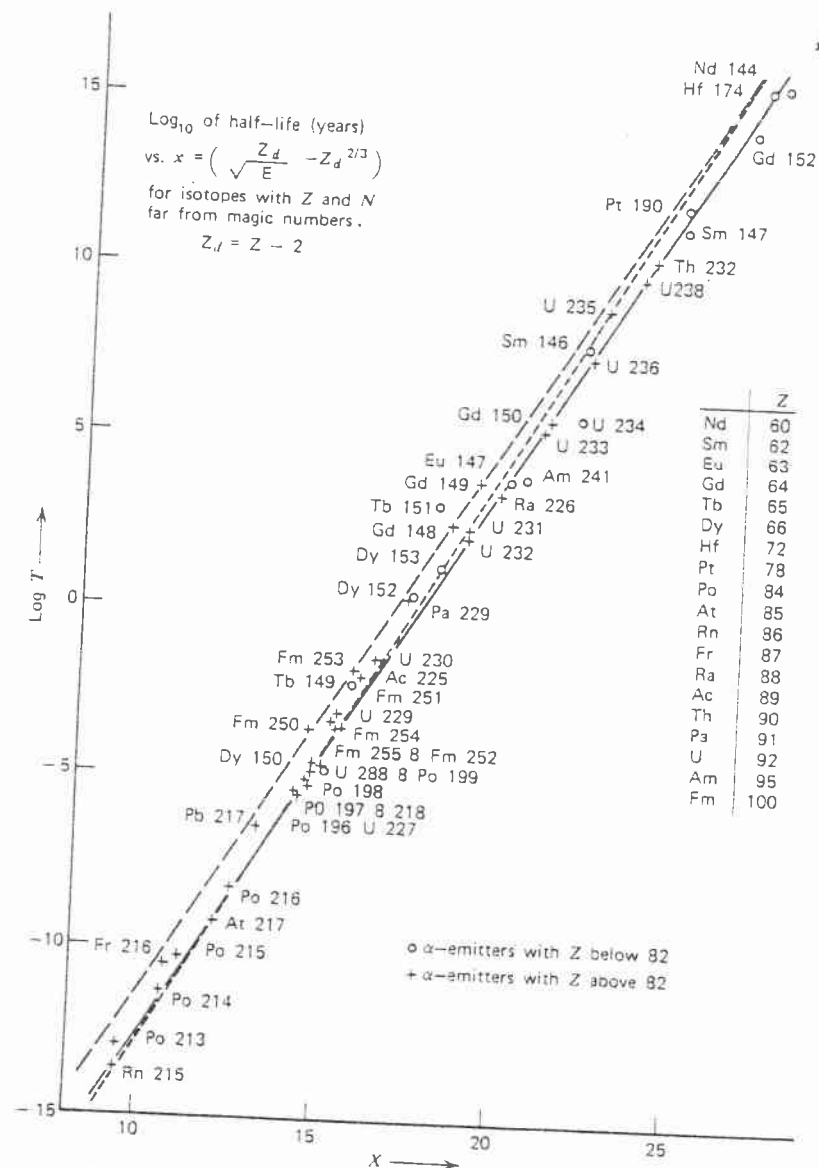
$$\frac{dN}{dt} = -\lambda$$

$$N = N_0 e^{-\lambda t}$$

$$\frac{1}{2} = e^{-\lambda t_{1/2}}$$

$$\ln 2 = \lambda t_{1/2}$$

$$t_{1/2} = \frac{\ln 2}{\lambda}$$



Plot of $\log_{10} 1/\tau$ versus $C_2 - C_1 Z_1 / \sqrt{E}$ with $C_1 = 1.61$ and a slowly varying $C_2 = 28.9 + 1.6Z_1^{2/3}$. (From E. K. Hyde, I. Perlman, and G. T. Seaborg, *The Nuclear Properties of the Heavy Elements*, Vol. I, Prentice-Hall, Englewood Cliffs, N.J. (1964), reprinted by permission.)

分類:

編號: 8-55

總號:

Remarks:

· Even with such crude model, the agreement is impressive.

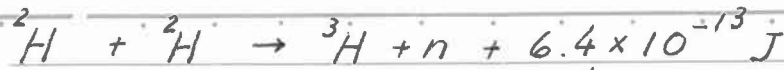
· For higher α energies, G depends on R .

· The idea was proposed in 1928

↓
first application of quantum mechanics
to nuclear physics.

For a more detailed discussion, see Appendix F

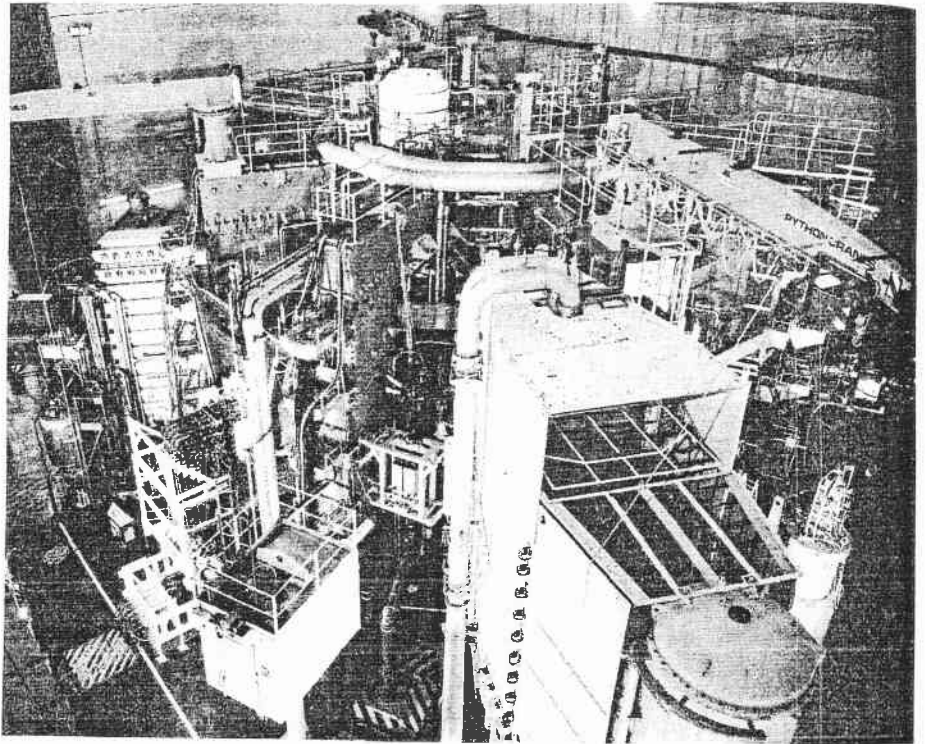
Nuclear fusion



↓
release of energy

↓
solution of the energy problem

This process is inhibited from happening because of the Coulomb repulsion between the two deuterons. The reaction rate can become useful only by a combination of two effects: the fact that the Coulomb barrier can be tunneled through and by raising the gas of (ionized) deuterons to a



The Tokamak fusion reactor is designed to confine highly energetic charged particles by strong and cleverly arranged magnetic fields. This photograph is of the JET Tokamak and its auxiliary systems.

higher temperature, the number of deuterons with higher energy grows (See Chapter 12). More energetic deuterons are closer to the top of the barrier, and there the barrier is less wide than for low E . Thus it is more likely that deuterons of higher energy will tunnel through the barrier separating them. Detailed calculations show that it is necessary to achieve temperatures on the order of 10^7 K to have a practical reaction rate. In a hydrogen bomb such temperatures are achieved by means of compression initiated by an atomic bomb. To get to these temperatures in an unexplosive manner and to confine such a hot gas for a time long enough to extract the generated energy are the two great challenges facing this field* (• Fig. 8-12). While much progress has been made over the last 40 years of research in this field, no immediate breakthrough is in sight.

TUNNELING THROUGH MULTIPLE BARRIERS: RESONANT TUNNELING

In the previous subsection we examined tunneling of a particle through a single barrier. As seen in Fig. 6.4b, when $E < V_0$, the tunneling probability monotonically increases as either E increases or the barrier thickness shrinks. There is no interesting resonant feature in the tunneling probability. If we examine the tunneling of particles through a potential region made up of not one single barrier, but two (or more) barriers as shown in Fig. 6.14, we find that the transmission or tunneling coefficient has resonant features.

A typical resonant tunneling structure has a form shown in Fig. 6.14. It consists of regions A and B where the particle is "free," enclosing a series of potential barriers and wells. An important resonant tunneling structure is the double-barrier resonant tunneling structure, which has the form shown in Fig. 6.14b. This structure is used for many important device applications. As shown in Fig. 6.14b, the quantum well enclosed by the two barriers has "quasi-bound" levels. If the barriers were infinitely thick, these levels would simply be the bound states in a quantum well, as discussed in Chapter 4. However, because of the finite barrier thickness, the quasi-bound states have wavefunctions that "leak" out of the well region, but the wavefunctions are primarily confined to the well region. When the energy of a particle (say, approaching from region A) approaches one of these quasi-bound energies, the transmission coefficient approaches unity.

The general problem of the resonant tunneling structure requires numerical computation, but if we assume that the structure is made up of a series of regions over which the potential energy is constant, it is possible to get analytical results. The approach is quite similar to the one we used in the last subsection—one writes

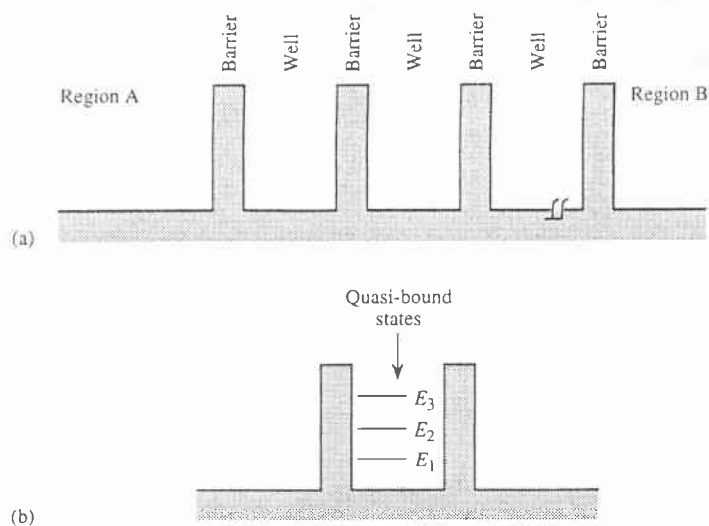


Figure 6.14: (a) A general potential profile which will show resonant tunneling behavior. (b) A double-barrier resonant tunneling structure. In the well formed between the two barriers, one has quasi-bound states with energies E_1, E_2, E_3, \dots . As the particle energy approaches these energies, the transmission coefficient approaches unity.

out the general solutions for the wavefunction in each region, matches boundary conditions, eliminates the coefficients involving the wavefunction of the intermediate regions, and then obtains the transmission and reflection coefficients.

In optics, we know that if light passes through multiple media, interference effects allow transmission peaks at certain frequencies. A similar effect occurs when particles impinge on more than one barrier. An interesting barrier is the double barrier structure shown in Fig. 6.15, which can be fabricated from two semiconductors. As shown in Fig. 6.15, the conduction band profile of such a structure produces a quantum well of size W enclosed by two thin barriers of thickness a and barrier height V_0 .

We may think of the quantum well formed by the double-barrier structure as having quasi-bound or resonant states at energy E_1, E_2, E_3 , etc., as shown in Fig. 6.15. If the barriers were very thick the electrons in the levels E_1, E_2, E_3 would not be able to "leak out" of the well. However, since the barriers have a finite thickness, the electron wavefunctions leak out through the barrier. Now consider an electron with energy E impinging on the double-barrier structure (resonant tunneling structure) as shown from the left. If the energy of the electron aligns with the well energies E_1, E_2, E_3 , etc., the electron is able to tunnel through the structure with unit probability. Otherwise, the tunneling probability is very small. This leads to sharp structures or resonances in the transmission probability versus electron energy curves, as shown in Fig. 6.15.

The tunneling probability for the double-barrier structure is given by an approach similar to the one used in Section 6.3 for a single-barrier. However, in

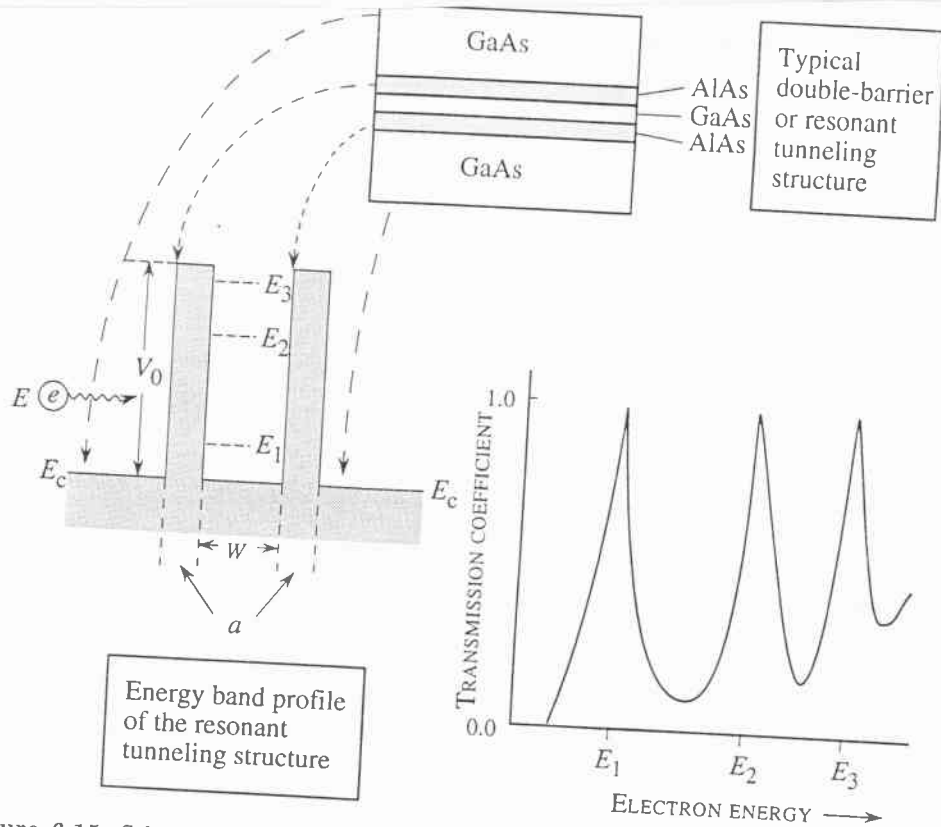


Figure 6.15: Schematic of a typical double barrier resonant tunneling structure. The energies E_1, E_2, E_3 , etc. represent the energies in the well of width W . The transmission coefficient goes to unity when the electron energy coincides with these resonant energies.

this case, the boundary conditions have to be matched at both the barriers. The detailed problem is straightforward, but involves tedious algebra. We will simply give the solution here. We first reexamine the single-barrier results.

The tunneling probability through a single barrier of height V_0 and width a is given by

$$T_{1B} = \frac{4E(V_0 - E)}{V_0^2 \sinh^2 \gamma a + 4E(V_0 - E)} \quad (6.30)$$

with

$$\gamma = \frac{1}{\hbar} \sqrt{2m(V_0 - E)}$$

which is the result obtained in Section 6.3.1.

Also, as in Section 6.3.1, we have, for the reflection amplitude from the first barrier,

$$r_{1B} = \frac{(k_1^2 + \gamma^2)(1 - e^{-2\gamma a})}{(k_1 + i\gamma)^2 - (k_1 - i\gamma)^2 e^{-2\gamma a}}$$

$$= \frac{(k_1^2 + \gamma^2) \sinh \gamma a}{(k_1^2 - \gamma^2) \sinh \gamma a + i2k_1\gamma \cosh \gamma a}$$

with a reflection probability

$$R_{1B} = |r_{1B}|^2 = \frac{V_0^2 \sinh^2 \gamma a}{V_0^2 \sinh^2 \gamma a + 4E(V_0 - E)} \quad (6.31)$$

where

$$k_1 = \sqrt{\frac{2mE}{\hbar^2}}$$

We may define (as in optics) the phase change θ produced in the reflected wave due to the reflection from a single barrier through the relation

$$r_{1B}^2 = R_{1B} e^{-2i\theta} \quad (6.32)$$

The angle θ is given by

$$\tan \theta = \frac{2k_1\gamma \cosh \gamma a}{(k_1^2 - \gamma^2) \sinh \gamma a} \quad (6.33)$$

These results have been repeated here, since the transmission probability through the double-barrier structure is expressed in terms of R_{1B} , T_{1B} and θ , given above.

For the double-barrier structure shown in Fig. 6.15, the transmission probability has sharp resonances as a function of the particle energy. In the case of a symmetric barrier, we get the following relation:

$$T_{2B} = \left[1 + \frac{4R_{1B}}{T_{1B}^2} \sin^2 (k_1 W - \theta) \right]^{-1} \quad (6.34)$$

where R_{1B} and T_{1B} are the single-barrier reflection and tunneling probabilities, and θ is the angle defined in Eqns. 6.32 and 6.33. From the form of Eqn. 6.34, we can see that the transmission probability becomes unity at certain well-defined particle energies. Away from these *resonant* energies, the transmission coefficient can become very small. Thus the transmission probability has very sharp features.

6.5.1 Application Example: Resonant Tunneling Diode

Semiconductor diodes incorporating the double-barrier resonant structure are known as *resonant tunneling diodes*. Resonant tunneling devices have potential for very-high-speed applications and are therefore being studied in great detail. The operation of a resonant tunneling structure is understood conceptually by examining Fig. 6.16a. For small applied voltages (case A in Fig. 6.16a) the tunneling probability of electrons with energies near the Fermi level energy is very small and, as a result, very little current flows through the structure. At point B, when the Fermi energy lines up with the quasi-bound state, a maximum amount of current flows through the structure, since the tunneling probability reaches unity. Further increasing the bias results in the energy band profile (point C), where the current through the structure decreases with increasing bias. Applying a larger bias results in a strong *thermionic emission* and thus, the current increases substantially, as shown at point D

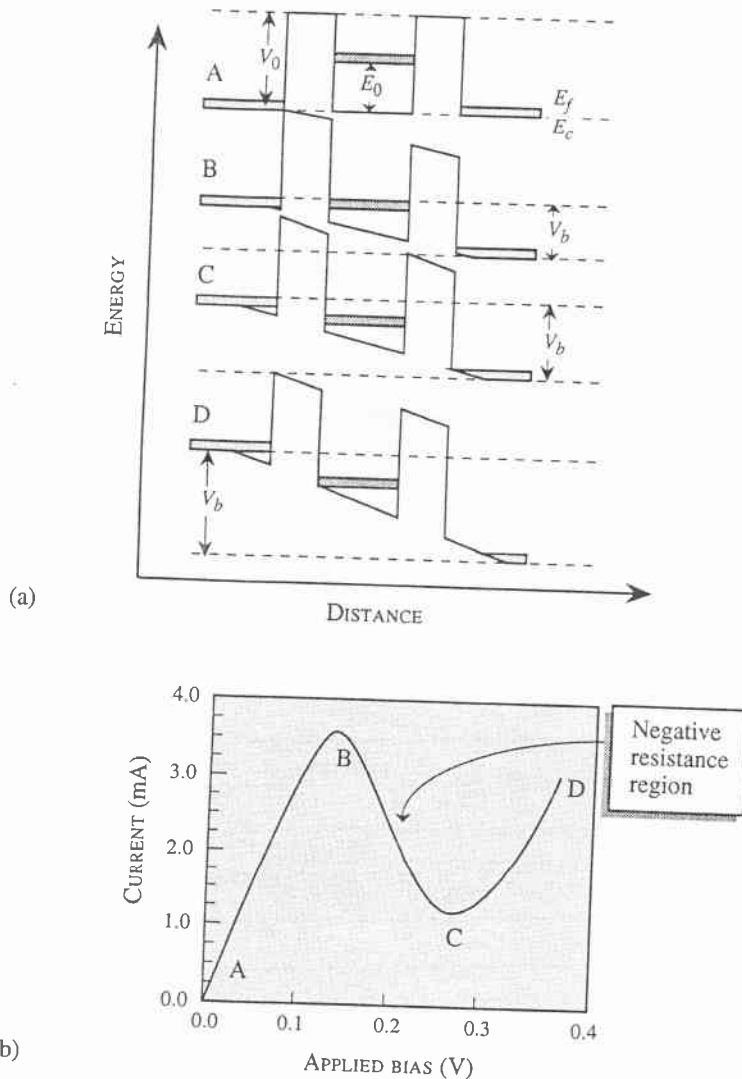


Figure 6.16: (a) Schematic explanation of the operation of resonant tunneling devices showing the energy band diagram for different bias voltages. (b) Typical current-voltage characteristic for the resonant tunneling diode.

A typical current-voltage-re. for the diode is shown in Fig. 6.16b

Of particular interest is the negative-resistance region, which can be exploited for low power high speed digital devices, as well as for microwave devices

TUNNELING IN SUPERCONDUCTING JUNCTIONS

In Chapter 4, Section 4.6.2, we have briefly described how materials can act as superconductors. In these materials at low temperatures electrons pair up to form Cooper pairs. These pairs are bosons and not fermions. The lowest energy state where electron pairs are bosons is separated from normal electron states by a small energy gap where no states are allowed. This gap is only about a millielectron volt and plays a very important role in how electrons tunnel into superconductors.

Let us consider a thin insulator sandwiched between two metals, as shown in Fig. 6.17a. Normal metals are characterized by two important properties: i) the Fermi level is in the middle of the band and electrons occupy states essentially up to the Fermi level. There is no energy gap in this conduction band; ii) In normal metals, electrons act as fermions and as they travel they suffer scattering.

When a bias is applied to the metal-insulator-metal junction electrons can tunnel from one side to the other and current flows. At small applied bias the current-voltage characteristics are essentially linear as shown in Fig. 6.17a.

Now let us consider a junction in which an insulator is sandwiched between two superconductors as shown in Fig. 6.17b. In this case we remind ourselves of two important properties of superconductors; i) Carriers move in pairs of charge $2e$ in the superconducting state; ii) the pairs suffer *no scattering* during transport. Thus long-range phase coherence is maintained in the wavefunction of electrons. This allows us to describe the carrier transport and current flow by simply solving the Schrödinger equation.

For the superconducting junction if the insulator is thin electron pairs can tunnel through the barrier. However, unlike the case in normal metals these electron pairs can move around a closed wire to complete the current, since there is no scattering path. As a result, current flows *even in the absence of any applied bias*. When a bias is applied the current is found to be constant up to a critical voltage V_c . Beyond this voltage electrons tunnel across the superconducting gap and normal Ohmic conduction occurs. The current-voltage relations for a superconductor are shown in Fig. 6.17b. The highly non-linear current-voltage relations are very useful for devices such as mixers where two different microwave signals can be "mixed" to produce sum and difference frequencies.

The detailed analysis of the current in a superconductor tunnel junction (called Josephson junction) is somewhat involved, but is given below for completeness. Let us consider first the case where no potential is applied across the junction.

We consider the simple case in which the two superconductors are identical. Let ψ_1 represent the probability amplitude for the electron pairs on one side of the junction, and ψ_2 the amplitude on the other side. The time-dependent Schrödinger equation $i\hbar\partial\psi/\partial t = H\psi$ can be used to describe the coupling and time-dependence of the electron pairs on one side across the junction. The equations for ψ_1 and ψ_2

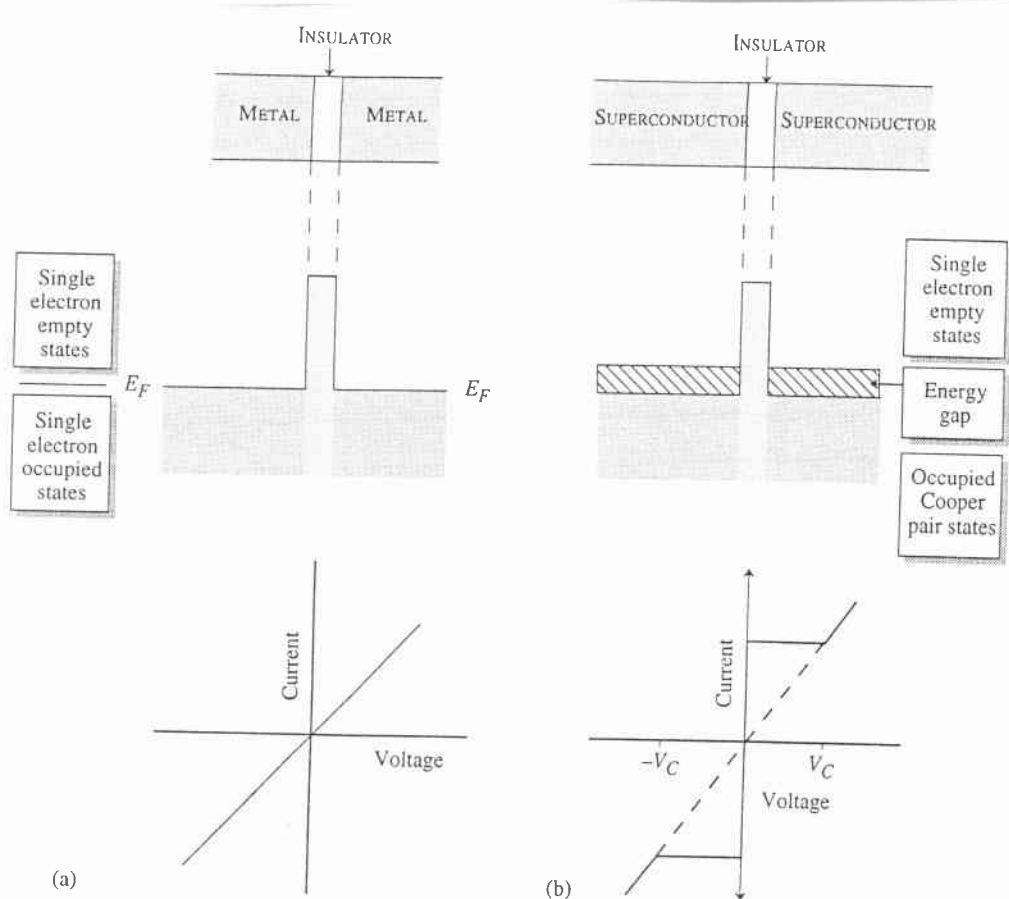


Figure 6.17: (a) A schematic of a metal-insulator-metal junction with the band profile seen by electrons and the current-voltage relation. (b) A schematic of a superconductor-insulator-superconductor junction.

are (choosing the energy of the pairs as zero)

$$\begin{aligned}
 i\hbar \frac{\partial \psi_1}{\partial t} &= H_{12} \psi_2 \\
 i\hbar \frac{\partial \psi_2}{\partial t} &= H_{12} \psi_1
 \end{aligned}
 \tag{6.35}$$

where the matrix element $H_{12} = \langle \psi_1 | H | \psi_2 \rangle = \langle \psi_2 | H | \psi_1 \rangle$ represents the coupling of the electron pairs across the insulator. This matrix element is proportional to the tunneling probability across the barrier.

If n_1 and n_2 are the pair densities on the two sides of the junction, we may write

$$\psi_1 = \sqrt{n_1} e^{i\theta_1}; \quad \psi_2 = \sqrt{n_2} e^{i\theta_2}
 \tag{6.36}$$

This gives, from Eqn. 6.35,

$$\frac{\partial \psi_1}{\partial t} = \frac{1}{2\sqrt{n_1}} e^{i\theta_1} \frac{\partial n_1}{\partial t} + i\psi_1 \frac{\partial \theta_1}{\partial t} = -\frac{i}{\hbar} H_{12} \psi_2 \quad (6.37)$$

$$\frac{\partial \psi_2}{\partial t} = \frac{1}{2\sqrt{n_2}} e^{i\theta_2} \frac{\partial n_2}{\partial t} + i\psi_2 \frac{\partial \theta_2}{\partial t} = -\frac{i}{\hbar} H_{12} \psi_1 \quad (6.38)$$

We multiply Eqn. 6.37 by $\sqrt{n_1} e^{-i\theta_1}$ to obtain (we define $\delta = \theta_2 - \theta_1$)

$$\frac{1}{2} \frac{\partial n_1}{\partial t} + in_1 \frac{\partial \theta_1}{\partial t} = -\frac{i}{\hbar} H_{12} \sqrt{n_1 n_2} e^{i\delta}$$

Similarly, we have

$$\frac{1}{2} \frac{\partial n_2}{\partial t} + in_2 \frac{\partial \theta_2}{\partial t} = -\frac{i}{\hbar} H_{12} \sqrt{n_1 n_2} e^{-i\delta}$$

Equating the real and imaginary terms within each of these equations, we get

$$\begin{aligned} \frac{\partial n_1}{\partial t} &= \frac{2H_{12}}{\hbar} \sqrt{n_1 n_2} \sin \delta ; \quad \frac{\partial n_2}{\partial t} = -\frac{2H_{12}}{\hbar} \sqrt{n_1 n_2} \sin \delta \\ \frac{\partial \theta_1}{\partial t} &= -\frac{H_{12}}{\hbar} \left(\frac{n_2}{n_1} \right)^{1/2} \cos \delta ; \quad \frac{\partial \theta_2}{\partial t} = -\frac{H_{12}}{\hbar} \left(\frac{n_1}{n_2} \right)^{1/2} \cos \delta \end{aligned}$$

We now assume that $n_1 \sim n_2$, which gives

$$\frac{\partial \theta_1}{\partial t} = \frac{\partial \theta_2}{\partial t} \Rightarrow \frac{\partial \delta}{\partial t} = 0$$

and

$$\frac{\partial n_2}{\partial t} = -\frac{\partial n_1}{\partial t}$$

The current flow across the junction is

$$J \propto \frac{\partial n_2}{\partial t} = -\frac{\partial n_1}{\partial t}$$

or

$$J = J_0 \sin \delta = J_0 \sin(\theta_2 - \theta_1) \quad (6.39)$$

The prefactor J_0 is proportional to the coupling matrix element or the tunneling probability of the pairs across the junction. An interesting feature of this result is that *there is a current flow across the junction in the absence of an applied voltage*. The current density lies between J_0 and $-J_0$, depending upon the phase difference $\theta_2 - \theta_1$.

Let us now consider what happens when a small voltage V is applied across the junction. As a result of this voltage, there is a net energy difference of $2eV$ as a Cooper pair crosses the junction. As a result, one side of the junction has an energy of $-eV$ and the other has an energy eV . These terms lead to the following equations:

$$\begin{aligned} i\hbar \frac{\partial \psi_1}{\partial t} &= H_{12} \psi_2 - eV \psi_1 \\ i\hbar \frac{\partial \psi_2}{\partial t} &= H_{12} \psi_1 + eV \psi_2 \end{aligned} \quad (6.40)$$

Proceeding as we did for the $V = 0$ case we get

$$\frac{\partial n_1}{\partial t} = \frac{2H_{12}}{\hbar} \sqrt{n_1 n_2} \sin \delta; \quad \frac{\partial n_2}{\partial t} = -\frac{2H_{12}}{\hbar} \sqrt{n_1 n_2} \sin \delta \quad (6.41)$$

$$\frac{\partial \theta_1}{\partial t} = \frac{eV}{\hbar} - \frac{H_{12}}{\hbar} \left(\frac{n_2}{n_1}\right)^{1/2} \cos \delta; \quad \frac{\partial \theta_2}{\partial t} = -\frac{eV}{\hbar} - \frac{H_{12}}{\hbar} \left(\frac{n_1}{n_2}\right)^{1/2} \cos \delta \quad (6.42)$$

Once again, using $n_1 \sim n_2$, we get

$$\frac{\partial(\theta_2 - \theta_1)}{\partial t} = \frac{\partial \delta}{\partial t} = -\frac{2eV}{\hbar}$$

Upon integrating this equation, we get

$$\delta(t) = \delta(0) - \frac{2eVt}{\hbar}$$

The current across the junction is now

$$J = J_0 \sin \left(\delta(0) - \frac{2eVt}{\hbar} \right) \quad (6.43)$$

The current oscillates with a frequency

$$\omega = \frac{2eV}{\hbar} \quad (6.44)$$

This observation is used for precise measurement of $\frac{e}{\hbar}$. If the applied voltage is increased beyond a critical voltage, as shown in Fig. 6.17b, the current reverts to an ohmic behavior, since the pairs are able to excite into the single-particle electronic spectra where the transport is not by Cooper pairs.

The tunneling properties of Josephson junctions can be exploited, along with the use of magnetic fields, to produce low-power digital logic devices and extremely sensitive magnetic field measurement instruments. These applications are discussed in Appendix C.

TOPICS STUDIED	KEY OBSERVATIONS
Tunneling of particles	<p>In quantum mechanics, when particles are treated as waves, they can traverse through regions where their energy is less than the potential energy. Their trajectories are completely different from what one expects from classical physics.</p>
Tunneling as a stationary state problem	<p>The time-independent problem can be used to calculate the tunneling behavior of particles. Physically, the time-independent problem corresponds to a constant flux of particles in space. A number of analytical and numerical approaches have been developed to solve such problems.</p>
Applications of tunneling	<p>Tunneling of particles has many important applications in technology. These include:</p> <ul style="list-style-type: none"> • Scanning tunneling microscopes for studying precise positions of atoms on a surface. • Producing low-resistance ohmic contacts for semiconductor devices. • Tunnel diodes for microwave applications. • Field emission devices. • Radioactive materials for medical and anthropological uses.
Tunneling through multiple barriers	<p>When particles tunnel through multiple barriers, the tunneling probability has strong resonances as a function of particle energy. This concept is exploited in a number of devices.</p>

Summary table.

分類:
編號: 8-66
總號:

MAGIC OF TECHNOLOGY

- A biologist is developing a model to understand how cockroaches move through the sewer system. For some reason the scientist does not want to spend the next few months with these critters. Technology comes to the rescue. The world's most adaptable creatures are injected with a *dye*, which sends out signals that can be tracked from the streets above.

- Children playing in a lush forest somewhere in Africa come across a strange jawbone of an animal. They have seen nothing like this before and start to use it as a pretend weapon. A passing paleontologist sees them at play and asks to borrow the bone. A few days later a worldwide press release announces: *JAWBONE OF A 20 MILLION YEAR OLD DINOSAUR DISCOVERED.*

- A high-density semiconductor memory manufacturing plant has developed a new *oxidation process* that will be used for gigabit memory chips. However, the engineers find that the yield of the process is extremely low. A team of researchers starts to look at the precise arrangement of silicon and oxygen atoms on the surface using a *scanning tunneling microscope*. They discover that whenever the starting silicon atoms are *bunched up* in a certain way the process fails. This causes the engineers to be more precise in preparing their wafers and the yield shoots up.

- A high-precision machine tool company is developing advanced materials for ball bearings that don't wear out so soon. Special ball bearings are prepared with a *built-in diagnostic tool*. As microscopic wear occurs in the bearings during use; a signal is sent out giving the exact level of degradation.

- Scientists at a research institute are following a promising lead to attack cancerous cells individually. They have developed a *homing* molecule which goes and binds itself to the offending cells. On top of this molecule the researchers manage to place an *armed* atom with a *zap-gun!* Once the homing molecule attaches to the cancerous cell, the zap-gun kills the cell.

In other institutes, scientists are developing *tracer* techniques to study complex biological reactions, blood flow through damaged arteries, and thyroid disorders. Similar techniques are being exploited by chemical companies, agriculture scientists, anthropologists, etc.

✓

Decay of Black Holes

Once inside the event horizon, nothing—not even light—can escape the gravitational pull of a black hole.⁵ That was the view held until 1974, when the brilliant British astrophysicist Stephen Hawking proposed that black holes are indeed radiant objects, emitting a variety of particles by a mechanism involving tunneling through the (gravitational) potential barrier surrounding the black hole. The thickness of this barrier is proportional to the size of the black hole,

⁵A brief introduction to black holes is found in Clifford Will's essay "The Renaissance of General Relativity", p. 50.



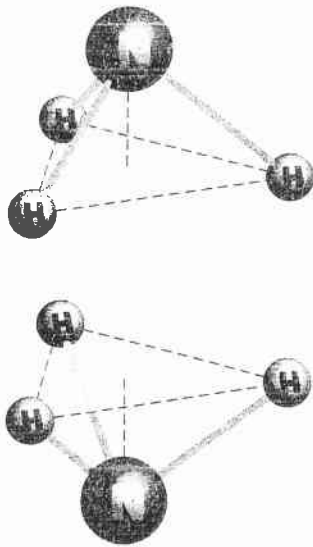
Stephen W. Hawking (1942–), a British astrophysicist, has made major contributions to problems in cosmology, including the theory of black holes. (MMP/Manni Mason's Pictures)

For readable accounts of tunneling from black holes, see S. W. Hawking, "The Quantum Mechanics of Black Holes," *Sci. Am.*, January 1977, pp. 34–40; and J. D. Beckenstein, "Black-hole Thermodynamics," *Phys. Today*, January 1980, pp. 24–31. The second title is somewhat more advanced, and contains additional references.

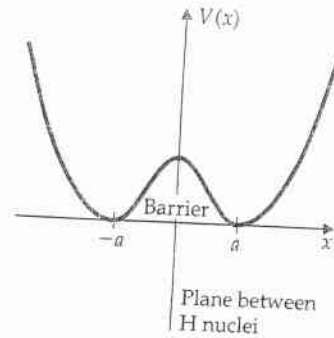
so that the likelihood of a tunneling event initially may be extremely small. As the black hole emits particles, however, its mass and size steadily decrease, making it easier for more particles to tunnel out. In this way emission continues at an ever increasing rate, until eventually the black hole radiates itself out of existence in an explosive climax! Thus, Hawking's scenario leads inexorably to the decay and eventual demise of any black hole. Calculations indicate that a black hole with the mass of our Sun would survive against decay by tunneling for about 10^{66} years. On the other hand, a black hole with the mass of only a billion tons and roughly the size of a proton (such mini black holes are believed to have been formed just after the Big Bang origin of the Universe) should have almost completely evaporated in the 10 billion years that have elapsed since the time of creation.

Ammonia Molecule NH_3

In ammonia, the three hydrogen nuclei are at the corners of an equilateral triangle, with the nitrogen nuclei at the apex of a pyramid.



Two arrangements of the nuclei of the ammonia (NH_3) molecule, each classically stable, place the nitrogen nucleus above and below, respectively, the plane of the equilateral triangle formed by the hydrogen nuclei.



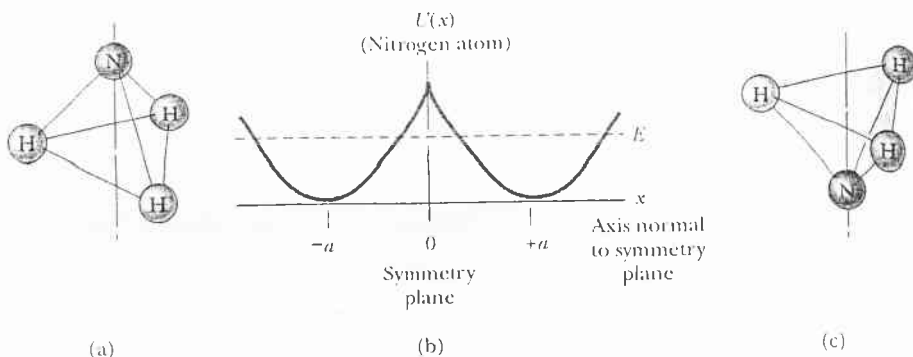
The potential energy of the nitrogen nucleus in ammonia as a function of the distance from the midpoint of the plane of the three hydrogen nuclei. The double well corresponds to two classically stable positions.

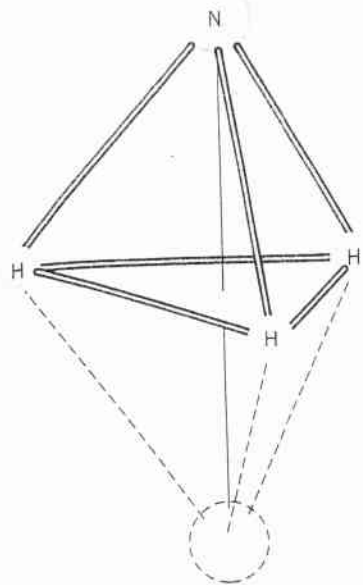
The potential energy function can be approximated by

$$V(x) = \frac{1}{2} M \omega^2 (|x| - a)^2$$

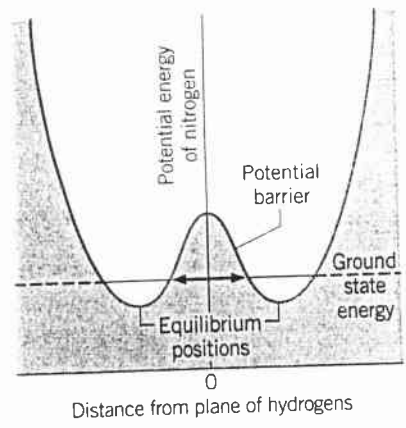
double oscillator model

ω is the classical frequency of vibration for the nitrogen atom around either of the equilibrium points $x = \pm a$



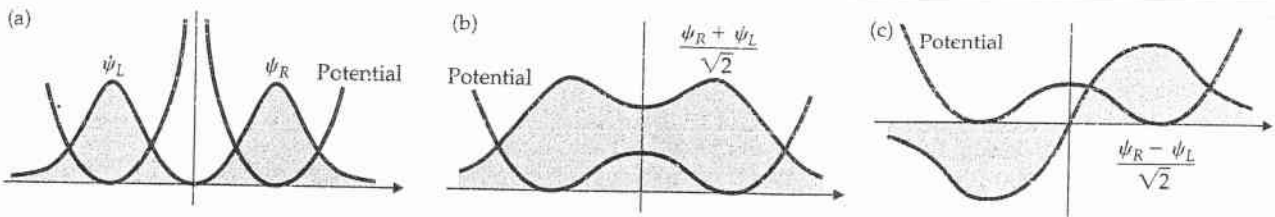


A schematic diagram of the ammonia molecule. The Coulomb repulsion of the three hydrogens establishes a barrier against the nitrogen atom moving to a symmetric position (shown in dashed lines) on the opposite side of the plane of hydrogens.



The potential energy seen by the nitrogen atom in an ammonia molecule. The nitrogen can penetrate the barrier and move from one equilibrium position to another.

This problem can be solved by solving the Schrodinger equation



(a) The wave functions for the nitrogen nucleus in ammonia in either of the two stable positions (potential-energy minima) if there were no mixing of the two due to tunneling. Tunneling implies that the wave functions with fixed energies are (b) the symmetric (even) superposition of the two wave functions in (a) or (c) the antisymmetric (odd) superposition of the two wave functions in (a).

$$\psi_+ = \frac{1}{\sqrt{2}} (\psi_R + \psi_L) \quad E_+$$

$$\psi_- = \frac{1}{\sqrt{2}} (\psi_R - \psi_L) \quad E_-$$

$E_+ < E_-$ (from the consideration of the node.)

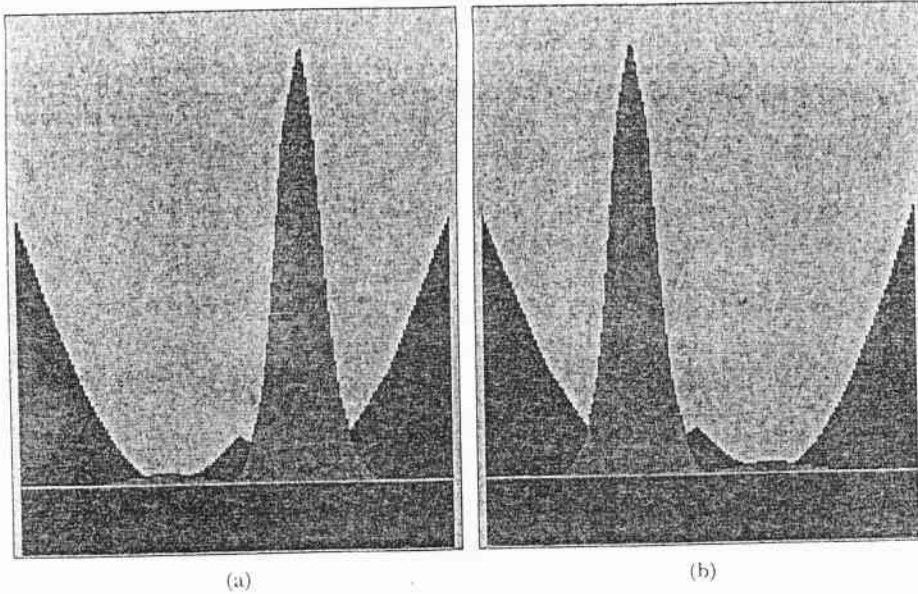
Both E_+ and E_- are less than $V(0)$

$$\psi(x, t) = A_+ \psi_+ e^{-iE_+ t/\hbar} + A_- \psi_- e^{-iE_- t/\hbar}$$

If A_+ , A_- are determined by the requirement that $|\psi(x, 0)|^2$ is on the right side then $\psi(x, t)$ can be calculated at all later time.

In a computer simulation for the ammonia problem, we see the nitrogen may appear at some later time.
 \Rightarrow tunneling has occurred.
 \Rightarrow the oscillating frequency can be calculated.

✓



(a) The nonstationary state formed from the superposition of the ground and first excited states represents the nitrogen atom initially localized in the right-side compartment of the double oscillator well. (b) Some time later, the nonstationary state of Figure 6.18a reassembles in the left-side compartment of the double oscillator well, indicating the nitrogen atom is now on the opposite side of the basal plane: the molecule has undergone inversion.

Since the flopping frequency is in the microwave range, the ammonia molecule can serve as an amplifier for microwave radiation. The *ammonia maser* operates on this principle. Because of the small energy difference between the ground and first excited states of the ammonia molecule, ammonia vapor at room temperature has roughly equal numbers of molecules in both states. Having opposite electric dipole moments, these states are easily separated by passing the vapor through a nonuniform electric field. In this way, ammonia vapor can be produced with the unusually large concentrations of excited molecules needed to create the *population inversion* necessary for maser operation. A spontaneous deexcitation to the ground state of one molecule releases a (microwave) photon, which, in turn, induces other molecules to deexcite. The result—much like a chain reaction—produces a photon cascade: an intense burst of coherent microwave radiation. The operation of masers and lasers is discussed in more detail in *later chapters*.

The N atom is bound to the molecule, so its states lie well below the central maximum of the potential. The central maximum presents a barrier to the N atoms in the lower states through which they slowly tunnel back and forth.¹⁷ The oscillation frequency $f = 2.3786 \times 10^{10}$ Hz when the atom is in the state characterized by the energy E_1 in Figure 6-31b. This frequency is quite low compared with those of most molecular vibrations, a fact that allowed the N atom tunneling frequency in NH_3 to be used as the standard in the first *atomic clocks*, devices that now provide the world's standard for precision timekeeping.

Appendix D

Summary of Some Solid State Results

TOPICS STUDIED	KEY OBSERVATIONS
Electrons in free space	<ul style="list-style-type: none"> • Electrons have an energy $E = \frac{\hbar^2 k^2}{2m_0} + V_0$ • Density of states define the number of allowed solutions (or energy levels) per unit volume per unit energy. Density of states is a very important concept and is dependent on the dimensions of the system.
Electrons in a periodic potential	<ul style="list-style-type: none"> • The wavefunction has a plane wave-like behavior $\Psi \sim u_k e^{i\mathbf{k}\cdot\mathbf{r}}$ where u_k is periodic. • The energy of the electron is not continuous. Allowed energy bands are separated by bandgaps. • A new parameter $\hbar\mathbf{k}$ is introduced. For most purposes, $\hbar\mathbf{k}$ acts as a momentum of the electron inside the crystal.
Crystalline structures	<ul style="list-style-type: none"> • Perfect periodicity exists in the arrangement of atoms or molecules—produced by placing a basis on lattice sites.
Crystalline semiconductors	<ul style="list-style-type: none"> • Semiconductors such as Si, Ge and C have a diamond structure with an underlying fcc lattice. • Semiconductors such as GaAs and InAs have a zinc blende structure with an underlying fcc lattice.
Ferroelectric crystals	<ul style="list-style-type: none"> • Such crystals have a built-in electric dipole due to the arrangement of positively and negatively charged atoms in the structure.

Summary table.

TOPICS STUDIED

KEY OBSERVATIONS

Kronig-Penney model for bandstructure

A simple model for electronic properties in a periodic structure. The outcome of this model is:

- There are a series of allowed energy bands separated by bandgaps.
- Electrons cannot have energies in the bandgap region.

Insulators, semiconductors, and metals

- If, at 0 K, the highest occupied band is filled completely and the next band (separated by a bandgap) is completely empty, a semiconductor or insulator results.
- If the highest band is partially filled, a metal results.

Valence and conduction bands

- The highest occupied band in a semiconductor at 0 K is called the *valence band*.
- A completely filled band cannot carry any current, so the conductivity of a pure semiconductor at 0 K is zero.

Summary table.

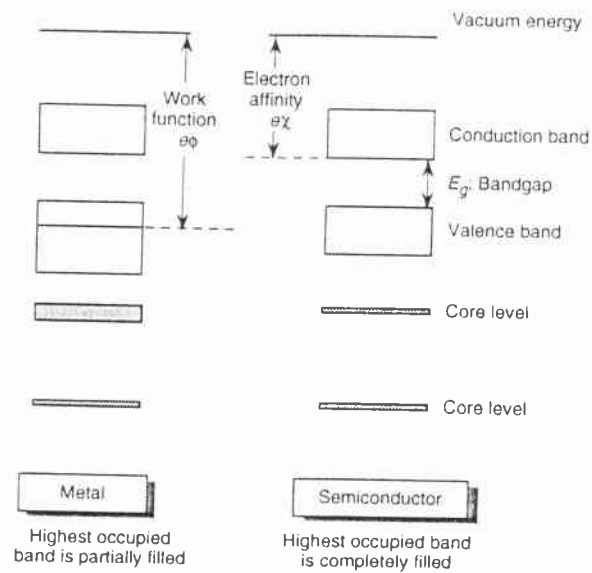


Figure 4.19: A schematic description of electron occupation of the bands in a metal and semiconductor (or insulator). In a metal, the highest occupied band at 0 K is partially filled with electrons. Also shown is the metal work function. In a semiconductor at 0 K, the highest occupied band is completely filled with electrons and the next band is completely empty. The separation between the two bands is the bandgap E_g . The electron affinity and work function are also shown.

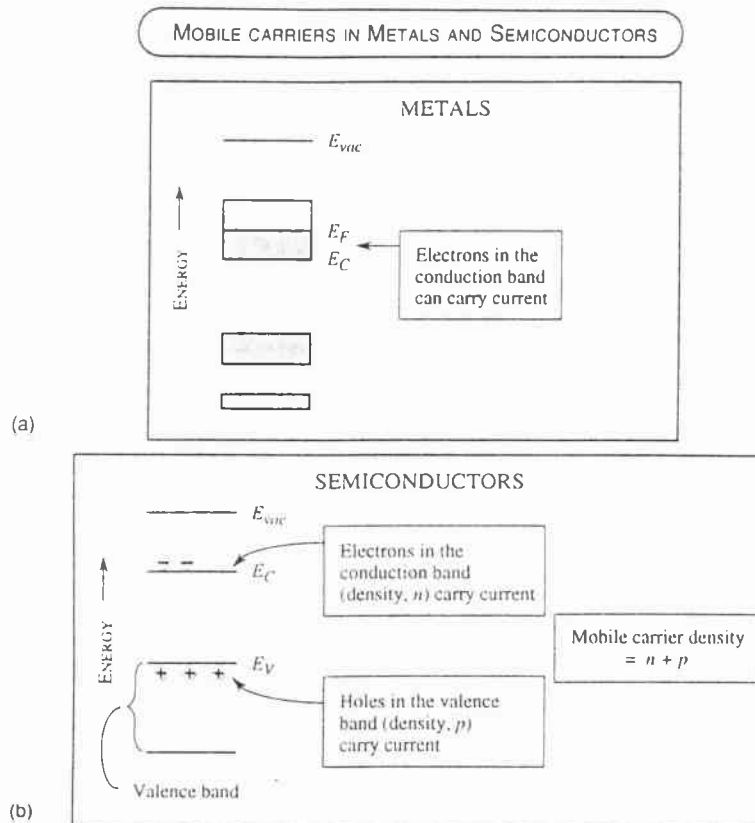


Figure 4.27: (a) A schematic showing mobile carrier (capable of carrying current) in metals; (b) In semiconductor, only electrons in the conduction band holes in the value band can carry current.

INTRINSIC CARRIER CONCENTRATION

From our discussion on metals and semiconductors we see that in a metal, current flows because of the electrons present in the highest (partially) filled band. This is shown schematically in Fig. 4.27a. The density of such electrons is very high ($\sim 10^{22} \text{ cm}^{-3}$). In a semiconductor, on the other hand, no current flows if the valence band is filled with electrons and the conduction band is empty of electrons. However, if somehow empty states or holes are created in the valence band by removing electrons, current can flow through the holes. Similarly, if electrons are placed in the conduction band, these electrons can carry current. This is shown schematically in Fig. 4.27b. If the density of electrons in the conduction band is n and that of the holes in the valence band is p , the total mobile carrier density is $n + p$.

How do holes appear in the valence band and how do electrons occupy the conduction band? In a pure semiconductor, at finite temperatures the thermal energy of the crystal knocks some electrons from the valence band into the conduction

band. When this happens, an electron-hole pair is produced. In the pure semiconductor, the electron density is equal to the hole density and is denoted by n_i and p_i , the subscript i standing for intrinsic. It is also possible to create holes in the valence band and electrons in the conduction band by using impurity atoms with special properties. This process is called doping, and we will discuss this in the next chapter.

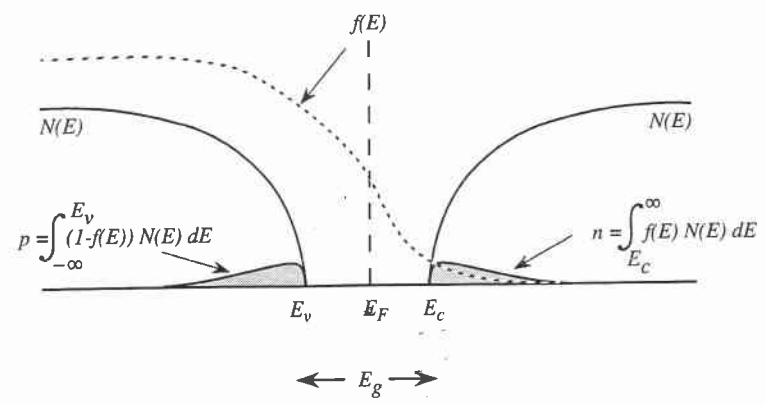


Figure 4.28: A schematic of the density of states of the conduction and valence band. N_c and N_v are the electron and hole density of states. Also shown is the Fermi function giving the occupation probability for the electrons. The resulting electron and hole concentrations are shown. For an intrinsic semiconductor $n = p$, since each electron produced in the conduction band leaves behind a hole in the valence band.

Essay

THE SCANNING TUNNELING MICROSCOPE



Roger A. Freedman

The basic idea of quantum mechanics, that particles have properties of waves and vice versa, is among the strangest found anywhere in science. Because of this strangeness, and because quantum mechanics mostly deals with the very small, it might seem to have little practical application. As we will show in this essay, however, one of the basic phenomena of quantum mechanics—the tunneling of particles—is at the heart of a very practical device that is one of the most powerful microscopes ever built. This device, the *scanning tunneling microscope* or *STM*, enables physicists to make highly detailed images of surfaces with resolution comparable to the size of a *single atom*. Such images promise to revolutionize our understanding of structures and processes on the atomic scale.

Before discussing how the STM works, we first look at a sample of what the STM can do. An image made by a scanning tunneling microscope of the surface of a piece of gold is shown in Figure 1. You can easily see that the surface is not uniformly flat, but is a



Paul K. Hansma

Department of Physics,
University of California,
Santa Barbara

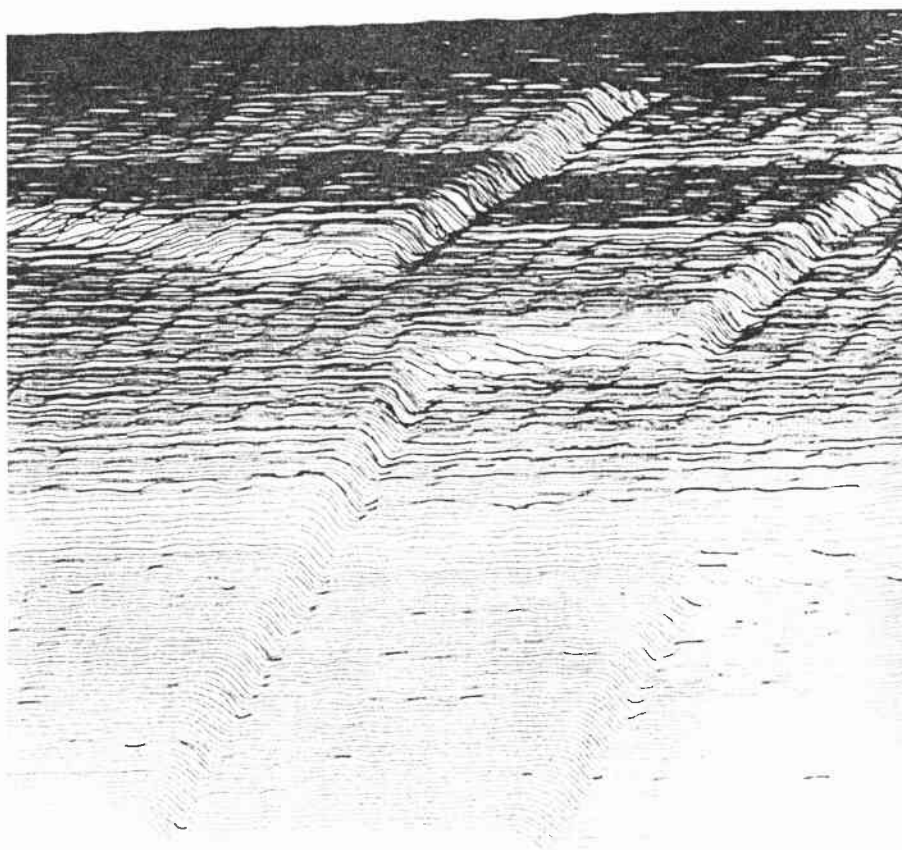


Figure 1 Scanning tunneling microscope image of the surface of crystalline gold. Successive scans are approximately 1.5 Å apart. The figure is from G. Binnig, H. Rohrer, Ch. Gerber, and E. Stoll, *Surface Sci.*, 144:321, 1984.

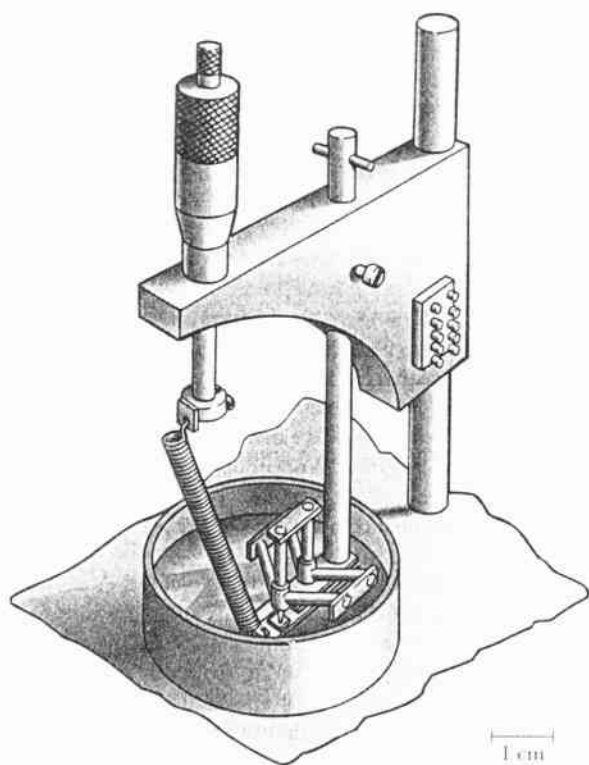


Figure 2 One design for a scanning tunneling microscope (STM). The sample to be studied is mounted on a plate in the cylindrical dish. The probe extends beneath the left tripod. The micrometer attached to the spring is used to position the sample.

series of terraces separated by steps that are only one atom high. Gentle corrugations can be seen in the terraces, caused by subtle rearrangements of the gold atoms.

What makes the STM so remarkable is the fineness of the detail that can be seen in images such as Figure 1. The *resolution* in this image—that is, the size of the smallest detail that can be discerned—is about 2 Å (2×10^{-10} m). For an ordinary microscope, the resolution is limited by the wavelength of the waves used to make the image. Thus an optical microscope has a resolution of no better than 2000 Å, about half the wavelength of visible light, and so could never show the detail displayed in Figure 1. Electron microscopes can have a resolution of 2 Å by using electron waves of wavelength 4 Å or shorter. From the de Broglie formula $\lambda = h/p$, the electron momentum p required to give this wavelength is $3100 \text{ eV}/c$, corresponding to an electron speed $v = p/m_e = 1.8 \times 10^6 \text{ m/s}$. Electrons traveling at this high speed would penetrate into the interior of the piece of gold in Figure 1, and so would give no information about individual surface atoms.

The image in Figure 1 was made by Gerd Binnig, Heinrich Rohrer, and collaborators at the IBM Research Laboratory in Zurich, Switzerland. Binnig and Rohrer invented the STM and shared the 1986 Nobel prize in physics for their work. Such is the importance of this device that unlike most Nobel prizes, which come decades after the original work, Binnig and Rohrer received their Nobel prize just six years after their first experiments with an STM.

One design for an STM is shown in Figure 2. The basic idea behind its operation is very simple, as shown in Figure 3. A conducting probe with a very sharp tip is brought near the surface to be studied. Because it is attracted to the positive ions in the surface,

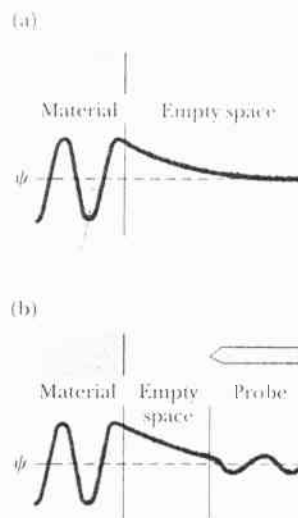


Figure 3 (a) The wavefunction of an electron in the surface of the material to be studied. The wavefunction extends beyond the surface into the empty region. (b) The sharp tip of a conducting probe is brought close to the surface. The wavefunction of a surface electron penetrates into the tip, so that the electron can “tunnel” from surface to tip. Compare this figure to Figure 6.2a.

Suc-
hrer,

an electron in the surface has a lower total energy than would an electron in the empty space between surface and tip. The same thing is true for an electron in the tip. In classical Newtonian mechanics, electrons could not move between the surface and tip because they would lack the energy to escape either material. But because the electrons obey quantum mechanics, they can "tunnel" across the barrier of empty space between the surface and the tip. Let us explore the operation of the STM in terms of the discussion of tunneling in Section 6.1.

For an electron in the apparatus of Figures 2 and 3, a plot of the energy as a function of position would look like Figure 6.2b. The horizontal coordinate in this figure represents electron position. Now L is to be interpreted as the distance between the surface and the tip, so that coordinates less than 0 refer to positions inside the surface material and coordinates greater than L refer to positions inside the tip. The barrier height $U = q\phi$ is the potential energy difference between an electron outside the material and an electron in the material. That is, an electron in the surface or tip has potential energy $-U$ compared with one in vacuum. (We are assuming for the moment that the surface and tip are made of the same material. We will comment on this assumption shortly.) The kinetic energy of an electron in the surface is E so that an amount of energy equal to $(U - E)$ must be given to an electron to remove it from the surface. Thus $(U - E)$ is the work function of an electron in the surface.

For the potential energy curve of Figure 6.2b, one could expect as much tunneling from the surface into the tip as in the opposite direction. In an STM, the direction in which electrons tend to cross the barrier is controlled by applying a voltage between the surface and the tip. With preferential tunneling from the surface into the tip, the tip samples the distribution of electrons in and above the surface. Because of this "bias" voltage, the work functions of surface and tip are different, giving a preferred direction of tunneling. This is also automatically the case if the surface and tip are made of different materials. In addition, the top of the barrier in Figure 6.2b will not be flat but will be tilted to reflect the electric field between the surface and the tip. If the barrier energy U is large compared with the difference between the surface and tip work functions, however, and if the bias voltage is small compared with $\phi = U/q$, we can ignore these complications in our calculations. Then all the results for a square barrier given in Section 6.1 may be applied to an STM. Detailed discussions of the effects that result when these complications are included can be found in the article by P. K. Hansma and J. Tersoff and in the Nobel prize lecture of Binnig and Rohrer (see Suggestions for Further Reading).

The characteristic scale of length for tunneling is set by the work function $(U - E)$. For a typical value $(U - E) = 4.0$ eV, this scale of length is

$$\begin{aligned} \delta &= \frac{\hbar}{\sqrt{2m_e(U - E)}} = \frac{\hbar c}{\sqrt{2m_e c^2(U - E)}} \\ &= \frac{1.973 \text{ keV} \cdot \text{\AA}}{\sqrt{2(511 \text{ keV})(4.0 \times 10^{-3} \text{ keV})}} = 0.98 \text{ \AA} \approx 1.0 \text{ \AA} \end{aligned}$$

The probability that a given electron will tunnel across the barrier is just the transmission coefficient T (Equation 6.9). If the separation L between surface and tip is not small compared with δ , then the barrier is "wide" and we can use the approximate result of Problem 5 for T . The current of electrons tunneling across the barrier is simply proportional to T . The tunneling current density can be shown to be

$$j = \frac{e^2 V}{4\pi^2 L \delta \hbar} e^{-2L/\delta}$$

In this expression e is the charge of the electron and V is the bias voltage between surface and tip.

bet
cur
typ
cur
cre.
bey
L is
is s
In
app

pla
an
onl
mig
eas
san
call
rer

cur
is f
sur

(a

Schematic view

One scan

Multiple scans

We can see from this expression that the STM is very sensitive to the separation L between tip and surface. This is because of the exponential dependence of the tunneling current on L (this is much more important than the $1/L$ dependence). As we saw earlier, typically $\delta \approx 1.0 \text{ \AA}$. Hence increasing the distance L by just 0.01 \AA causes the tunneling current to be multiplied by a factor $e^{-2(0.01 \text{ \AA})/(1.0 \text{ \AA})} \approx 0.98$; that is, the current decreases by 2%—a change that is measurable. For distance L greater than 10 \AA (that is, beyond a few atomic diameters), essentially no tunneling takes place. This sensitivity to L is the basis of the operation of the STM: monitoring the tunneling current as the tip is scanned over the surface gives a sensitive measure of the topography of the surface. In this way the STM can measure the height of surface features to within 0.01 \AA , or approximately one one-hundredth of an atomic diameter.

The STM also has excellent lateral resolution, that is, resolution of features in the plane of the surface. This is because the tips used are *very* sharp indeed, typically only an atom or two wide at their extreme end. Thus the tip samples the surface electrons only in a very tiny region approximately 2 \AA wide, and so can “see” very fine detail. You might think that making such tips would be extremely difficult, but in fact it’s relatively easy: sometimes just sharpening the tip on a fine grinding stone (or even with fine sandpaper) is enough to cause the tip atoms to rearrange by themselves into an atomically sharp configuration. (If you find this surprising, you’re not alone, Binnig and Rohrer were no less surprised when they discovered this.)

There are two modes of operation for the STM, shown in Figure 4. In the *constant current mode* (Fig. 4a), a convenient operating voltage (typically between 2 mV and 2 V) is first established between surface and tip. The tip is then brought close enough to the surface to obtain measurable tunneling current. The tip is then scanned over the surface

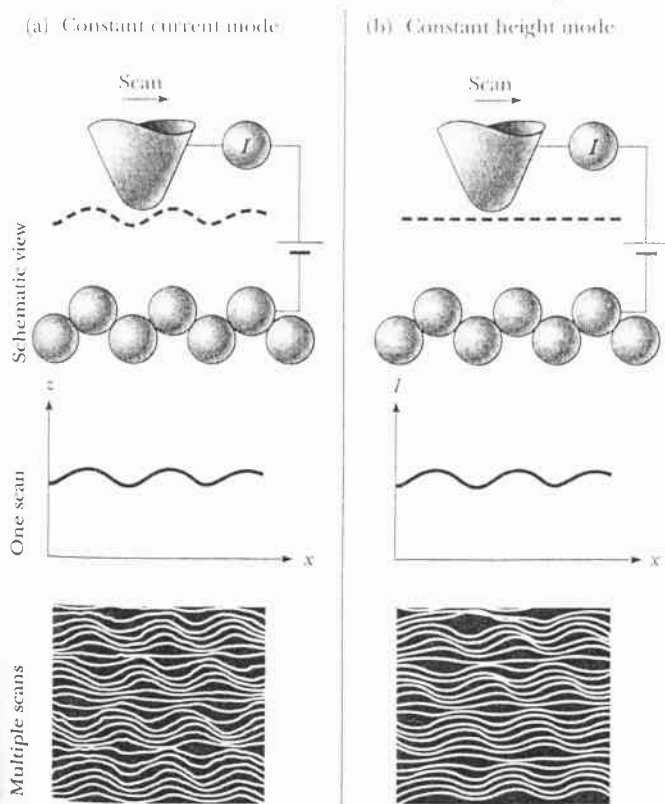


Figure 4 Scanning tunneling microscopes can be operated in either (a) the constant current mode or (b) the constant height mode. The images of the surface of graphite were made by Richard Sonnenfeld at the University of California at Santa Barbara. The constant height mode was first used by A. Bryant, D. P. E. Smith, and C. F. Quate, *Appl. Phys. Lett.* 48:832, 1986.

while the tunneling current I is measured. A feedback network changes the vertical position of the tip, z , to keep the tunneling current constant, thereby keeping the separation L between surface and tip constant. An image of the surface is made by plotting z versus lateral position (x, y) . The simplest scheme for plotting the image is shown in the graph below the schematic view. The height z is plotted versus the scan position x . An image consists of multiple scans displaced laterally from each other in the y direction.

The constant current mode was historically the first to be used and has the advantage that it can be used to track surfaces that are not atomically flat (as in Fig. 1). The feedback network, however, requires that the scanning be done relatively slowly. As a result, the sample being scanned must be held fixed in place for relatively long times to prevent image distortion.

Alternatively, in the *constant height mode* (Fig. 4b), the tip is scanned across the surface at constant voltage and nearly constant height while the current is monitored. In this case the feedback network responds only rapidly enough to keep the average current constant, which means that the tip maintains the same average separation from the surface. The image is then a plot of current I versus lateral position (x, y) , as shown in the graph below the schematic. Again, multiple scans along x are displayed laterally displaced in the y direction. The image shows the substantial variation of tunneling current as the tip passes over surface features such as individual atoms.

The constant height mode allows much faster scanning of atomically flat surfaces (100 times faster than the constant current mode), since the tip does not have to be moved up and down over the surface "terrain." This fast scanning means that making an image of a surface requires only a short "exposure time." By making a sequence of such images, researchers may be able to study in real-time processes in which the surfaces rearrange themselves—in effect making an STM "movie."

Individual atoms have been imaged on a variety of surfaces, including those of so-called *layered materials* in which atoms are naturally arranged into two-dimensional layers. Figure 5 shows an example of atoms on one of these layered materials. In this image it is fascinating not only to see individual atoms, but also to note that some atoms are missing. Specifically, there are three atoms missing from Figure 5. Can you find the places where they belong?

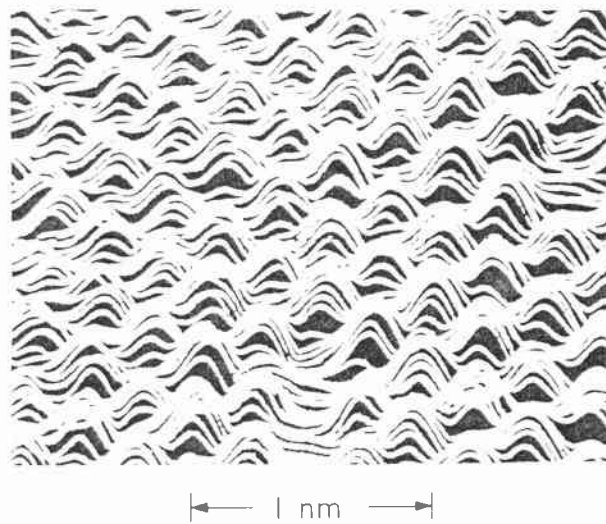


Figure 5 Image of atoms on a surface of tantalum disulfide (TaS_2) immersed in liquid nitrogen. $1 \text{ nm} = 10^{-9} \text{ meter} = 10 \text{ \AA}$. The figure is from C. G. Slough, W. W. McNair, R. A. Coleman, B. Drake, and P. K. Hansma, *Phys. Rev. B* 34:994, 1986.

Figure
figure

An
the su
the sp
take p
This s
in it, a
as an i
water
water.

As
obtain
for ion
were s
comes
this pa
on thi
plated
surface
seeing

Wh
have r
with st
rings c
ring a
the th
the un
lie dir
them.
been i
above
7, sinc

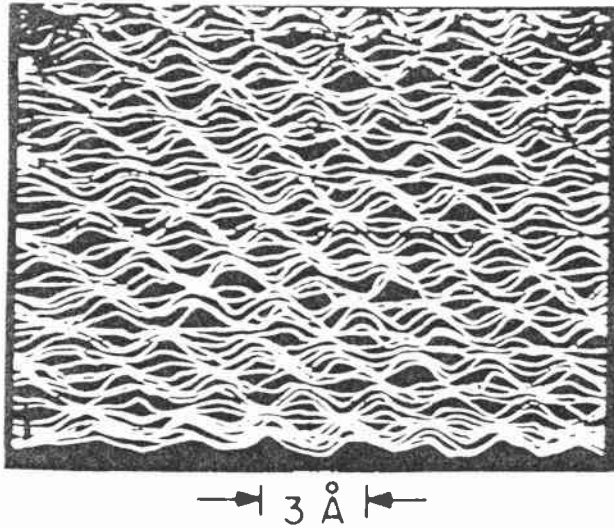


Figure 6 Image of a graphite electrode in an electrolyte used for silver plating. The figure is from R. Sonnenfeld and B. Schardt, *Appl. Phys. Lett.* 49:1172, 1986.

Another remarkable aspect of the STM image in Figure 5 is that it was obtained with the surface and tip immersed in liquid nitrogen. We assumed earlier in this essay that the space between the surface and tip must be empty, but in fact electron tunneling can take place not just through vacuum but also through gases and liquids—even water. This seems very surprising since we think of water, especially water with salts dissolved in it, as a conductor. But water is only an *ionic* conductor. For electrons, water behaves as an insulator just as vacuum behaves as an insulator. Thus electrons can flow through water only by tunneling, which makes scanning tunneling microscopy possible “under water.”

As an example, Figure 6 shows individual carbon atoms on a graphite surface. It was obtained for a surface immersed in a silver-plating solution, which is highly conductive for ions but behaves as an insulator for electrons. (The sides of the conducting probe were sheathed with a nonconductor, so that the predominant current into the probe comes from electrons tunneling into the exposed tip. The design of STM used to make this particular image is the one shown in Fig. 2.) Sonnenfeld and Schardt observed atoms on this graphite surface before plating it with silver, after “islands” of silver atoms were plated onto the surface, and after the silver was electrochemically stripped from the surface. Their work illustrates the promise of the scanning tunneling microscope for seeing processes that take place on an atomic scale.

While the original STMs were one-of-a-kind laboratory devices, commercial STMs have recently become available. Figure 7 is an image of a graphite surface in air made with such a commercial STM. Note the high quality of this image and the recognizable rings of carbon atoms. You may be able to see that three of the six carbon atoms in each ring *appear* lower than the other three. All six atoms are in fact at the same level, but the three that appear lower are bonded to carbon atoms lying directly beneath them in the underlying atomic layer. The atoms in the surface layer that appear higher do not lie directly over subsurface atoms, and hence are not bonded to carbon atoms beneath them. For the higher-appearing atoms, some of the electron density that would have been involved in bonding to atoms beneath the surface instead extends into the space above the surface. This extra electron density makes these atoms appear higher in Figure 7, since what the STM maps is the topography of the electron distribution.

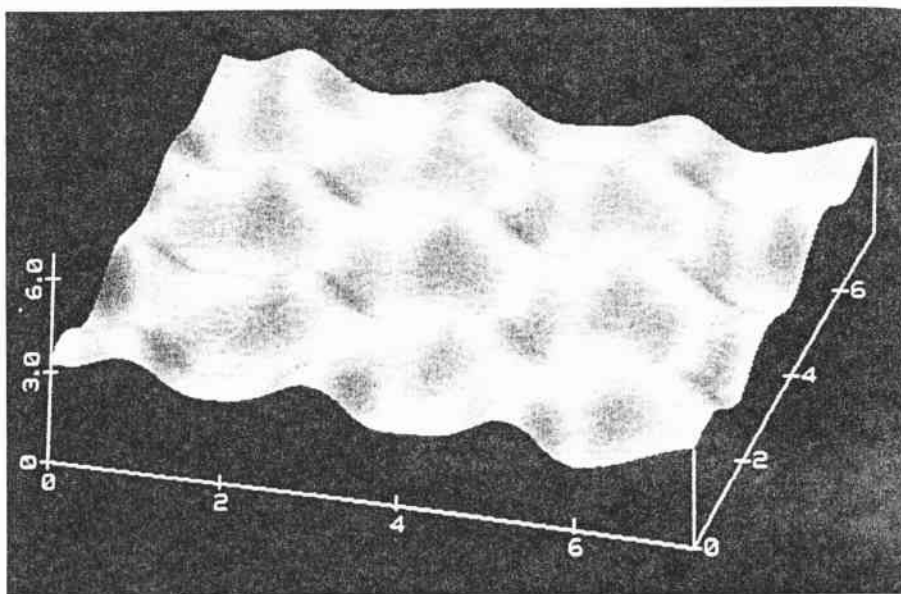


Figure 7 Image of a graphite surface in air, obtained with a commercial STM: the Nanoscope II from Digital Instruments in Goleta, California.

The availability of commercial instruments should speed the use of scanning tunneling microscopy in a variety of applications. These include characterizing electrodes for electrochemistry (while the electrode is still in the electrolyte), characterizing the roughness of surfaces, measuring the quality of optical gratings, and even imaging replicas of biological structures.

Perhaps the most remarkable thing about the scanning tunneling microscope is that its operation is based on a quantum mechanical phenomenon—tunneling—that was well understood in the 1920s, yet the STM itself wasn't built until the 1980s. What other applications of quantum mechanics may yet be waiting to be discovered?

Suggestions for Further Reading

- G. Binnig, H. Rohrer, Ch. Gerber, and E. Weibel, *Phys. Rev. Lett.* 49:57, 1982. The first description of the operation of a scanning tunneling microscope.
- G. Binnig and H. Rohrer, *Sci. Am.*, August 1985, p. 50. A popular description of the STM and its applications.
- C. F. Quate, *Phys. Today*, August 1986, p. 26. An overview of the field of scanning tunneling microscopy, including insights into how it came to be developed.
- P. K. Hansma and J. Tersoff, *J. Appl. Phys.* 61:R1, 1987. A comprehensive review of the "state of the art" in scanning tunneling microscopy.
- G. Binnig and H. Rohrer, *Rev. Mod. Phys.* 59:615, 1987. The text of the lecture given on the occasion of the presentation of the 1986 Nobel prize in physics.

The Scanning Tunneling Microscope

A new kind of microscope reveals the structures of surfaces atom by atom. The instrument's versatility may extend to investigators in the fields of physics, chemistry and biology

by Gerd Binnig and Heinrich Rohrer

"The surface was invented by the devil," said the illustrious physicist Wolfgang Pauli. Pauli's frustration was based on the simple fact that the surface of a solid serves as the boundary between it and the outer world. Whereas an atom within a solid is surrounded by other atoms, an atom at a surface can interact only with other atoms on the surface, with atoms beyond the surface or with those immediately under it. The properties of the surface of a solid therefore differ radically from those of the interior. For instance, to minimize energy, surface atoms often arrange themselves differently from the other atoms in a solid. The resulting complexities of surface structures have long thwarted efforts to derive precise experimental and theoretical descriptions of them.

At the IBM Zurich Research Laboratory we have developed a device that makes it possible to characterize in a quantitative way such surface complexities: the scanning tunneling microscope. Our microscope enables one to "see" surfaces atom by atom. It can even resolve features that are only about a hundredth the size of an atom. Such a tool has important implications, for example, in the microelectronic industry. As the silicon chip, which is the key element in computer architecture, decreases in size its surface area increases sharply in relation to its volume. Therefore the surface becomes increasingly important in the chip's operation and in its interactions with other logic elements. The scanning tunneling microscope will probably contribute to the understanding of other physical, chemical and biological phenomena as well.

Scanning tunneling microscopy is the product of considerable evolution. Microscopy appears to have begun in the 15th century when simple magnifying glasses were made with which to

observe insects. In the late 17th century Antony van Leeuwenhoek developed the optical microscope, which revealed the existence of single cells, pathogenic agents and bacteria. Although optical microscopy has developed into a sophisticated, versatile technique, a physical limit hampers it: the optical microscope cannot resolve atomic structures. The reason is that the average wavelength of visible light is about 2,000 times greater than the diameter of a typical atom, which is about three angstrom units. (One angstrom unit is one ten-billionth of a meter.) In other words, trying to probe atomic structures with visible light is like trying to find hairline cracks on a tennis court by bouncing tennis balls off its surface.

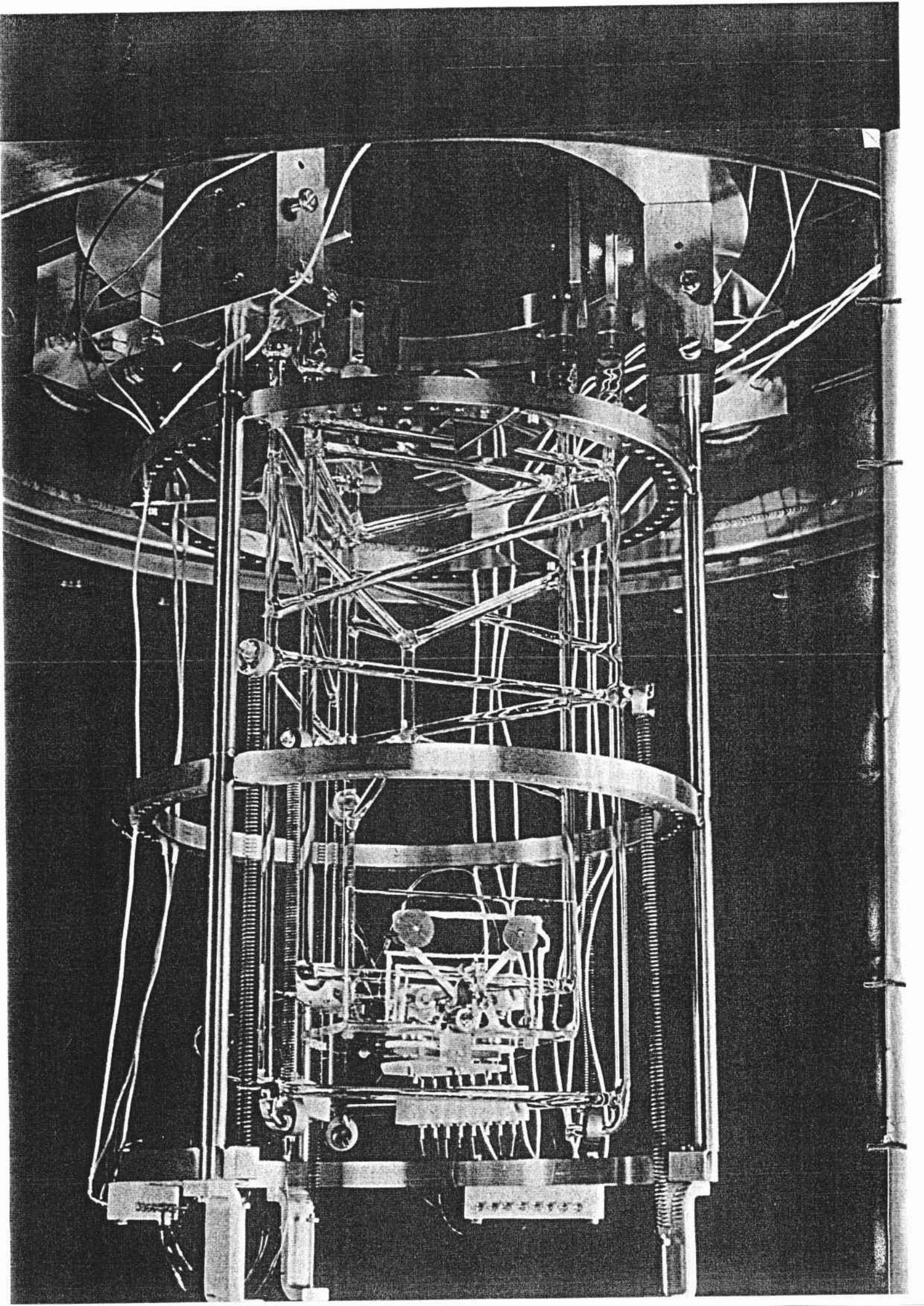
The first successful exploration of atomic structures grew out of a basic discovery of quantum mechanics. It is that light and other kinds of energy exhibit characteristics of both particles and waves. In 1927 Clinton J. Davisson and Lester H. Germer of the Bell Telephone Laboratories confirmed the wave nature of the electron. They also found that a high-energy electron has a shorter wavelength than a low-energy electron. An electron of sufficient energy exhibits a wavelength comparable to the diameter of an atom. This fact led to the invention of the electron microscope. With electron microscopy projections of atomic rows and even

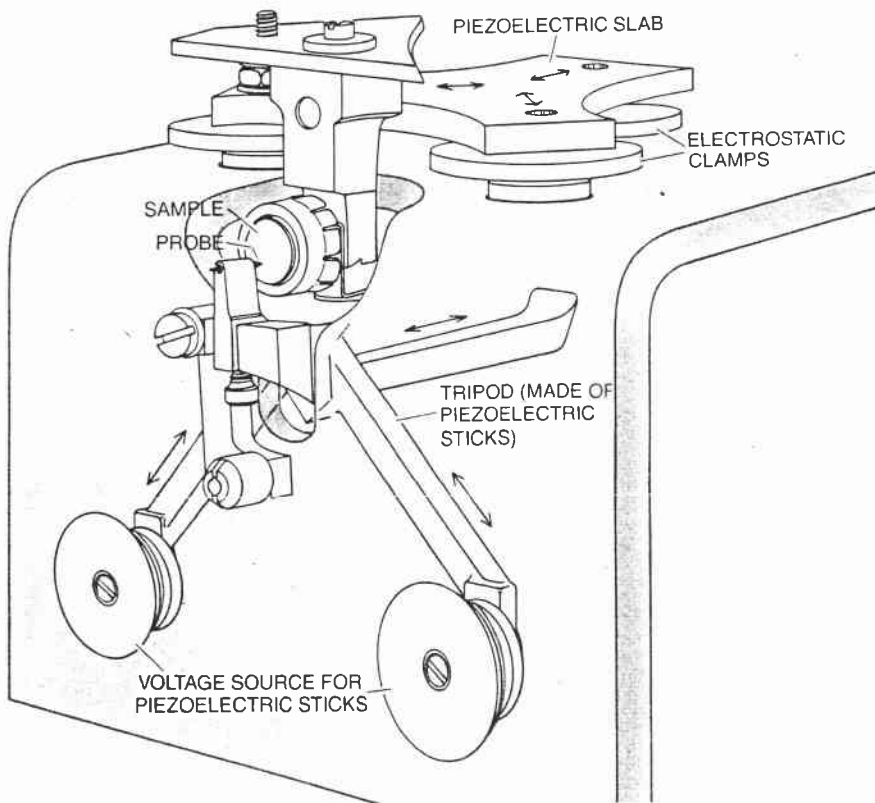
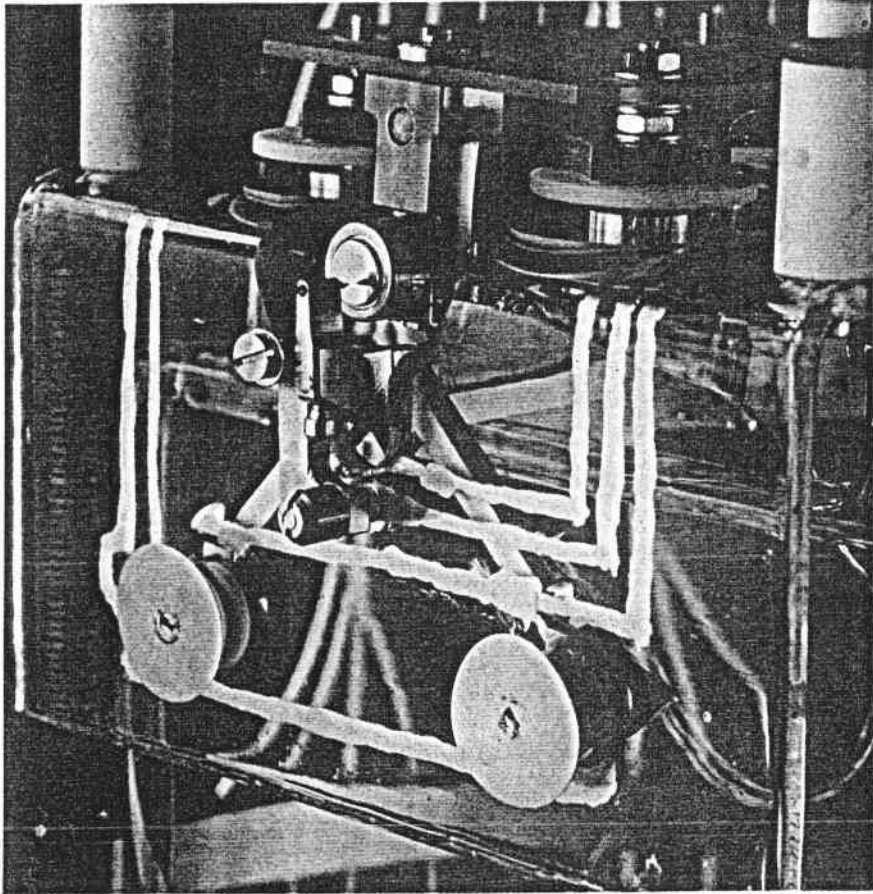
atomic orbitals in thin crystalline films have been observed.

Since the electron microscope has such a high resolving power, why was it necessary to develop a new kind of microscope? Although electron microscopy has proved to be extremely successful in observing the bulk features of crystalline materials, it cannot resolve surface structures except under very special circumstances. A high-speed electron penetrates deep into matter and so reveals little of the surface structure. A slow-moving electron is easily deflected by the charges and the electric and magnetic fields of the sample. In the 1950's Edwin W. Müller made some progress when he invented the field-ion microscope, an instrument that is highly sensitive to surfaces. Unfortunately its range of applicability is narrow: a sample must sit on a fine needle tip that is only a few angstroms wide and the sample must be stable against the high electric fields characteristic of the technique.

The principle of operation of the scanning tunneling microscope makes it possible to avoid these difficulties. The main difference between the scanning tunneling microscope and all other microscopes is that it uses no free particles; consequently there is no need for lenses and special light or electron sources. Instead the bound electrons already existing in the sample under

SCANNING TUNNELING MICROSCOPE has two stages, suspended from springs, that nestle within a cylindrical stainless-steel frame. The innermost stage contains the microscope mechanism. To achieve high-resolution images of surface structures the microscope must be shielded from even such small vibrations as those caused by footsteps and sound. The copper plates (attached to the bottom of the stainless-steel frame) and the magnets (attached to the bottom of the inner and outer stages) damp vibrations. Any disturbance causes the copper plates to move up and down in the field generated by the magnets. The movement induces eddy currents in the plates. The interaction of the eddy currents with the magnetic field retards the motion of the plates and hence the motion of the stages. For work required in a vacuum a steel cover is placed over the outer frame of the microscope.





MICROSCOPE DEVICE contains a sample and a scanning needle. Piezoelectric materials, which expand or contract when voltage is applied to them, enable the device to resolve features that are only about a hundredth the size of an atom. A piezoelectric drive positions the sample on a horizontal metal plate. A piezoelectric tripod then sweeps the scanning needle over the surface of the sample, simultaneously achieving high stability and precision.

investigation serve as the exclusive source of radiation.

To understand this principle imagine that the electrons bound to the surface of the sample are analogous to the water of a lake locked in by the shore. Just as some of the lake water seeps into the surrounding land to form groundwater, so some of the electrons on the sample's surface leak out and form an electron cloud around the sample. According to classical physics, no electron cloud exists because reflection at the sharp boundaries of surfaces confines the particles. In quantum mechanics, however, each electron behaves like a wave: its position is "smeared out." This accounts for the existence of electrons beyond the surface of matter. The probability of finding an electron beyond the surface of a conductor falls rapidly, in fact exponentially, with distance from the surface. Since the electrons appear to be digging tunnels beyond the surface boundary, the effect is traditionally known as tunneling.

The first experimental verification of tunneling was made about a quarter of a century ago by Ivar Giaever of the General Electric Company. A thin, rigid insulating layer was used to separate two metal plates called electrodes. The gap between the electrodes was small enough to allow the electron clouds associated with the electrodes to overlap slightly. A potential difference between the electrodes, induced by applying voltage to them, causes electrons to flow from one electrode to the other through the overlapping clouds. The flow is analogous to the flow of groundwater between two adjacent lakes when one lake is higher than the other.

We built our scanning tunneling microscope by making a few basic changes in the standard tunneling configuration. First we replaced one of the electrodes with the sample we wanted to investigate. Then we replaced the other electrode with a sharp, needlelike probe. Finally we replaced the rigid insulating layer with a nonrigid insulator such as liquid, gas or vacuum so that we could scan the needle tip along the contours of the sample's surface.

To scan the surface we push the tip toward the sample until the electron clouds of each gently touch. The application of a voltage between the tip and the sample causes electrons to flow through a narrow channel in the electron clouds. This flow is called the tunneling current. Since the density of an electron cloud falls exponentially with distance, the tunneling current is ex-

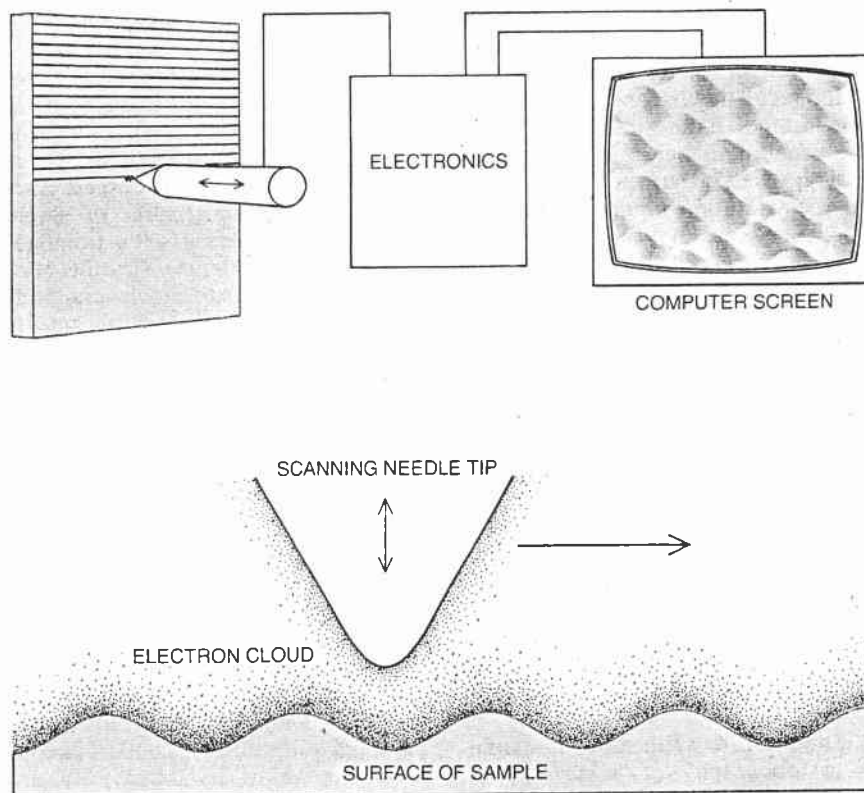
tremely sensitive to the distance between the tip and the surface. A change in the distance by an amount equal to the diameter of a single atom causes the tunneling current to change by a factor of as much as 1,000.

We exploit the sensitivity of the tunneling current to produce exquisitely precise measurements of the vertical positions of the atoms on the sample's surface. As the tip is swept across the surface a feedback mechanism senses the tunneling current and maintains the tip at a constant height above the surface atoms. In this way the tip follows the contours of the surface. The motion of the tip is read and processed by a computer and displayed on a screen or a plotter. By sweeping the tip through a pattern of parallel lines a three-dimensional image of the surface is obtained. A distance of 10 centimeters on the image represents a distance of 10 angstroms on the surface: a magnification of 100 million.

How is it possible to move the needle over a sample while maintaining a gap between the tip and the surface that is less than 10 angstroms and achieve a stability and precision that is better than .1 angstrom? First, the microscope must be shielded from vibrations such as those caused by sound in the air and by people walking around in a building. Second, the drives of the needle must be highly precise. Finally, the tip must be as sharp as the limits of rigidity and stability allow.

Two stages, or sections, suspended from springs, nestle within the stainless-steel cylindrical frame of the microscope and protect the tunneling gap from vibration. Both stages, triangular in cross section, are made of glass rods. The second stage slips into the first stage, from which it is suspended by three springs. The first stage in turn is suspended from the outer frame, also by three springs. The second stage carries the heart of the microscope: it contains both the sample and the scanning needle.

When the entire microscope sits in a vacuum, air resistance is minimal and the first and second stages could, if they were disturbed, bounce up and down almost indefinitely. To stop this motion we rely on the phenomenon of eddy-current damping. We let copper plates attached to the bottom of the first and second stages slide between magnets attached to the outer frame. As each plate slides up and down, the magnetic field causes the conducting electrons of the copper to move around, inducing a so-called eddy current. The reaction between the eddy current and the magnetic field retards



ELECTRON TUNNELING is the phenomenon that underlies the operation of the microscope. An electron cloud occupies the space between the surface of the sample and the needle tip (*bottom*). The cloud is a consequence of the indeterminacy of the electron's location (a result of its wavelike properties); because the electron is "smeared out," there is a probability that it can lie beyond the surface boundary of a conductor. The density of the electron cloud decreases exponentially with distance. A voltage-induced flow of electrons through the cloud is therefore extremely sensitive to the distance between the surface and the tip. As the tip is swept across the surface a feedback mechanism senses the flow (called the tunneling current) and holds constant the height of the tip above the surface atoms (*top*). In this manner the tip follows the contours of the surface. The motion of the tip is read and processed by a computer and displayed on a screen or a plotter. Sweeping the tip through a pattern of parallel lines yields a high-resolution, three-dimensional image of the surface.

the motion of the plate and thereby protects the microscope from even the smallest vibrations.

Once the gross vibrations have been stopped the sample can be positioned. This is done with a specially developed drive that carries the sample across a horizontal metal plate on the second stage. The body of the drive consists of a slab of piezoelectric material that expands or contracts when voltage is applied. The drive has three metallic feet, arranged in triangular fashion, that are coated with a thin layer of insulating material. They can be clamped to the metal plate by establishing a voltage between them and the metal plate.

We move the drive in the following manner. Suppose, for instance, we clamp only one foot and apply a voltage to the piezoelectric body so that it contracts. The other two feet will move slightly. We then clamp those two feet, release the third foot and remove the applied voltage so that the

body expands back to its original size. The drive has just moved one step. The step width can be varied between 100 and 1,000 angstroms. Since the drive can rotate about each of its feet, it can walk along the plate in any desired direction.

When the drive has carried the sample to the wanted tunneling position, we begin scanning the surface of the sample. We use a rigid tripod made of three piezoelectric sticks to move the tip of the scanning needle. When we apply a voltage to expand or contract one of the sticks, the other two bend slightly. Consequently the tip moves in a straight line over distances as great as 10,000 angstroms. Furthermore, this motion is quite sensitive to the magnitude of the applied voltage: a voltage on the order of .1 volt results in a motion of 1.0 angstrom. The precision of the tripod's drive is so good that at present only vibration limits the vertical resolution of the sample's surface. This resolution at present is in the

range of approximately a few hundredths of an angstrom.

The lateral resolution of the surface is limited by the sharpness of the tip. In this instance nature has been kind to the vacuum tunneler. It is relatively easy to make a sharp tip that yields a lateral resolution of about six to 12 angstroms: one simply grinds the end of a needle, which is usually made of tungsten.

To achieve a lateral resolution of two angstroms, however, the needle must have a single atom sitting securely on top of its tip. Such an atom usually comes from the sample itself. It is dislodged by high electric fields that are caused by applying a voltage difference of from two to 10 volts between the sample and the tip. Since luck plays a large role in the final stage, we are trying to sharpen the tip by bombarding it with a high-energy beam of ions. This causes the atoms on the surface to sputter away in a highly controlled manner.

In addition to delineating the atomic topography of a surface, the scanning tunneling microscope reveals atomic composition. The tunneling current depends both on the tunnel distance and the electronic structure of the surface and on the fact that

each atomic element has an electronic structure uniquely its own.

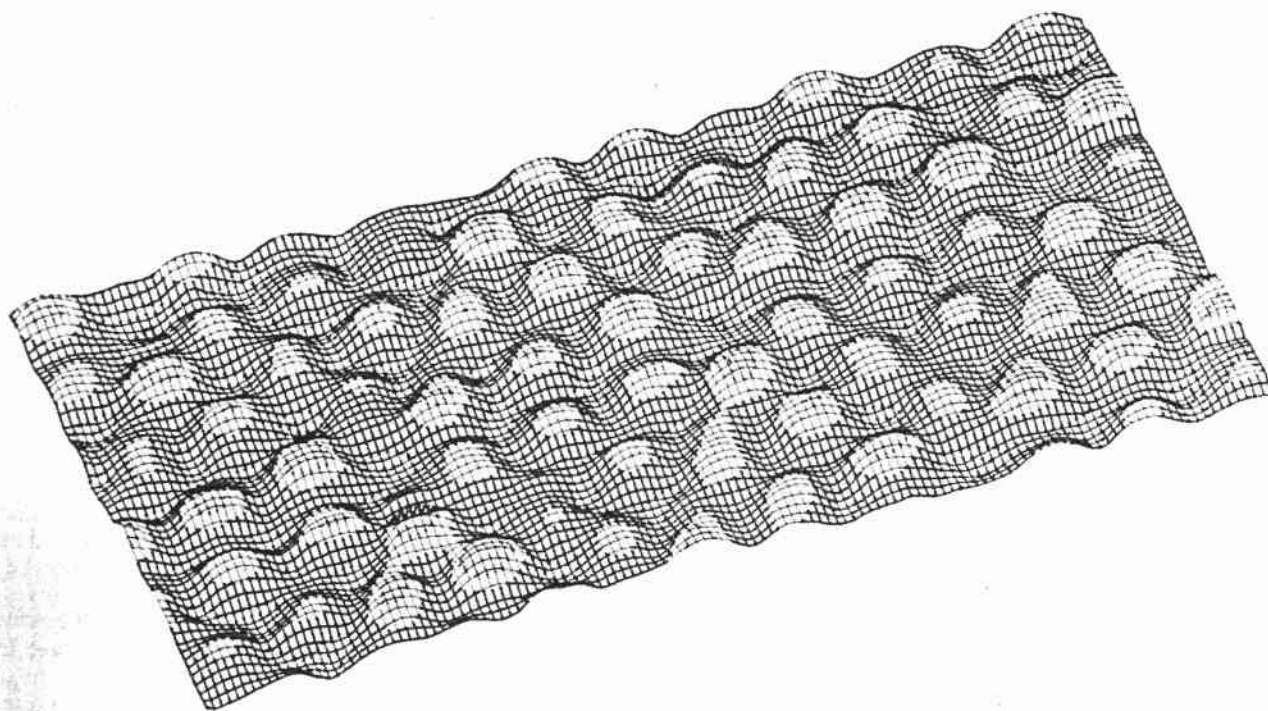
The ability of the microscope to resolve both topography and electronic structure will make it useful to investigators in physics, chemistry and biology. We first pursued the simplest case: the topographic structures of single crystals characterized by a homogeneous surface structure. Crystals consist of identical atomic layers built one on top of another. While results from scattering experiments indicate that the top layer is different from and more complex than the others, the precise structure of this layer was hard to determine.

The best-known surface structure is the diamond-shaped unit cell of silicon. Since each of the four edges of the cell measures seven atomic spacings, the cell is referred to as the 7-by-7. Each 7-by-7 contains 12 bumps that have not been visualized before. Each bump apparently corresponds to a single atom. The arrangement of the surface atoms is, although aesthetically pleasing, quite complex. This is in contrast to the relatively simple structure of any bulk layer found in silicon. Its unit cell, 49 times smaller in area than the 7-by-7, contains only two atoms. Another great difference between the two kinds of layers is that the surface

layer is much rougher than any bulk layer. Although the surface pattern is now known and a vast amount of information about it has been gained from other experiments, the reason this and not a different structure forms is not yet understood.

Another crystal whose surface structure is now better understood is the gold crystal. We found that when we cut the crystal in a direction parallel to its atomic layers, the resulting face is smooth. A cut in a direction diagonal to the atomic layers results in a rougher face. Just as one learns from studying the earth's crust how it was formed millions of years ago, so we have learned from studying these surfaces how they took shape. Current theories reveal that the diagonally cut surface assumes its jagged nature because such a configuration has a lower energy and is consequently stabler than a smooth configuration.

A more exotic branch of physics, the study of superconductivity, has also benefited from the application of scanning tunneling microscopy. A superconducting material is characterized by its complete lack of electrical resistance. The use of superconductors to make cables that are free from power losses could save enormous amounts of energy. The colliding-beam acceler-



SURFACE OF SILICON as disclosed by the scanning tunneling microscope consists of a pattern of diamond-shaped unit cells. Each cell measures 27 angstrom units (one angstrom unit is one ten-billionth of a meter) on a side. The cell is called the 7-by-7 because each side measures seven atomic units. Each 7-by-7 contains 12

bumps that are arranged in two groups of six. The bumps, which have never before been resolved, apparently correspond to the surfaces of individual atoms. They stand as much as 1.3 angstroms above the rest of the surface. The image was formed by applying a voltage so that electrons flowed from the needle tip to the surface.

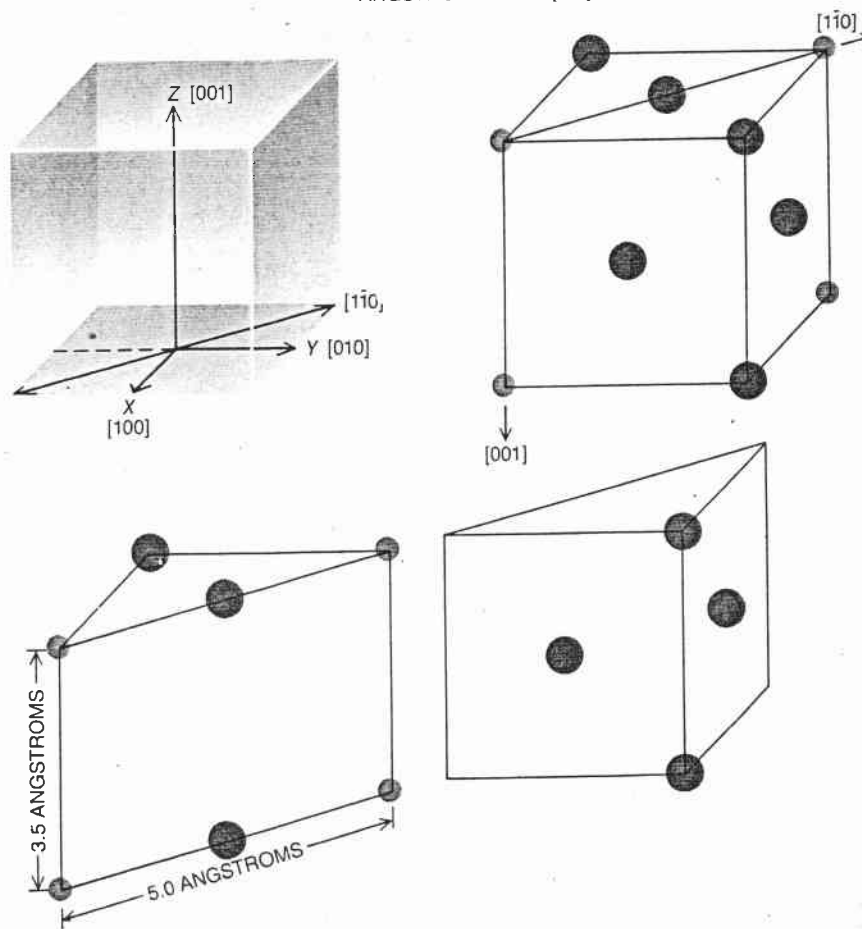
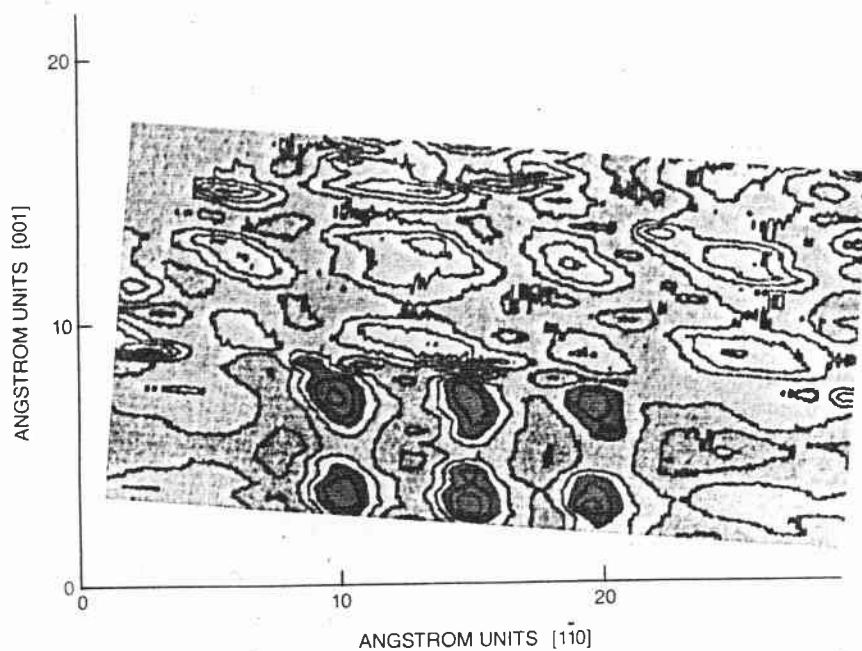
ator at Fermilab uses superconducting magnets to achieve high magnetic fields while saving energy. There is a catch, however. Superconductivity is only known to occur in some conductors that have been chilled below a critical temperature, typically a few degrees above absolute zero (-273 degrees Celsius).

A group of Stanford University investigators led by Calvin F. Quate has developed a scanning tunneling microscope that operates effectively at low temperatures. The workers first used their microscope to map the electronic structure of the surfaces of several conductors at room temperature. Then they chilled the conductors below the critical temperature of each and recorded the changes in electronic structure. The group can now document the growth of regions of superconductivity on surfaces.

The scanning tunneling microscope has also led to new understanding of certain chemical interactions. Our group has now observed on an atomic scale the adsorption of oxygen by nickel [see illustration at right]. Our finding confirms the results from earlier scattering experiments: The spacing of the oxygen atoms bound to the nickel surface varies according to direction. In particular, oxygen atoms that lie in one specific direction, designated $[001]$, are separated by one lattice spacing, or the distance between two adjacent nickel atoms in that direction. Oxygen atoms that lie in another direction, designated $[1\bar{1}0]$, are separated by two or five lattice spacings but never by one, three or four. We suspect that some kind of screening effect between the electric charges of the nickel and oxygen atoms is responsible for the anomaly, but more investigation is needed to determine the actual details of the physical interaction.

All the applications we have so far discussed have hinged on the ability of the microscope to detect structures whose dimensions are measured in mere fractions of an angstrom. Such high resolution is not always necessary. Even where the resolution of the scanning tunneling microscope is no better than some tens of angstroms, we expect on the basis of previous results that it will yield novel information and stimulate significant progress. In particular the possibility of operating the scanning tunneling microscope in air at ordinary pressure will in many applications more than compensate for any loss in resolution.

One such application is found in the study of friction. In order to minimize friction energy losses, investigators are



OXYGEN ADSORBED ON NICKEL (*top*) is observed on an atomic scale. The oxygen atoms (*color*) are 3.5 angstroms apart in one direction, designated $[001]$, and 5.0 angstroms apart in the other, $[1\bar{1}0]$. The face-centered cubic model of the nickel crystal (*bottom*) suggests the reason. The geometry of the model dictates that if the lattice spacing between two adjacent nickel atoms in the $[001]$ direction is 3.5 angstroms, the spacing in the $[1\bar{1}0]$ direction must be 2.5 angstroms. The electronic repulsion between two oxygen atoms is too great, however, to allow them to rest stably at lattice points separated by a mere 2.5 angstroms. Therefore oxygen atoms lying along the $[1\bar{1}0]$ direction must be separated by at least two lattice spacings, which corresponds to the observed 5.0-angstrom distance. Separations of five lattice spacings are sometimes seen, but never separations of three or four. Additional investigation may yet disclose the underlying reasons for the anomaly.

interested in learning more about the structure and causes of surface roughness of industrial materials. Recent studies suggest that the scanning tunneling microscope is ideally suited to the required work.

Our microscope has also demonstrated its usefulness in biology, even though at present it can achieve lateral resolutions of only 10 angstroms. In this case the relatively poor resolving power of the microscope is more than compensated for by its ability to provide a direct and nondestructive method of viewing biological samples.

Other microscopes in some sense partially destroy the samples on which they have been focused. In standard electron microscopy, for instance, samples must be coated with a thin layer of metal and, because they must be studied in a vacuum, they dry out. Since water molecules are an important part of biological substances, this might change the samples in an undesirable—and uncontrollable—way. In the scanning tunneling microscope

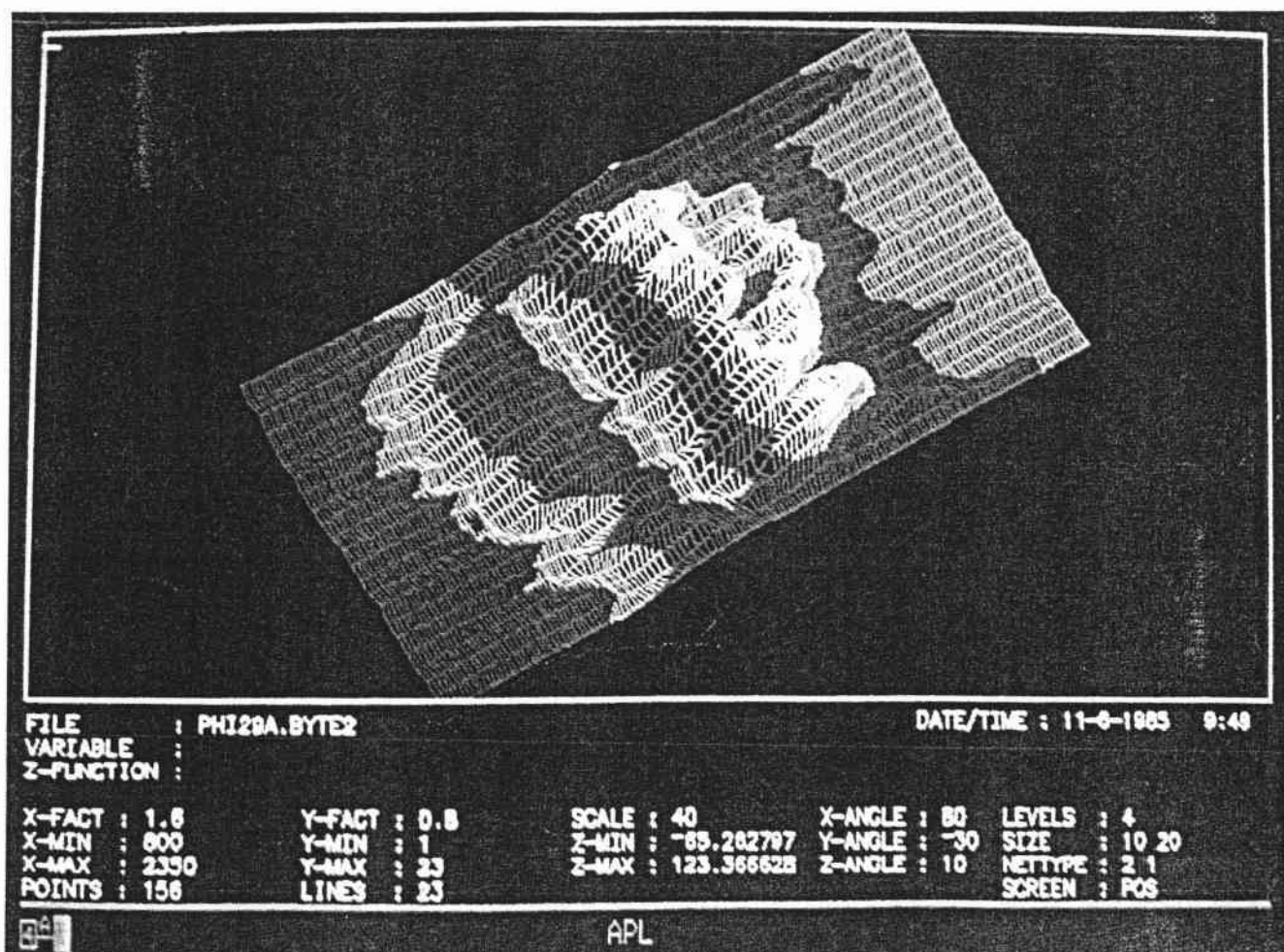
water can even be used as the insulating layer between the sample and the probing needle. (Water is a relatively poor conductor unless it contains ions such as those formed when sodium chloride dissolves in it.) Exploiting the sensitivity of the scanning tunneling microscope, we have, with the help of E. Courtens of the IBM Zurich Research Laboratory and H. Gross and J. Sogo of the Swiss Federal Institute of Technology, scanned the surface of the nucleic acid DNA. We observed a series of zigzags corresponding to its helical structure.

In a collaborative effort with Arturo Baró, Nicolas Garcia and Rodolfo Miranda of the Autonomous University of Madrid and José L. Carascosa of IBM Spain, we found that the head of the virus known as phi 29 measures $400 \times 300 \times 200$ angstroms. The structure of the connection between the head and the tail of the virus, called the collar, which appears to play a significant role in the process of infection, has been unraveled; the results agree

with those obtained by means of image-processed electron micrographs.

Apart from imaging, the probe tip will also be useful for testing electronic circuits. As components continue to shrink, the probes that test them must also be continuously miniaturized. The tip then serves as both a local voltage probe and a current source.

In all the foregoing applications it is vital that the imaging process not destroy or even alter the object. But the scanning tunneling microscope also offers promise as a tool for spurring specific chemical processes. One of the unique features of the microscope is its highly focused low-energy electron beam, or tunnel current. The energies of the beam lie within the range of those of most chemical processes. Therefore by tuning the beam to specific energies workers can cause particular reactions to occur. This mode of operation and the other capabilities of the instrument appear to open an entire new gamut of investigative possibilities.



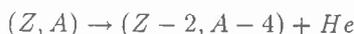
COLLAR OF VIRUS PHI 29 connects the head of the virus to its tail. Raw, unprocessed electron micrographs such as this one have

aided in unraveling the structure of the collar, an understanding of which is critical in controlling the spread of some viral infections.

Appendix F Radioactivity

In general, radioactivity can involve any of the following processes:

(i) α -Decay: In α -decay, a helium nucleus is emitted from the radioactive nucleus. The general reaction is written as (Z is the atomic number, A is the atomic mass)



The original nucleus has 2 units less charge and 4 units less mass.

(ii) β -Decay: In β -decay, a negative electron is emitted from the nucleus, leaving the nucleus with one more charge and the same mass



(iii) γ -Decay: this case, the original nucleus is an excited state (usually produced when another atom decays) and relaxes by emitting γ -rays.

Let us develop an understanding of radioactive decay by studying α -decay. In this process we can think of the nucleus as containing α -particles, i.e., 2 neutrons + 2 proton composites. There is a strong binding energy to keep the nucleus intact. However, in radioactive materials the nuclear structure is such that the highest energy nucleus can tunnel out of the nuclear potential.

In Fig. 6.13, we show a model potential for an α -particle as a function of its distance from the nucleus. At large distances from the nucleus, the potential energy is the electrostatic energy between a helium ion and the nucleus. At very small distances, the potential is the nuclear potential and is attractive and of the form shown in Fig. 6.13. The general potential is assumed to be of the form

$$\begin{aligned} V(r) &= -V_0, \quad r < r_0 \\ &= \frac{2Z'e^2}{4\pi\epsilon_0 r}, \quad r > r_0 \end{aligned} \quad (6.19)$$

where Z' is the charge of the final nucleus and the factor 2 is due to the charge of the helium nucleus.

Let us consider the limits of the integral for the tunneling probability. One limit is $r = r_0$ and the other can be seen to occur at (E is the energy of the α -particle) the point where $E = V(r)$. This gives for the other limit, a value r_1 where

$$r_1 = \frac{2Z'e^2}{4\pi\epsilon_0 E} \equiv \frac{A}{E} \quad (6.20)$$

Using these limits, we have, for the tunneling probability T (m is the mass of the α -particle),

$$\begin{aligned} \ln T &= -2 \int_{r_0}^{r_1} \left(\frac{2m}{\hbar^2} \right)^{1/2} \left(\frac{2Z'e^2}{4\pi\epsilon_0 r} - E \right)^{1/2} dr \\ &= -2 \left(\frac{2mE}{\hbar^2} \right)^{1/2} \int_{r_0}^{r_1} \left(\frac{r_1}{r} - 1 \right)^{1/2} dr \end{aligned} \quad (6.21)$$

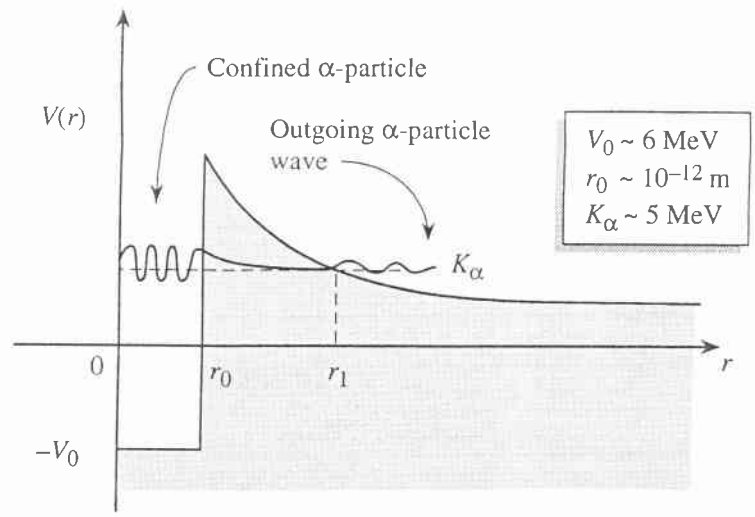


Figure 6.13: Model for the potential energy of an α -particle near a nucleus.

A solution of the integral gives the following result for the tunneling out probability of α -particles:

$$\ln T = \frac{4e}{\hbar} \left(\frac{m}{\pi \epsilon_0} \right)^{1/2} Z'^{1/2} r_0^{1/2} - \frac{e^2}{\hbar \epsilon_0} \left(\frac{m}{2} \right)^{1/2} Z' E^{-1/2} \quad (6.22)$$

If energy is expressed in MeV, r_0 in 10^{-15} m, we get

$$\ln T = 2.97 Z'^{1/2} r_0^{1/2} - 3.95 Z' E^{-1/2} \quad (6.23)$$

As α -particles leave the nucleus the nucleus transforms from one element to another. This process is known as radioactive decay. It is possible to describe the radioactive decay of an element by the equation

$$N(t) = N(0) \exp -\lambda t \quad (6.24)$$

An approximate expression for the rate λ can be obtained from the intuitive relation

$$\lambda = \nu T \quad (6.25)$$

where ν is the frequency with which the α -particle "strikes" the potential barrier. Inside a nucleus we can picture that there are N α -particles that can be produced by the proper association of protons and neutrons. The attempt frequency ν can then be written as

$$\nu = \frac{Nv}{2r_0} \quad (6.26)$$

where v is the velocity of the α -particles:

$$v = \sqrt{\frac{2E}{m}} \quad (6.27)$$

Isotope	$K_\alpha(\text{MeV})$	$t_{1/2}$	$\lambda(\text{s}^{-1})$
^{232}Th	4.01	$1.4 \times 10^{10} \text{ y}$	1.6×10^{-18}
^{238}U	4.19	$4.5 \times 10^9 \text{ y}$	4.9×10^{-18}
^{230}Th	4.69	$8.0 \times 10^4 \text{ y}$	2.8×10^{-13}
^{230}U	5.89	20.8 d	3.9×10^{-7}
^{210}Rn	6.16	2.4 h	8.0×10^{-5}
^{220}Rn	6.29	56 s	1.2×10^{-2}
^{222}Ac	7.01	5 s	0.14
^{215}Po	7.53	1.8 ms	3.9×10^2
^{218}Th	9.85	0.11 μs	6.3×10^6

Table 6.1: Half-lives and α -particle energies of some elements.

The parameter λ is related to the half-life, $t_{1/2}$ (i.e., the time it takes for half of the original atoms to decay), by the relation

$$t_{1/2} = \frac{0.693}{\lambda} \tag{6.28}$$

In Table 6.1 we show half-lives of some elements that decay by emitting α -particles. We can see that the half-life ranges from billions of years to microseconds. Radioactivity is used in a number of important technologies. We will briefly discuss a few applications.

Tracer Applications: An important application of radioactive materials is for tracer applications. This application is based on two properties: i) similarity in chemical properties of a radioactive atom (an isotope) and other atoms of an element. This allows one to follow movement of an element through chemical, physical or biological steps; ii) detection of the chemical species by examining the unique half-life of the radioactive tracer. Uses of tracer radioactive elements have been made in

- Tracking of cockroaches through city sewer systems. In this application, the insect is injected with a small radioactive material and the emission is tracked.
- Tracking of leaks in piping systems.
- In the metal industry, wear-and-tear of tools is tracked by radioactive tagging of tools and examining the radioactivity content of shavings, etc.
- A widespread use of tracers is in the field of medical diagnostics where a trace radioactive element is injected in the bloodstream and its movement is following through the body.

Treatment of Tumors: Advances in drug technology have allowed pharmaceutical companies to make drugs where radioactive elements (e.g., iodine) can be incorporated into specially designed molecules. These molecules, when injected into the bloodstream, can distinguish between healthy and tumor cells. They attach themselves to the tumor cells where the radioactive element delivers local radiation,

destroying the unhealthy cells. Since the radiation is preferentially delivered, there are few side effects.

Carbon-Dating: A very useful application of radioactivity is for dating objects such as fossils, bodies buried in glaciers, and even the Turin shroud. It is known that ^{12}C and ^{13}C are stable while ^{14}C is radioactive with a half-life of 5700 years. The disintegration of ^{14}C produces ^{14}N . Cosmic rays in the atmosphere produce ^{14}C which is then dispersed through the biosphere. The fraction of ^{14}C in the total carbon content in the biosphere (living organism) is fairly stable. However, when an organism dies, it no longer gets ^{14}C from the atmosphere, and the ^{14}C content starts to decrease. By measuring the residual ^{14}C in an object, it is possible to find the time of "death" in reference to contemporary time. The years before present, t , are given by

$$t = \frac{1}{\lambda} \ln \frac{A_o}{A_s} \tag{6.29}$$

where A_o is the contemporary activity, A_s is the radioactivity in the object. Carbon dating is one of the most accurate ways of determining the age of life forms which have been dead for a long time. The accuracy of the method is such that objects can be dated to within decades.